Universidade de Aveiro Departamento de Engenharia Mecânica
2016

Ismael Alagili Sassi Ehtiwesh

Avaliação exergética, energética, económica e ambiental de centrais de energia solar concentrada na Líbia

Exergetic, energetic, economic and environmental evaluation of concentrated solar power plants in Libya

Universidade de Aveiro Departamento de Engenharia Mecânica
2016

Ismael Alagili Sassi Ehtiwesh

Avaliação exergética, energética, económica e ambiental de centrais de energia solar concentrada na Líbia

Exergetic, energetic, economic and environmental evaluation of concentrated solar power plants in Libya

Tese apresentada à Universidade de Aveiro para cumprimento dos requisitos necessários à obtenção do grau de Doutor em Engenharia Mecânica, realizada sob a orientação científica do Prof. Doutor Antonio Carlos Mendes de Sousa, Prof. Doutor Fernando José Neto da Silva do Departamento de Engenharia Mecânica da Universidade de Aveiro.

Este trabalho de investigação foi financiado pelo ministério do Ensino Superior da Líbia no âmbito da bolsa n° 469-2009.

I dedicate this work to my beloved father and mother

o júri

Presidente

Doutor Nelson Fernando Pacheco da Rocha
Professor Catedrático, Universidade de Aveiro.

Doutor Fausto Miguel Cereja Seixas Freire
Professor Auxiliar, Faculdade de Ciências e Tecnologia, Universidade de Coimbra.

Doutor Margarida Isabel Cabrita Marques Coelho
Professora Auxiliar, Universidade de Aveiro.

Doutor Fernando José Neto da Silva
Professor Auxiliar, Universidade de Aveiro.

Doutor Maria Cândida Lobo Guerra Vilarinho
Professora Auxiliar, Universidade do Minho.

Doutor Ana Isabel Palmero-Marrero
Professora Auxiliar Convidada, Faculdade de Engenharia, Universidade do Porto.

Palavras-Chave

energia solar; centrais elétricas solares; CSP; armazenamento de energia térmica; modelação numérica; análise exergética; termoeconómica; impacto ambiental; LCA

Resumo

O projeto de Doutoramento aborda o potencial de usar centrais de energia solar concentrada (CSP) como um sistema de produção de energia alternativa disponível na Líbia. Uma análise nas vertentes exergética, energética, económica e ambiental foi realizada para um tipo particular destas centrais – um sistema de 50 MW com receção parabólica, porém ela é suficientemente geral para ser aplicada a outras configurações. A originalidade do estudo, para além da modelação e análise da configuração selecionada encontra-se na utilização do estado da arte em termos da análise exergética combinada com a avaliação do ciclo de vida (LCA).

A modelação e simulação da central CSP selecionada são efetuadas no terceiro capítulo tendo em consideração as duas componentes: ciclo de potência e campo de coletores solar. O modelo computacional para a análise do sistema foi desenvolvido com base em equações algébricas que descrevem o sistema, e que são resolvidas usando o *software* EES. Deste modo, são definidas as propriedades em cada ponto de interesse para os diferentes elementos do sistema, o que assim permite determinar as energias, eficiências e irreversibilidades desses elementos. O modelo desenvolvido tem o potencial de se tornar uma ferramenta de grande utilidade para o projeto preliminar de engenharia de centrais CSP, e também para a avaliação da eventual reconfiguração de centrais elétricas solares comerciais em operação. Além disso, o modelo pode ser utilizado no estudo de viabilidade da operação de centrais CSP, através da análise energética, económica e ambiental, para regiões diferentes da que foi escolhida no presente estudo -Trípoli (Líbia). O cenário total da viabilidade da operação da central CSP é completado através da análise horária com base anual apresentada no quarto capítulo. Esta análise permite a comparação de diferentes sistemas e, eventualmente permite fazer a seleção com base nas componentes económicas e energéticas, que são determinadas dentro do contexto do *software* greenius. A análise também toma em conta o impacto de financiamento e incentivos dados aos projetos no custo da produção de energia. O principal resultado desta análise é a verificação que o desempenho é mais elevado, com o consequente menor custo nivelado da eletricidade, para a Líbia em comparação com o Sul da Europa (Espanha). Assim a Líbia tem o potencial de se tornar um candidato atrativo para o estabelecimento de centrais CSP com o objetivo, como foi considerado em várias iniciativas europeias, de exportar eletricidade gerada através de fontes de energia renováveis de países do Norte de África e Médio Oriente para a Europa. A análise apresenta uma breve revisão do custo corrente da eletricidade e o potencial para reduzir o custo da energia a partir da tecnologia de receção parabólica de centrais CSP. A avaliação do ciclo de vida com base exergética (ELCA) e a avaliação do ciclo de vida convencional são realizadas para a centrais CSP específicas no quinto capítulo. Os objetivos são 1) avaliar o impacto ambiental e custo, em termos de do ciclo

de vida exergético do sistema; 2) identificar pontos fracos em termos da irreversibilidade dos processos; e 3) verificar se as centrais CSP podem reduzir o impacto ambiental e o custo de geração de eletricidade em comparação com centrais que consomem combustível fóssil. O capítulo ainda apresenta uma análise termoeconómica com base na metodologia do custo específico da exergia (SPECO), que avalia o custo relacionado com a destruição de exergia. A análise verificou que o impacto mais importante é a contribuição apresentada pelo campo solar (79%), e os materiais com maior impacto são: aço (47%), sal fundido (25%) e óleo sintético (21%). A análise ELCA mostra que a maior demanda de exergia é devida ao aço (47%); a análise existe uma considerável demanda de exergia relacionada com o sal fundido e ainda o óleo sintético. Em comparação com as centrais que consomem combustível fóssil (NGCC e óleo) a central sistema CSP apresenta menor impacto ambiental, enquanto o pior desempenho ambiental é o da central com queima de óleo seguida pela central a gás natural (NGCC). Na central CSP, o campo solar apresenta o custo mais elevado, enquanto o gerador de vapor, entre os componentes do ciclo de potência, apresenta o maior custo. O armazenamento de energia térmica permite que as centrais CSP superem a intermitência de radiação solar para responder à procura de energia elétrica independentemente das condições climáticas, e também possam estender a produção de eletricidade para além da disponibilidade da radiação solar diária. A análise numérica do transiente térmico de um sistema de armazenamento de gradiente térmico é realizada durante a fase de carregamento. O sistema de equações que descreve o modelo numérico é resolvido através da utilização de diferenças finitas implícitas no tempo usando o *software* Matlab. Os resultados da análise indicam que as previsões estão em boa concordância com os dados experimentais para a evolução no tempo da região de gradiente térmico, em particular para regiões mais afastadas da entrada. Nesta região os desvios observados são provavelmente causados pelo alto nível de turbulência devido à penetração do jato no seio do tanque de armazenamento. O modelo analítico simples para simular a turbulência que foi desenvolvido melhora os resultados. Esta abordagem não requer esforço computacional adicional e determina a difusidade térmica efetiva ao longo do tanque.

Keywords solar energy; solar power plants; CSP; thermal energy storage; numerical modeling; exergetic analysis; thermoeconomic; environmental impact; LCA

Abstract

The PhD project addresses the potential of using concentrating solar power (CSP) plants as a viable alternative energy producing system in Libya. Exergetic, energetic, economic and environmental analyses are carried out for a particular type of CSP plants. The study, although it aims a particular type of CSP plant – 50 MW parabolic trough-CSP plant, it is sufficiently general to be applied to other configurations. The novelty of the study, in addition to modeling and analyzing the selected configuration, lies in the use of a state-of-the-art exergetic analysis combined with the Life Cycle Assessment (LCA). The modeling and simulation of the plant is carried out in chapter three and they are conducted into two parts, namely: power cycle and solar field. The computer model developed for the analysis of the plant is based on algebraic equations describing the power cycle and the solar field. The model was solved using the Engineering Equation Solver (EES) software; and is designed to define the properties at each state point of the plant and then, sequentially, to determine energy, efficiency and irreversibility for each component. The developed model has the potential of using in the preliminary design of CSPs and, in particular, for the configuration of the solar field based on existing commercial plants. Moreover, it has the ability of analyzing the energetic, economic and environmental feasibility of using CSPs in different regions of the world, which is illustrated for the Libyan region in this study. The overall feasibility scenario is completed through an hourly analysis on an annual basis in chapter Four. This analysis allows the comparison of different systems and, eventually, a particular selection, and it includes both the economic and energetic components using the “greenius” software. The analysis also examined the impact of project financing and incentives on the cost of energy. The main technological finding of this analysis is higher performance and lower levelized cost of electricity (LCE) for Libya as compared to Southern Europe (Spain). Therefore, Libya has the potential of becoming attractive for the establishment of CSPs in its territory and, in this way, to facilitate the target of several European initiatives that aim to import electricity generated by renewable sources from North African and Middle East countries. The analysis is presented a brief review of the current cost of energy and the potential of reducing the cost from parabolic trough-CSP plant. Exergetic and environmental life cycle assessment analyses are conducted for the selected plant in chapter Five; the objectives are 1) to assess the environmental impact and cost, in terms of exergy of the life cycle of the plant; 2) to find out the points of weakness in terms of irreversibility of the process; and 3) to verify whether solar power plants can reduce environmental impact and the cost of electricity generation by comparing them with fossil fuel plants, in particular, Natural Gas Combined Cycle (NGCC) plant and oil thermal power plant. The analysis also targets a thermoeconomic analysis using the specific exergy costing (SPECO) method to evaluate the level of the cost caused by exergy destruction. The main technological findings are that the most important contribution impact lies with the solar field, which reports a value of 79%; and the materials with the

highest impact are: steel (47%), molten salt (25%) and synthetic oil (21%). The “Human Health” damage category presents the highest impact (69%) followed by the “Resource” damage category (24%). In addition, the highest exergy demand is linked to the steel (47%); and there is a considerable exergetic demand related to the molten salt and synthetic oil with values of 25% and 19%, respectively. Finally, in the comparison with fossil fuel power plants (NGCC and Oil), the CSP plant presents the lowest environmental impact, while the worst environmental performance is reported to the oil power plant followed by NGCC plant. The solar field presents the largest value of cost rate, where the boiler is a component with the highest cost rate among the power cycle components. The thermal storage allows the CSP plants to overcome solar irradiation transients, to respond to electricity demand independent of weather conditions, and to extend electricity production beyond the availability of daylight. Numerical analysis of the thermal transient response of a thermocline storage tank is carried out for the charging phase. The system of equations describing the numerical model is solved by using time-implicit and space-backward finite differences and which encoded within the Matlab environment. The analysis presented the following findings: the predictions agree well with the experiments for the time evolution of the thermocline region, particularly for the regions away from the top-inlet. The deviations observed in the near-region of the inlet are most likely due to the high-level of turbulence in this region due to the localized level of mixing resulting; a simple analytical model to take into consideration this increased turbulence level was developed and it leads to some improvement of the predictions; this approach requires practically no additional computational effort and it relates the effective thermal diffusivity to the mean effective velocity of the fluid at each particular height of the system.

Altogether the study indicates that the selected parabolic trough-CSP plant has the edge over alternative competing technologies for locations where DNI is high and where land usage is not an issue, such as the shoreline of Libya.

Table of Contents

List of Tables

List of Figures

Nomenclature

Symbols

A_p	Parabolic reflector aperture [m]
$\dot{C}_D$	Cost rate associated with exergy destruction [€/h]
c	Specific heat capacity [J/kg-K]
C	Cost per unit exergy [€/W-h]
CED	Cumulative energetic demand [J]
CExD	Cumulative exergetic demand [J]
ch	Chemical exergy [J]
D	Diameter [m]
d	The coefficient of damage
DNI	Direct Normal Insolation [W/m²]
$\dot{E}_D$	Exergy destruction rate [W]
E_t	Electricity generation in the year t
E_x	Exergy [J]
F_t	Fuel expenditures in the year t
h	Enthalpy [J/kg]
h	Convective heat transfer coefficient [W/m²-K]
h_v	Volumetric interstitial heat transfer coefficient [W/m-K]
I	Irreversibility [J/kg]
It	Investment expenditures in the year t
IAM	Incidence angle modifier
IMP	The impact category [Pt]
k	Physical exergy [J]
K	Pressure drop coefficient [bar-s²/kg²]
K_{th}	Thermal conductance [W/m-K]
l_{mix}	Mixing length [m]
L	Height of the tank [m]
LCE	Levelized cost of electricity [€/kWhe]
LCOE	Required Tariff
$\dot{m}$	Mass flow rate [kg/s]
m	Mass [kg]
M_t	Operations and maintenance expenditures in the year t
n	Amount of energy [J]
n	Expected lifetime of the system

NTU	Number of transfer units
Nu	Nusselt number
P	Pressure [Pa]
Pr	Prandtl number
Q	Heat transfer [W]
r	Radius [m]
r	Discount rate
r_{ex}	The relation of exergy to energy [J]
R_a	Rayleigh number
R_e	Reynolds number
s	Entropy [J/kg-K]
S_{gen}	Entropy generation [J/K]
T	Temperature [K]
t	Time [s]
u	Velocity [m/s]
U	Average exit velocity and the orifice diameter [m/s]
UA	Overall heat transfer coefficient [W/K]
U_w	Coefficient of thermal losses to the environment [W/m²-K]
W	Work [W]
x	Steam quality
X	Downstream distance [m]
z	Height [m]

Greek Symbols

a	Fitting constant designed
a_w	Relation between thermal losses area and tank volume [m^{-1}]
α	Thermal diffusivity [m²/s]
α_a	The coating absorptance
β	Volumetric thermal expansion coefficient [m^{-1}]
γ	The fraction of the direct solar radiation reflected by mirrors
ε	Effectiveness
ε	Emissivity
ε	Porosity of the storage medium (void fraction)
η	Efficiency
ν	Kinematic viscosity [m^2/s]
Π	Dimensionless temperature

ρ	Density [kg/m³]
ρ_{cl}	The clean mirror reflectance
σ	Stefan-Boltzmann constant [W/m^2-K^4]
σ	Standard deviation related to the spread of the profile across the centerline
τ_e	Envelope transmittance
ϑ	Velocity [m/s]

Subscripts

*	Sub index indicating dimensionless quantities
eff	Sub index that refers to the effective storage medium
o	Atmosphere
SF	Solar field
th	Thermal

Abbreviations

CH	Switzerland (Geographical boundary)
CSP	Concentrate solar power
DALYs	The number of year life lose and the years lived disabled
ELCA	Exergetic Life Cycle Assessment
EQ	Ecosystem quality
GHI	Global horizontal irradiation
GLO	Global (Geographical boundary)
HCE	Heat collection element
HH	Human health
HPT	High pressure turbine
HTF	Heat transfer fluid
LCA	Life Cycle Assessment
LCE	Levelized cost of energy
LCI	Life cycle inventory
LCIA	Life cycle impact assessment
LFR	Linear Fresnel
LPT	Low pressure turbine
LS3	Luz parabolic design third generation
M	Momentum
NGCC	Natural gas combined cycle
OCE	Oceanic (Geographical boundary)

PCM	Phase change material
PDF	The loss of species for a specific area and over a particular time span
PTPP	Parabolic trough power plant
R	Resources
RER	Europe (Geographical boundary)
SEGS	Solar energy generation systems
SPECO	Specific exergy costing
STPP	Solar thermal power plant
T	Turbulence
TES	Thermal energy storage
w	Water
ZFE	Zone of flow establishment

Chapter 1

Introduction

1.1 Overview

The emphasis of the present study is the renewable production of energy. Sustainability and energy are issues that are relevant to all sectors of the Society, including the well-being in the future of mankind in the planet Earth. They should not be treated in separate; however, the immediacy of the need for energy is ever-present in every corner of the world, although with differing degrees of intensity, in a wide range of sectors from electricity production to food. Obviously the impacts are experienced in such diverse areas as environment, public health, national security, economy, education and quality of life. In the world, energy use and conversion are intrinsically linked to gross domestic product; unfortunately, the most prosperous and technologically developed nations are also those that have the highest energy consumption per capita. Taking into consideration that most of the energy is based on fossil fuels, there is an ecological urgent requirement that their use be phased out in favor of renewable sources of energy, which may be considered one of the great challenges of this century. The situation is aggravated with the rapid economic expansion of developing countries with large populations with increasingly

higher purchasing power; the worst case scenario is the developing countries adopting energy consumption models of the developed countries. Moreover, the world population is rapidly growing, and some studies predict a world population of 9 billion around 2040 [1] taking the 7 billion people living on this planet today as the base value. The global demand for energy will be dramatic and it can be reasonably questioned whether it will be sustainable maintaining an increasing level of economic growth and of living standards.

The International Energy Outlook 2013 predicts that the energy consumption will increase by 56% by 2040 taking as reference 2010 [2]. The expected increased demand for energy will have a further economic impact due to a potential increase in fuel prices – this trend already is noticeable and it is a result of new growing economies. The energy infrastructure is greatly dependent on fossil fuels like oil, coal and gas. These resources are finite and, notwithstanding major advances in extraction technologies, best estimates indicate that in the coming century, at current rates of consumption, the world will be running out of oil and gas reserves. The depleting of the reserves will require more advanced and eventually more expensive technologies, and in some cases such as hydraulic fracturing (fracking), potentially environmentally harmful. However, the argument to find alternatives to fossil fuels should not be their depletion, but the production of greenhouse gases, in particular carbon dioxide. The increase in carbon dioxide concentration in the earth's atmosphere up to 2013 [3] is dramatic; there was an approximate increase of 19.4% in the mean annual concentration, from 354.35 parts per million by volume (ppmv) of dry air in 1990 to 396.48 ppmv in 2013. There is a nearly general consensus that carbon dioxide is responsible for global warming and climate change; if the occurrence of disasters related to extreme weather is an indication, then it is urgent the shifting from fossil to alternative energy sources, like solar and wind.

Renewable energy sources have the advantage of not compromising the ecosystem and, in general, they have relatively minor environmental impacts. In

addition, in sociological and political terms, the trade of renewable energy does not foster violent extremism and/or national security problems. These particular problems are currently associated with the trade of fossil fuels in many regions of the world; concurrently, the price stability can be jeopardized and being at the mercy of the market drifts. Fossil fuels, although being the engines of progress and development for well over one century, are harmful to the environment and, with dwindling reserves; there is an ever-increasing need to find alternatives. The ongoing challenge is to find the alternative energy source that can meet simultaneously environmental requirements, immediate societal needs, and affordability in terms of cost and access. It should be mentioned, in the global context, that nowadays, more than 12% of the world population is undernourished; 12% of the world population lacks access to potable drinking-water source, 37% has no access to sanitation facilities with obvious serious public health impacts [4]. Based on all these inequities and inequalities, which may have its roots in limited access to energy, the energy paradigm must change to attain sustainability on Earth and, in particular, not only the survivability but the well-being of mankind.

In fact, nowadays, energy is one of the time stamps or dating elements that can be used to describe society; the type of energy that society uses is a sign of how modern or how ancient that society is. The invention of the steam engine in the 1700s enabled the conversion of thermal energy into kinetic energy; thus, in antiquity, there were kinetic and thermal energy, but there was no way to convert the thermal energy into kinetic energy. However, with the Industrial Revolution, the use of the steam engine increases. Once the steam engine was available, it could take the heat to motion; as a consequence, machines and factories became a societal reality. Throughout the 20^{th} century, energy consumption has mostly been a story of growth. During the last few decades, there was steady growth in the energy consumption despite energy saving measures and increased efficiency. In the 70s, during a relatively short period, the energy consumption dropped primarily due to geopolitical reasons, which led to an oil crisis and consequently high energy prices. In addition,

fossil fuels have been the dominant primary energy source in modern history. Fossil fuels have advantages that are hard to replace, particularly, in terms of energy density and performance. Renewables and nuclear still represent, as compared to fossil fuels, a very small fraction of the global energy consumption.

The advantages of the solar energy are that the source – the Sun - is free and renewable, inexhaustible and matches reasonably well peak demand, which, in general, is not the case of wind power. The prospects for solar power generation are very good, considering that systems performance are markedly improving, while prices are dropping. Legal global restrictions in greenhouse gases emissions may make solar power generation economically competitive with fossil fuels power generation. Essentially, there are three different approaches to the use of solar energy: one is the solar thermal, where the solar energy can be used in a variety of applications including space and water heating. Solar thermal is pretty simple, and usually the heating fluid operates at relatively low temperatures – typically below 100ºC. Solar thermal used in applications in which the use of heat is the purpose. Others related to power production, occurs through the concentrated solar power (CSP) using the solar energy to create steam that then generates electricity and through solar photovoltaic (PV) panels where direct electricity production is obtained. Solar photovoltaic panels are used for direct electricity production, converting radiant energy photons to electrical energy electrons. It operates commonly with scattered/reflected light, and it is sensitive to cloud cover, like any other solar system; the presence of clouds will diminish the solar irradiation. Efficiency of PV systems is still low, but the progress in this area over the last decades has been dramatic making them a viable competitor for not only distributed but also centralized power.

CSP technology is a system for centralized power generation and it involves several energy conversions. It transforms radiant energy to thermal energy to make steam, which then goes through a steam turbine to produce mechanical energy that then activates magnets of the electrical generator to produce electricity. It requires

direct normal radiation, consequently, it does not work with a scattered light; this is the reason why it needs a concentrator to heat up the working fluid. Concentrated solar power plants are becoming one of the most promising technologies to produce clean and sustainable energy; therefore their use in the future is expected to increase [5]. CSP technologies cover a large array of different options, of which, the most common are: parabolic trough, central receivers (power tower), parabolic dish and linear Fresnel. The parabolic trough is the one with a wider usage [6,7] and which is considered in this study. However, the central receiver technology is becoming increasingly important, particularly in the US and Spain. The parabolic dish technology has the advantages of having a low requirement in what concerns water consumption, but the technology still has very high capital costs [8]. CSP plants (CSPs) consist of three main systems: the solar field, the power conversion cycle and the thermal energy storage system (TES) [9]. The solar field consists of a ray of mirrors that track and reflect the sun's rays into a receiver when the concentrated sunlight strikes the boiler pipes to heat the water. Steam produced by the heated water is piped from the boiler to a turbine where electricity is generated. CSP in this way becomes a dispatchable renewable energy when using TES. TES can expand the time of power generation, and is normally charged at the peak of solar energy for the duration of the day-time while the stored heat is released at night or when there is not enough solar radiation. There are technological challenges when using CSP with TES; it can be stored energy in different materials, such as concrete, molten salt or ceramic. Energy storage is a critical factor in the advancement of solar thermal power systems that generate electricity [10]; it can offer the potential to deliver electricity without fossil-fuel backup and to meet peak demand, independently of weather conditions. In contrast to totally dispatchable fossil sources, CSP without TES is an incomplete energy resource depending on the hourly and daily supply of solar radiation; this radiation is variable on a daily and monthly basis; therefore, it is not totally reliable. Given these constraints, solar radiation capture and use need to be optimized to maximize power production. The long-term strategy for CSP, considering possible limitations of TES, is for it to be fully integrated into a power grid with

adequate adaptation with auxiliary facilities and a generational mix that includes variable generation sources such as wind and even fossil fuel.

1.2 Literature Review

The south side of the Mediterranean coastline has a very high annual direct normal irradiation (DNI) [11], which makes Libya a privileged potential user of solar power generation technologies. In fact, Europe is studying the feasibility of building renewable energy projects with particular emphasis on concentrated solar power plants along the shores of the Mediterranean and in the North African desert, such as the Desertec initiative [12]. This Desertec energy project, which has as partners several Mediterranean countries, is an excellent example of the realization of the concept of cooperation between Europe and Africa. The plants will be in African soil and connected to a grid that links North Africa to Europe, and in this way supporting local economic development through this innovative collaboration. CSP plants in Libya can use state-of-the-art technologies, which use relatively well-known and abundant materials; in their production it will be possible to minimize environmental impacts, including toxic emissions and limited use of water. Taking into consideration these premises, CSPs will be attractive not only to the investors, but also to consumers. The grid connecting the southern and northern Mediterranean coasts will have a new underwater cable between Africa and Europe. The high voltage direct current cable will be laid across the Mediterranean seabed and it will have an extension of six hundred kilometers.

Under this scenario, the utilization of solar power systems has an enormous potential in Libya; the Mediterranean coast of Libya offers outstanding conditions of CSP rollout, namely: very high DNI, little precipitation, large amount of free flat land and it is close to Europe. Undoubtedly, the eventual sales of the CSP generated electricity to Europe will be a prime motivation to start these CSP projects, despite the large investment required. High capital costs of solar devices over their lifetime can

be amortized and solar technology can be competitive against other technologies [13].

There is a considerable body of literature dealing with different solar energy options for electricity generation using CSP technologies. In particular, a few studies aim to advance the parabolic trough technology for power generation. Ya-Ling He et al. [14] reported a detailed procedure for the modeling of the parabolic trough solar power plant with organic Rankine cycle within the energy simulation package TRNSYS; the influence of several design and operating parameters on the performance of the collector field and the complete system was examined. The authors concluded that with the increase in HTF velocity, the heat collecting efficiency increases quickly at the beginning; however, it is almost independent of the HTF velocity when the velocity reaches a determined value. In addition, it was shown that the heat collecting efficiency increases with the increase in DNI. Moreover, the heat loss of the solar collector increases when the interlayer pressure between absorber tube and glass tube is less than 10 Pa. However, with further increase of the pressure, the reduction of the loss is practically negligible. Derbal et al. [15] conducted the modeling and numerical simulation of a 150 MW integrated solar combined cycle plant (with 20% solar) in the area of Hassi R'mel (Algeria) – this region is close to Libya and consequently the environmental conditions are similar to those of the present study. The combined cycle plant uses a gas turbine with exhaust heat recovery for steam generation; the overall efficiency obtained is about 49% at nominal power output. The study of Montes et al. [16] presents a multiple economic optimization of a solar-only parabolic trough plant by considering five different layouts – all of them with the same power block but different solar field sizes. The study concludes that with increasing sized solar field, without thermal storage, the return on the investment worsen; this result is somewhat obvious, as solar thermal energy available beyond the steam plant nominal rating would be wasted. In addition, the size and configuration of the solar field have a significant environmental impact. Lippke [17] simulated the part-load behavior of the 30 MWe Kramer Junction solar

electric generating systems located at Boron, California. The results indicate that the solar radiation intensity greatly influences the optimum temperature of the steam and of the heat transfer fluid. Reddy et al. [18] carried out an energetic and exergetic analysis for the year round operation of a parabolic trough power plant for two different locations in India. The study demonstrates that the main energetic loss takes place at the Rankine heat engine circuit through the condenser, followed by the collector-receiver unit. The energetic efficiency of the system was increased by 1.49% and the exergetic efficiency was increased by 1.51% for the more favorable location, when the operating pressure was increased from 90 bar to 105 bar. Poullikkas [19] carried out a feasibility study aiming to investigate whether the installation of parabolic trough solar power systems in the Mediterranean region is economically feasible taking as a base study the available solar potential of Cyprus. Based on the findings of the study, the installation of a parabolic trough solar thermal power plant in the Mediterranean area can be profitable and economically feasible under appropriate conditions, which are dependent primarily on the size of the plant, the degree of thermal storage, the initial cost and the cost of land. In addition, the results demonstrated that the additional benefit resulting from CO_2 emissions trading price of 30 €/t for all cases tested within the simulations was at 0.024 €/MWh. The study demonstrates that by increasing the size of the parabolic trough solar thermal power plant from 25 MW to 100 MW, the investment becomes increasingly attractive.

Furthermore, one of the main advantages of solar radiation is that it allows the conversion of electromagnetic radiation to electricity to occur without environmentally harmful discharges. However, other stages of the fuel cycle contribute to environmental damage. This is a critical point since the environmental performance has become a key issue especially in the conceptual and design stages of a large-scale project; therefore, projects should be investigated and implemented to minimize its impact on the environment. Life Cycle Assessment (LCA) has emerged as one of the preferred tools to assess environmental impact of a selected product or process over its life and it encompasses all stages, including raw materials selection,

production, use and disposal. LCA is an objective procedure to evaluate the environmental burdens associated with a product, process, or activity by identifying and quantifying energy and material usage and environmental releases. In this way, it is possible to assess competing measures and opportunities to be identified and ultimately implemented to yield environmental impact minimization.

Combined exergetic and Life Cycle Assessment is used in the present study to evaluate the CSP plant along its life cycle in terms of environmental impacts and energetic performance. LCA, as already mentioned, is a tool which can be used not only to investigate the contribution of each life cycle stage to the total environmental load, but also to enable the identification of environmental hotspots and to provide opportunities for process improvement and optimization of either the plant or a specific life cycle stage. On other hand , the use of the exergy balance as a tool to assess industrial processes, can overcome the limitations of a simple energy analysis; the exergy analysis allows the evaluation of the thermodynamic performance of energy systems and the determination of the energy quality disintegration during energy transfer and conversion [20]. Exergy, which is derived from the second law of thermodynamics, is useful in the identification of the irreversibilities associated with the energy flow and its conversion. The exergy analysis allows the evaluation of the maximum available work in terms of quality and quantity for a critical assessment of the thermodynamic performance of any energy producing system; it has been widely used in the design, simulation and performance evaluation of energy systems.

Cornelissen [21] proposed a method that involves exergetic considerations into the LCA framework. The integration of the two methodologies within one combined method has largely enhanced their respective strengths, while reducing their individual weaknesses. The combination of exergy and LCA, known as exergetic life cycle assessment (ELCA), enables the production of exergy scores for a large number of materials and processes, which, in particular for resource use and

resource depletion scores, may prevail over conventional life cycle assessment methods [22]. ELCA analysis is considered to be the most appropriate instrument to quantify environmental impact related to the depletion of natural resources [21] and its implementation is clearly the same as that of LCA; however, it requires a far more comprehensive database namely the exergetic values of all inputs in addition to highly detailed disaggregated data of the processes involved. In addition, ELCA is a universally applicable tool to evaluate process efficiency and to investigate the sustainability of heterogeneous systems. Therefore, in the recent past ELCA has been favored in the evaluation of the sustainability of complex systems and technologies.

There are few studies of LCA applied to CSP plants and most of them are primarily focused on some parts and/or subunits of CSP power plants [23-29]. Lechón et al. [23] assessed the environmental impacts of the electricity generated using a 17 MW central tower and 50 MW parabolic trough solar thermal power plants in Spain and identified opportunities to improve the systems in what concerns the environmental impact reduction. The estimated greenhouse gases emissions were approximately 200 g/kWh (CO_2 - equivalent), which is lower than those of competing fossil technologies. Piemonte et al. [24] conducted a LCA for the molten salt CSP plant combined with a biomass back-up burner. The findings were very encouraging - using the reference weighing set proposed by the Swiss LCA Group, the CSP plant has a large number of advantages over the conventional power plants. Weinrebe et al. [25] reported a LCA analysis of two generic solar thermal power plants with fossil co-firing of natural gas and dry cooling towers; the reference plants selected were 80 MW solar energy generation systems (SEGS) parabolic trough plant and 30 MW Phoebus power tower plant. The study illustrated that emissions related to electricity generation of solar plants in 'solar only' mode were typically one order of magnitude below the corresponding emissions of conventional plants. In addition, the hybrid operation presented emissions 2 to 4 times lower than those from conventional plants. Oro et al. [26] reported a comparative analysis of the environmental impact of

three different types of thermal storage systems. The systems are sensible solid heat storage, sensible liquid heat storage (2-tank model), and latent heat storage (phase change material). The analysis reported that the sensible liquid storage system is the one with the highest environmental impact. The solid medium has the lowest impact, since its design is very simple and the thermal storage capacity is relatively small. Kuenlin et al. [27] presented a comparative LCA study for four different CSP plants: parabolic trough, central tower, Fresnel and parabolic dish. The dish plant has the best environmental performance, while the parabolic trough plant is the one with the worst environmental performance as a result of using the synthetic oil as the network HTF (Heat Transfer Fluid) and the molten salt. Klein and Rubin [28] conducted a comparative study of the life cycle greenhouse gas emissions, water consumption, and direct on-site land use. They associated one MWh of electricity generation from solar thermal power plants with wet and dry cooling and with three energy backup units (minimal backup, molten salt thermal energy storage and natural gas-fired heat transfer fluid heater). The study demonstrated that plants with natural gas have 4 to 9 times more greenhouse gas emissions than plants with thermal energy storage. The study also pointed out that CSPs with thermal energy storage generally have twice as many life cycle greenhouse gas emissions as the minimal backup plants. Asdrubali et al. [29] reports on LCA analyses of different types of electricity generation from renewable resource systems including a solar energy (PV and CSP). Wind power is the system with the lowest overall environmental impact, whereas geothermal power and PV are the technologies with the highest overall environmental impact values, while CSP presents a medium level environmental impact.

Moreover, several studies focused on exergetic analysis for thermodynamic and economic evaluation of CSPs and its related systems [30-51]. Hepbasli [30] conducted a comprehensive reviews on exergetic analysis and performance assessment of a wide range of renewable energy resources and sustainable development including solar thermal power plants. The same author in co-authorship performed a series of exergetic studies dealing with sustainable energy systems [31-

38]. In their assessment, exergy analysis is a very useful tool, which can be successfully used in the evaluation of renewable energy resources and energy-related systems. Sciubba [39] used the Extended Exergy Accounting method for evaluation and design optimization of a co-generative power plant, the method being described in detail in [40-43], demonstrating that exergy is indeed a practical instrument for performing design optimization tasks, and it can be a useful indicator for economic and environmental impacts. Singh et al. [44] conducted a second law analysis based on an exergy concept for evaluating the respective losses and exergetic efficiency of solar thermal power system components (collector field and power cycle). The analysis concluded that the main energy loss takes place at the condenser (power cycle), while the maximum exergetic losses take place at the collector/receiver assembly (collector field). Khaljani et al. [45] addressed the thermodynamic, exergo-economic and environmental evaluation of co-generation of heat and power taking into consideration three objective functions: first and second law efficiencies and the total cost rates of the system. The main finding of the study is that the exergy destruction cost rate is higher than the capital investment cost rate, while combustion chamber, heat recovery steam generator and gas turbine are the components with the highest total cost rate. Furthermore, exergo-economic analysis is an effective tool used to determine the cost effectiveness of thermal systems, with the intent of evaluating and enhancing the system performance in terms of its economic and thermodynamic indicators [46]. The specific exergy costing (SPECO) method [47,48] is used in the present study for the thermodynamic economic analysis; the main benefit of this method is allowing to calculate the cost of exergy destruction in each component of the energy system under consideration [48]. The method has been used for economic analysis of thermal energy systems; among the most relevant work for the present study, the following publications were selected. Tsatsaronis et al. [48] demonstrated the usefulness of a new approach of exergy costing in exergo-economic analysis based on specific exergy by applying it to a simplified gas turbine system; the approach eliminates the need for auxiliary assumptions in the exergo-economic analysis and improves the accuracy of the

costing process by considering both the cost-formation and the monetary-value-use processes. Elsafi [49] conducted an exergo-economic analysis for a direct steam generation parabolic trough-CSP plant; the analysis indicates that the highest exergetic cost rate takes place in the solar field followed by the condenser. Cavalcanti and Motta [50] conducted an exergo-economic analysis of a solar-powered/fuel assisted Rankine cycle for a power plant located in Natal (Brazil) using the SPECO approach. The study concludes that the month of June (winter) has the lowest collector efficiency, higher fuel consumption and higher specific cost per exergy unit of electricity, while March presents the best results for these indicators. The system described is not an advantageous system from an exergo-economic point of view, and it was observed that the electricity cost rate per exergy is high comparison with other systems. Colpan and Yeşin [51] carried out a thermoeconomic analysis of the Bilkent combined cycle cogeneration plant using the SPECO method. Cost rate associated with exergy loss was found $135/h (≈ €119/h) for 15t/h process steam export. The capital cost of the power turbines is only affected by the cost rate of electricity output of the gas turbine.

Notwithstanding the quality of the aforementioned studies, none of them has combined life cycle assessment with exergetic analysis for the evaluation of CSPs. The novelty of the present analysis lies in combining both tools for CSPs in order to overcome some potential weaknesses of the two individual methodologies. ELCA was used in several studies with promising results but not for CSPs which is the aim of the present work. These studies were conducted for several different systems related to industrial fields such as hydrogen production [52,53], solar heating and cooling systems [54], resource consumption in built environment [55], biodiesel production [56], gas turbine power cycle [57], cement production process with waste heat power generation [20] and combined cycle power plant [58]. The major conclusion of these studies is that ELCA is a practical tool to investigate the resource and energy utilization and the environmental impact during all stages of the system life cycle.

The work of Bösch et al. [22] details the basis for the implementation of the Cumulative Exergy Demand method (CExD); the indicator CExD is introduced to report total exergy removal from nature to obtain a product, summing up the exergy of all resources required. CExD assesses the quality of energy demand and includes the exergy of energy carriers in addition to non-energetic materials. The exergy concept was applied to the resources contained in the Eco-invent database, considering chemical, kinetic, hydro-potential, nuclear, solar-radiative and thermal exergies. The impact category indicator is grouped into eight resource categories, namely: fossil, nuclear, hydropower, biomass, other renewables, water, minerals, and metals. Therefore, the indicator Cumulative Exergy Demand accounts for the exergy of resources that are removed from nature and thus are not accessible anymore for future exploitation. In comparison to other indicators, the study of Bösch et al. demonstrated that CExD provides a more differentiated and complete picture corresponding categories of Cumulative Exergy Demand (CED), and resource depletion categories in CML'01 and EI'99. Their study has the objective of presenting exergy scores for a large number of materials and processes and to compare the exergy scores with resource use and resource depletion scores from typical Life Cycle Assessment methods. The study illustrates that the exergy concept can be operationalized in product LCA. CxED is a suitable indicator to evaluate energy and resource demand, and more comprehensive indicator than the widely used Cumulative Energy Demand (CED). Where, CExD is a more comprehensive indicator than the widely used CED as a result of the consideration of the quality of energy and the integration of non-energetic resources. All of the eight CExD categories proposed are significant contributors to Cumulative Exergy Demand in at least one of the product groups analyzed. In product or service assessments and comparative claims, a careful and conscious selection of the appropriate CExD-categories is required based on the energy and resource quality demand concept to be expressed by CExD.

Over the above, energy storage is a critical factor in the advancement of solar power systems for the sustained generation of electricity. In addition, the

incorporation of thermal energy storage (TES) into the operation of concentrated solar power plants offers the potential of delivering electricity without fossil-fuel backup even during peak demand, independent of weather conditions and daylight. Furthermore, thermocline thermal energy storage systems have the potential of providing extended storage capability at reduced cost, when compared to 2-tank systems; as a consequence, thermocline technology has been receiving increased worldwide attention. However, large-scale utilization of the thermocline storage system is still hindered by several technical problems, among them time-dependence of temperature delivery and sizing requirements. The present study contributes to this specific area: modeling and analysis for a thermocline energy storage system is conducted aiming at a better understanding of the dynamic temperature response. The thermocline tank, as compared to other thermal storage systems such as the 2-tank technology, may decrease the construction cost on average reduces the materials and components (such as heat exchangers, pumps and etc.); in this context, for large single-tank, installations the cost reduction can be as high as 33% [59]. Despite this potential, some areas of the design and performance of thermocline systems still require further attention for future incorporation in commercial CSP plants.

Tesfay and Venkatesan [60] studied a one-dimensional model using Schumann equations and constant thermo-physical properties for the heat transfer fluid (HTF) and no heat loss to the environment. The study of Bayon and Rojas [61] presented a single phase one-dimensional model to conduct a parametric analysis, in which the relative importance of some design parameters. The study considers that the HTF and the filler bed at the same temperature for which only one governing equation is needed to solve. By contrast, a detailed two-temperature, two-dimensional model was presented by Yang and Garimella [62,63]; they studied the discharge process of the thermocline system with molten salt and filler material and the effect of non-adiabatic boundaries on the thermal performance of thermocline tanks. Flueckiger *et al.* [64] carried out a comprehensive thermo-mechanical analysis of the

tank walls, where they studied the thermal ratcheting phenomenon involving the tank walls, which is caused by temperature variations and the settling of the filler particles. Xu *et al.* [65] studied the heat transfer and fluid dynamics in the thermocline storage system using a two-dimensional and two-phase model. Particular emphasis was given to the influence of the interstitial heat transfer rate and the filler thermal conductivity, and it was concluded that a uniform cross-sectional temperature could be achieved with two insulation layers, and the thermocline region can cover more than one-third of the tank height at maximum thickness for a tank height of 14 meters. The same authors also published in [66,67] results concerning the effects of the fluid inlet velocity, inlet temperature, porosity, tank height and solid particle properties on the thermal performance of TES.

1.3 Objectives and Methodology Overview

The present study addresses the potential of concentrating solar power (CSP) plants with parabolic trough technology of becoming a viable alternative energy producing system. To this purpose, exergetic, energetic, environmental and economic performance analyses were carried out. The investigation is concentrated on a 50 MW parabolic trough-CSP plant and it takes into consideration the Libyan territory; the Tripoli region is selected as the specific location of the CSP plant based on its high solar irradiation, consumer proximity and density, and condenser cooling water availability. In the region prevails a large-scale Mediterranean climate, where the average annual levels of irradiation are very favorable to commercial solar applications [11]. The analysis encompasses two modeling components: the first one addresses the power cycle, which is a reheating Rankine cycle, while the second one aims the solar field, which consists of mirror receivers and tube absorbers. The thermodynamic characterization of the power cycle was conducted and the thermodynamic properties (P, T, v, x, h, s) are determined for the operating state points of the system. The flow through the components associated with the power cycle (boiler, turbine, condenser and pump) was assumed at steady-state, steady-

flow conditions. A computer model was developed for the analysis of the selected plant and it is based on algebraic equations describing the power cycle and the solar field; the system of equations of the model is solved using the Engineering Equation Solver (EES) software [68]. The model is designed to define the properties at each state point of the cycle and then, sequentially, to determine energy, efficiency and irreversibility for each power cycle component. The solar field model is based on the simplified methodology proposed by Forristall [69], where the heat transfer model for the heat collection is one dimensional and steady-state and it uses a thermal resistance analysis. The main goal of this model is the determination of the temperature of the heat transfer fluid (HTF) leaving the solar field. Consequently, the thermal performance and energy gained by the HTF can be calculated under different meteorological conditions, in addition to different configurations and HTFs, where the geometry and thermal properties, respectively, are predefined. Consequently, the developed model has the potential of becoming a useful tool for the preliminary design of CSPs and, in particular, for the configuration of the solar field using existing commercial plants. Moreover, it has the ability of analyzing the energetic, economic and environmental feasibility of using CSPs in different regions of the world, which was illustrated by analyzing Libyan region in the present study.

In addition, the overall energy scenario for the selected plant in terms of behavior and performance of its components is completed through an hourly analysis on an annual basis for different sites in Libya. This analysis allows the comparison of different systems and, eventually, a particular selection, and it includes both the economic and energetic facets, which are simulated within a “greenius” software [70]; the climate database is collected using the Meteonorm7 software [71]. The analysis also looks at the impact of project financing and incentives on the cost of energy. The cost reduction potential of eventual enhancements can also be evaluated within this analysis. Cost reduction is a crucial requirement for electricity generation from concentrating solar power plants to be cost competitive compared to that of fossil-fired plants. In this study, as the primary metric of the financial performance to

expresses the selling price of the energy, is used the levelized cost of electricity (LCE). In addition, it makes a sound case, based on the current cost of energy, for the potential for reducing the cost of energy from parabolic trough-CSP plant. An interesting, and to a great extent surprising, finding is higher values for performance and potentially lower LCE for Tripoli (Libya) as compared to Andalucia (Spain). Libya, in technological terms, has the potential of becoming attractive for establishing CSPs in its territory and, in this way, to facilitate the realization of several European initiatives that aim to import electricity generated by renewable sources from North African and Middle East countries.

Furthermore, the present study employs the state-of-the-art in what concerns exergetic analysis combined with Life Cycle Assessment (LCA) for CSP plants. The integrated analysis is used to evaluate the studied power plant. LCA was used to assess the environmental impacts of this particular type of CSP along its life cycle, taking into consideration the contribution of each life cycle stage to the total environmental load. LCA can enable the identification of environmental hotspots and can provide opportunities of process improvement as well as optimization of either the product or a specific stage of its life cycle stage. The Exergetic Life Cycle Assessment (ELCA) examines the flows of exergy within a system with the purpose of the reduction of exergy destruction and consequent improvement of efficiency. ELCA integrates exergetic considerations into the LCA framework and its advantage with respect to LCA is similar to that of the cumulative exergy content method with respect to energy analysis; considering exergy instead of energy allows a thermodynamically correct assessment of both the resource base and its final use. The thermodynamic economic analysis is conducted using the exergo-economic indicator in order to evaluate the level of the cost of each component of the plant caused by the exergetic destruction in each component and in the overall system. The research is concentrated on a 50 MW parabolic trough-CSP plant; and the data for the LCA was provided for a specific location with high solar irradiation, such as, as mentioned before, a particular region in Libyan territory. The analysis is designed to

support the decision making process of future CSP plants designs and their construction. In the SimaPro Software, CExD is directly taken from Eco-invent database. Exergy is used as a measure of the potential loss of "useful" energy resources; therefore, the methodology to be used in the present context will encompass the following steps: Development of LCA using Eco-indicator 99; performing ELCA using the Cumulative Exergy Demand indicator; and conducting a thermoeconomic analysis using the specific exergy costing (SPECO) approach. The data for the LCA was provided for a specific location with high solar irradiation, such as, for instance, a region in Libyan territory. Therefore, as already stated, the study intends to be a supporting tool to the decision process of future designs of CSPs, in particular, for the environmental and economic aspects.

Furthermore, the present study investigates, identifies and develops a numerical model for the thermal storage system that can simulate its behavior, and it has the potential of enabling enhancement of effectiveness, and economics and operational characteristics of solar parabolic trough electric systems. Moreover, the study places particular emphasis on the thermocline storage tank, taking into consideration that thermal energy storage allows CSPs to deliver electricity without fossil-fuel backup as well as to meet peak demand, independent on solar collection and fossil fuel backup. In addition, thermocline systems have the potential to provide storage capability at reduced cost, when compared to two-tank systems. Comprehensive transient, charging stage was simulated and analyzed with particular emphasis on heat transfer and fluid dynamics within the thermocline thermal storage technology. The numerical investigation carried out follows largely [61], the thermocline thickness and effectiveness are examined as a function of the thermocline motion, effective thermal diffusivity and height of the tank. The model was validated with the experimental data presented in the study of Zurigat et al. [72]. The numerical model based on the resulting system of equations is solved by using time-implicit and space-backward finite differences and it was encoded within the Matlab environment. The aim of this component of the model is to describe the thermocline tank behavior by means of a

result which accurately provides outlet temperature with time and can be implemented in any kind of code used for simulating the annual performance of a CSP power plant. The analyses of the thermal storage system led to the following findings: the predictions agree well with the experiments in what concerns the time evolution of thermocline region, particularly for the regions away from the top-inlet. The deviations observed in the near-region of the inlet are most likely due to the high-level of turbulence in this region due to the localized level of mixing; a simple analytical model to take into consideration this increased, turbulence level was developed and it leads to some improvement in the predictions.

1.4 Motivation

The PhD project aims to address the potential of CSPs of becoming a viable technology alternative for clean energy production in Libya, in line with the feasibility studies of supplying Europe with electricity produced by renewable energy plants but also with particular emphasis on concentrated solar power plants along the shores of the Mediterranean. Undoubtedly, the eventual sales of the CSP generated electricity to Europe will be a prime motivation to start these CSP projects, despite the large investment required. The projects will not only benefit European energy consumers, but also they will bring many socioeconomic benefits to Libya and its people. This collaboration has the potential of having far reaching effects; in particular it may bring renewed stability and prosperity not only to the regions involved in the project, but also to those in their neighborhood. Above all, this collaboration of equals embracing different continents and cultures may be an example how to establish peace through the elimination of social differences leading shared wealth and education opportunities. Energy projects similar to the one proposed in the present work have enormous potential in terms of socio-economic development, as it is anticipated that, at least, half of the project construction costs will be spent locally. In addition, the project will benefit Libya by creating a wide range of jobs, many of them requiring highly qualified personnel that, hopefully, the Libyan educational system will be able

to graduate. Research institutes and higher education institutions will have further motivation for conducting research and development toward practical applications of associated technologies. Essentially, the study aims to find out to what extent CSP plants can help to minimize environmental impacts through the reduction fossil fuels dependence; moreover, in the medium to the long term, it will be advantageous to have implemented the integration of CSP plants with sea water desalination systems, which will be capable of solving the problem of water scarcity in Libya.

1.5 Thesis Outline

The thesis is organized in seven chapters; Chapter one presents the problem definition, literature review, and objectives and motivation of the study. Chapter two aims to offer an introductory succinct description of solar energy and concentrated solar power technologies. Chapter three covers the modeling and analysis of the power plant under consideration. The overall energy scenario for the CSP in terms of behavior and performance of its components is completed through an hourly analysis on an annual basis in Chapter four. Chapter five addresses an exergetic, environmental and economic assessment, in terms of exergy of the entire life cycle of the plant. Chapter six investigates, identifies and develops a numerical model for the thermal storage system that can simulate its behavior. Comprehensive transient, charging stage was simulated and analyzed with particular emphasis on heat transfer and fluid dynamics within the thermocline thermal storage system. Last, Chapter seven contains the overall summary of the work and presents recommendations for future research.

Chapter 2

Concentrated Solar Power Systems

2.1 Solar Insolation

Solar energy is in the form of electromagnetic radiation with the wavelength spectrum from about 0.1µm to over 3µm [73]; most of this energy is concentrated in the visible and the near infrared wavelength range. The incident solar radiation (insolation), known as irradiance is given in units of power per square meter (W/m^2). The average amount of solar radiation falling on a surface normal to the rays of the Sun outside the atmosphere of the Earth is called the solar constant. This so-called solar constant, in fact, may take values between 1353 and 1370 W/m^2 depending on the geographical and climatic conditions [74]. Figure 2.1 shows the annual orbit of the Earth around the Sun. The distance between the Earth and the Sun changes over the year; the minimum is 1.471E+11 m on 21st of December (Winter solstice) and the maximum 1.521E+11 m on 21st of June (Summer solstice). The year-round average Earth-Sun distance is 1.496E+11 m. The amount of solar radiation intercepted by the Earth, consequently, varies during the year, the minimum being on 21st of December and the maximum on 21st of June [73]. The axis of the

Earth's daily rotation around itself is at an angle of 23.45° to the axis of its elliptical around the Sun. This tilt is the main reason of the seasonal variation of the solar radiation available at any location on the Earth. The angle between the Earth-Sun line and the plane through the equator is called the solar declination, which varies between - 23.45° on 21st of December to +23.45° on 21st of June [73].

The knowledge of the amount and quality of solar energy available at a particular location is very important for the design of any solar system. Although the insolation is relatively constant outside the Earth's atmosphere, local climate can cause wide variations in available insolation on the surface of the Earth from one location to another. In addition, the Sun's motion with respect to the Earth allows surfaces with different geographical coordinates to intercept different quantities of solar energy.

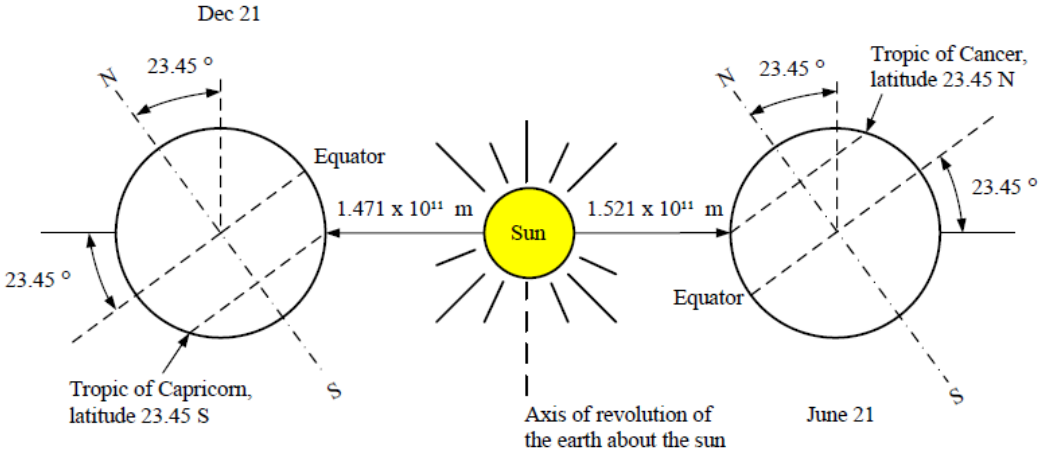

Figure 2.1: Motion of the Earth around the Sun [75].

Outside the fringes of the Earth's atmosphere, the Sun's energy is continuously available at the rate of 1.35 kW/m^2 [73]. As a result of the Earth's rotation, its asymmetric orbit around the Sun, and the contents of its atmosphere, a great fraction of this energy does not reach the Earth. Figure 2.2 illustrates the regions of high irradiation where solar energy conversion systems have the potential of producing the maximum amount of energy.

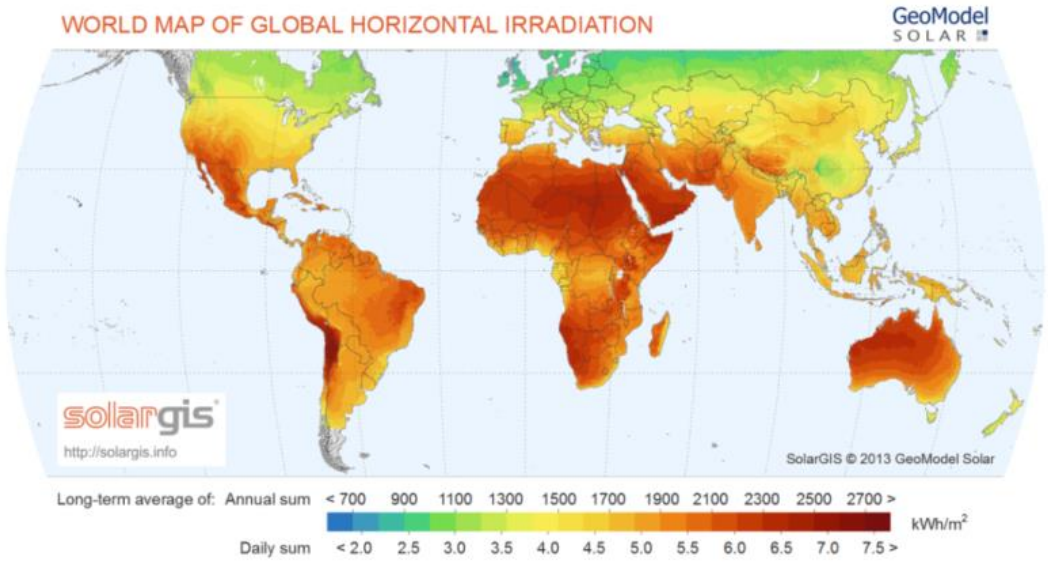

Figure 2.2: Areas of the world with high insolation [76].

Obviously, solar energy is available over the entire Earth, and, in theory, with appropriate sizing of the solar thermal energy system it will be possible to use in regions with average value of irradiation ~1200 kWh/m^2; however, in practice, this would not make any economic sense. Similar to any other energy-producing projects, those are solar based require for the selection of the location clear and detailed information and identification of the quantity, quality and timing of the solar energy available. Figure 2.3 illustrates the variation of insolation over a full day in middle of July at Tripoli. The red curve represents the global horizontal irradiation, i.e. the energy coming directly from the Sun and falling on a square meter of surface area, which is normal to the irradiation; the peak rate of incident solar energy occurs around noon with a value of 950 W/m^2. The green curve represents the rate of direct normal irradiation (DNI).

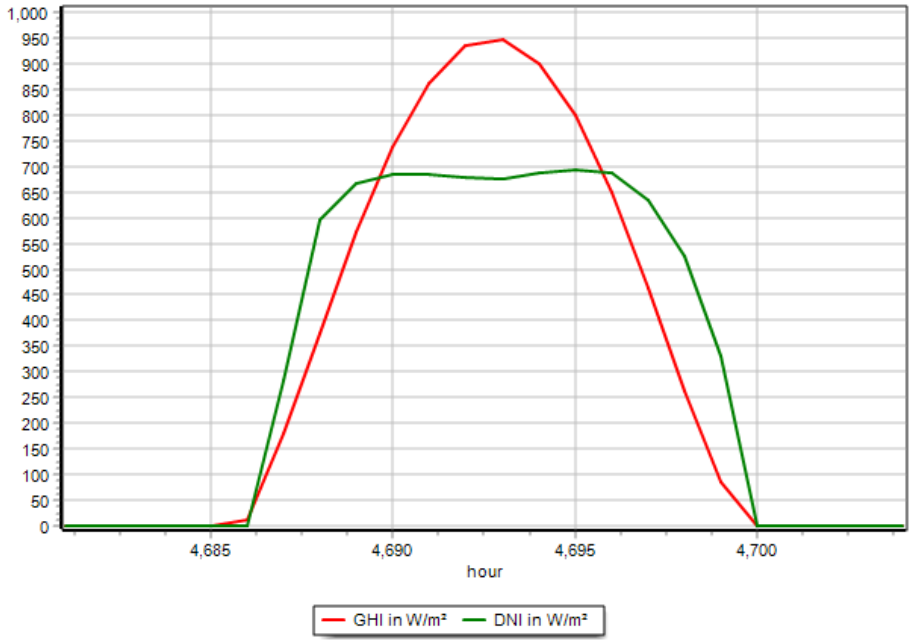

Figure 2.3: Insolation data for Tripoli in the middle of July obtained with greenius [70].

2.2 Solar Energy Generation

Solar technologies are typically characterized as active or passive solar depending on the way of capturing, converting and distributing solar energy. Active solar energy uses mechanical equipment in the collection, storage, and distribution of solar energy. The term “passive” refers to the harnessing of the energy coming from the Sun, usually in the form of heating, without the use of mechanical equipment; a particular example is the use of the envelope of buildings and their orientation to have heat gains of solar origin. There are many different types of solar energy systems which can be used to convert the solar irradiation into energy. Figure 2.4 shows schematically the basic solar system types. The solar energy can be captured and converted into heat, which is then supplied to a demand for thermal energy (thermal load) such as house heating, hot water heating or heat for industrial processes. This type of system may or may not include thermal storage, and usually includes an auxiliary source of energy so that the demand can be met during longer periods with no sunshine.

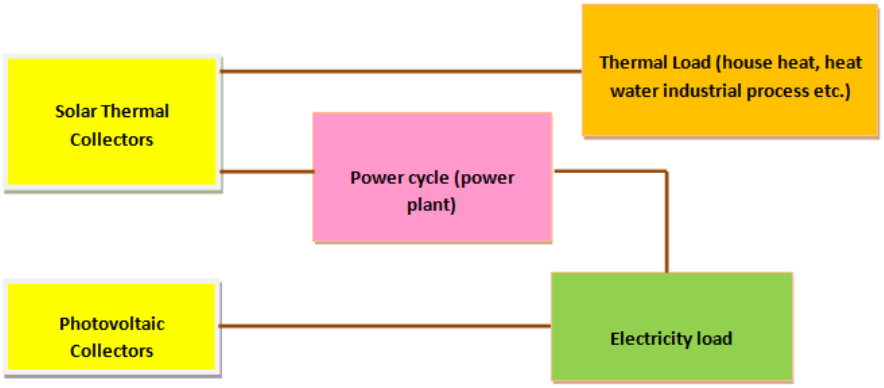

Figure 2.4: Diagram of basic solar energy conversion systems.

In addition, in case there is power (electricity) demand rather than heat, the solar energy can be used in the boiler of a power plant, or in a photovoltaic system with direct conversion of solar energy into electricity. Solar collectors concentrate sunlight with the purpose of heating a heat transfer fluid (HTF); when the aim is to generate electricity through a power plant, the HTF is raised to high temperatures. The HTF is circulated in the boiler (steam generator) to generate steam, which is expanded through the steam turbine that drives the electric generator to produce electricity.

Fossil-fuel energy-producing systems have led to a better quality of life and enhanced development; however, they are also the origin of many challenging problems. Foremost among them are those related to harmful impacts on the environment with an eventual contribution to global warming and climate change. In addition, the fossil-fuel resources are finite; therefore, there is an urgency to replace these energy sources for others that allow for sustainable development. It is recognized that renewable energy resources, at present, due technological and economic reasons, cannot replace fossil fuels; however, over the years that will be the goal. Therefore, renewable energy resources such as wind energy, hydro, photovoltaic conversion, biomass, tidal, geothermal energy and solar thermal power plants should increasingly contribute to the world's present energy demand and supply scenarios. In fact the European Commission produced the so-called climate

and energy package in the form of binding legislation aiming that demanding climate and energy targets for 2020 by achieved by the European Union (EU). These targets, known as the "20-20-20" targets, may be summarized as three main objectives for 2020: 1) 20% reduction in EU greenhouse gas emissions taking as a base 1990 levels; 2) 20% of the EU energy consumption is produced from renewable resources; and 3) 20% improvement of the current EU's energy efficiency. These targets may be too ambitious; however, they clearly indicate the urgent need for action in finding solutions and implementing them.

Among the renewable energy sources, solar power generation undoubtedly offers the most promising and viable option for the production of power [77]. Figure 2.5 presents the already-demonstrated and most promising solar power generation technologies.

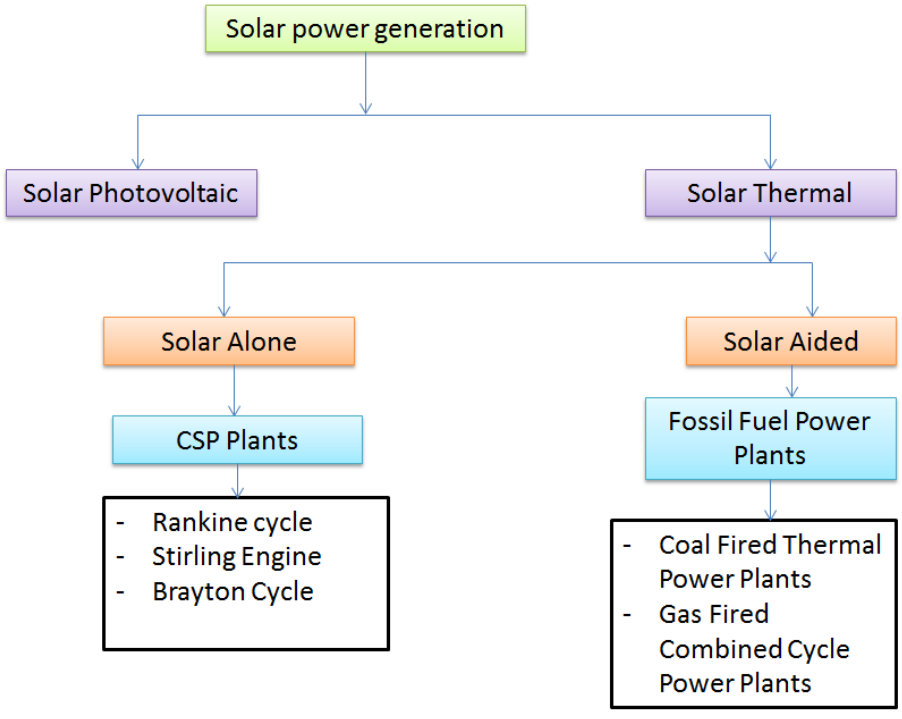

Figure 2.5: Diagram of solar power generation methods [77].

2.3 Concentrated Solar Power Technologies

Solar thermal power plants are becoming one of the most promising technologies to produce clean and sustainable energy. Consequently, the use of solar thermal energy in the future is expected to increase [5]. CSP power plants can expand the time of power production using thermal energy storage, which is normally charged at the peak of solar energy for the duration of the day-time while the stored heat is released during the night or when there is not enough solar radiation. The CSP operating principle is rather straightforward: CSP devices concentrate energy from the radiation of the Sun onto receivers; this concentrated energy is transferred to boilers, where the steam is produced. This steam expands through steam turbines or other types of engines, such as reciprocating steam engines, resulting into mechanical energy, which is converted through the electric generators into electricity. The main objective of the CPS technologies is to attain the highest temperature possible of the working fluid using, for instance, mirrors to concentrate the solar irradiation. This temperature, to a great extent, dictates the efficiency of the CSP plant. There are about seven primary applications of CSP generated exhaust heat, namely [78]:

i. **Heating water**: Water can be heated for many different purposes in domestic and public institutions, which is arguably one of the most important applications.

ii. **Industrial processes**: Hot water can be used to clean industrial equipment and machinery. Some sectors, including beverage bottling plants for example, require very large quantities of hot water for both production and maintenance.

iii. **Food refrigeration**: Absorption chilling can be used for food refrigeration (which will be maintained at a temperature of about 4 -7°C).

iv. **Agriculture**: Greenhouse plants and crops can benefit from heat at night and cooling during the day to maintain a set temperature over the year.

v. **Accelerating biogas production**: Biogas processing increases at higher temperatures; heat can be used to speed up the process of the digestion tank turning waste into fuel. This is significant because the biogas can quickly become its own source of renewable electricity or heat, or be further processed to provide a source of renewable fuel.

vi. **Space heating or cooling**: The free heat energy can also be used for space heating in homes, factories, dormitories, hospitals, etc. Conversely, with the use of absorption chillers, the same heat can provide cooling.

vii. **Generate even more electricity**: If only electricity is required and there is no use for the thermal energy for heating or cooling, then the Rankine cycle steam turbine (which can use lower temperature heat to generate power) can be used to increase the power output of the overall solar application.

In general, a priority is to maximize the investment. While a combined heat and power (CHP) solution may not meet the specific requirements of every site and region, however, there are many locations that could truly benefit from this combination, providing eventually CHP at lower price. CSP technologies cover a large array of different options, of which, the most common are: parabolic trough, central receivers, dish and linear Fresnel. The parabolic trough is the one with a wider usage and which is considered in this study. However, central receiver technology is becoming increasingly important, particularly in the US and Spain. Dish technology has the advantages of having low requirement in what concerns water consumption for surface cleaning, but the technology still has very high capital costs. Table 2.1 summarizes a comparison of these types; the comparison was prepared by the International Renewable Energy Agency (IRENA) [79]. These CSP technologies differ significantly from one to another, not only in what concerns technical and economic aspects, but also in relation to their reliability, maturity and operational experience at utility scale.

Table 2-1: Comparison of different CSP technologies [79].

	Parabolic Trough	Solar Tower	Linear Fresnel	Dish-Stirling
Typical capacity (MW)	10-300	10-200	10-200	0.01-0.025
Maturity of technology	Commercially proven	Pilot commercial Projects	Pilot projects	Demonstration projects
Technology development risk	Low	Medium	Medium	Medium
Operating temperature (°C)	350-550	250-565	390	550-750
Plant peak efficiency (%)	14-20	23-35	18	30
Annual solar-to-electricity efficiency (net) (%)	11-16	7-20	13	12-25
Annual capacity factor (%)	25-28 (no TES) 29-43 (7h TES)	55 (10h TES)	22-24	25-28
Collector concentration	70-80 suns	>1 000 suns	>60 suns (depends on secondary reflector)	>1 300 suns
Receiver/absorber	Absorber attached to collector, moves with collector, complex design	External surface or cavity receiver, fixed	Fixed absorber, no evacuation secondary reflector	Absorber attached to collector, moves with collector
Storage system	Indirect two-tank molten salt at 380°C (dT=100°C) or Direct two-tank molten salt at 550°C (dT=300°C)	Direct two-tank molten salt at 550°C (dT=300°C)	Short-term pressurized steam storage (<10 min)	No storage for Stirling dish, chemical storage under development
Hybridization	Yes and direct	Yes	Yes, direct (steam boiler)	Not planned
Grid stability	Medium to high (TES or hybridization)	High (large TES)	Medium (back-up firing possible)	Low
Cycle	Superheated Rankine steam cycle	Superheated Rankine steam cycle	Superheated Rankine steam cycle	Stirling
Steam conditions (°C/bar)	(380-540) 100	540 (100-160)	260/50	n.a.
Water requirement (m3/MWh)	3 (wet cooling) 0.3 (dry cooling)	2-3(wet cooling) 0.25(dry cooling)	3 (wet cooling) 0.2 (dry cooling)	0.05-0.1 (mirror washing)
Application type	On-grid	On-grid	On-grid	On-grid/ Off-grid
Suitability for air cooling	Low to good	Good	Low	Best
Storage with molten salt	Commercially available	Commercially available	Possible, but not proven	Possible, but not proven

To allow extended generation of electricity, CSP power plants use thermal energy storage (TES) technology. TES can be achieved by storing energy in different materials, such as, concrete, molten salt or ceramic. Energy storage is a critical factor in the advancement of solar thermal power systems that generate electricity [10]. In addition, the incorporation of thermal energy storage into the operation of CSPs offers the potential to deliver electricity without fossil-fuel backup as well as to meet peak demand, independent of weather conditions. TES systems would be charged during the peak of solar energy during the day-time, and the stored heat would be released where the solar power is not sufficient to operate at the required power. Although,

CSP is not well known as PV; however, it does account for a considerable amount of the existing universal renewable energy production. By 2013, there was about 3.4 GW of installed CSP operational capacity [80], in particular in the USA and Spain; the United States and India added CSP facilities to their grids in 2014. However, CSP activity continued in many countries, with South Africa and Morocco the most active markets in terms of construction and planning [81]. Spain remained the global leader in existing capacity. Most of the current installed capacity uses parabolic trough technology; however, the CSP technologies being installed are diversifying, where the largest CSP plant in operation is power tower technology in Ivanpah (USA) that uses a heliostat field collector. The largest CSP plants in operation are listed in Table 2.2 [80,82].

Table 2-2: Large operating CSP plants.

CSP Plant	Capacity (MW)	Technology	Storage
Ivanpah (USA)	392	Power Tower	
SEGS (Mojave desert, USA and Canada)	354	PTPP	
Mojave Solar project (Barstow, USA and Canada)	280	PTPP	
Solana Generating Station (Gila Bend, USA)	280	PTPP	6 h
Genesis Solar Energy Project (Blythe, USA and Canada)	250	PTPP	
Solaben (Spain)	200	PTPP	
Solnovo (Spain)	150	PTPP	
Andasol (Spain)	150	PTPP	7.5 h
Extresol (Spain)	150	PTPP	7.5 h
Dhursar (Integated solar combined cycle, India)	125	LFR	
Martin Next Generation Solar Energy center (USA)	75	PTPP	
Puerto Errado (Spain)	30	LFR	

2.3.1 Parabolic Trough Systems

Parabolic trough system is presently the most mature solar thermal electric technology. This is mainly due to available large commercial-scale plants - the first one has been operating in the California Mojave Desert since 1984. Large field of

collectors using mirrors, which are shaped as array parabolas to reflect the Sun's rays to the absorbing tube placed at the center of the arc of the trough, are used to supply thermal energy to the HTF. The heat receiving tube – the absorber tube, in general, is made of steel, and it is encapsulated by an evacuated glass tube to reduce the heat loss by convection; the heat receiving tube must be capable of sustaining very high temperatures (~400°C). The absorptivity of the absorbing tube is absolutely critical in the performance of the device. A recently developed coating can achieve an absorption rate of 95% at a temperature of 400°C, and the radiosity, which combines the emission and the reflected portion of the irradiation, represents less than 14% of the irradiation [83]. To increase the irradiation collection, usually, the parabolic troughs are arrayed to track the Sun path.

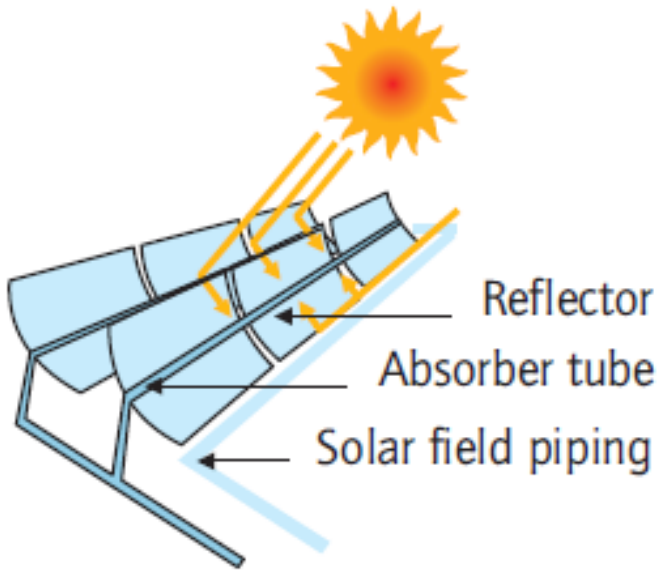

Figure 2.6: Parabolic trough system [84].

The existing parabolic trough power plants in commercial operation rely on synthetic oil as the HTF from collector pipes to boiler heat exchangers, where water is preheated, evaporated and then superheated. Most existing plants, however, have little or no thermal storage and rely on fossil fuels as a backup to guarantee their nominal power output. For instance, all CSP plants in Spain derive 12% to 15% of

their annual electricity generation from burning natural gas [84]. Some newer plants already have significant thermal storage capacities such as the Andasol power plant in Spain.

2.3.2 Power Tower Systems

Solar towers, and also known as central receiver systems, use a large number of small mirrors (Heliostats) to concentrate the Sun's rays on a central receiver that placed atop of the tower. Some commercial tower plants currently in operation use direct steam generation (DSG) in the receiver; some others use molten salts as both the heat transfer fluid and storage medium. This technology achieves very high temperatures up to 800°C, thereby increasing the efficiency at which heat is converted into electricity in the power block and reducing the cost of thermal storage. In addition, the concept is highly flexible; designers can choose from a wide variety of heliostats, receivers, transfer fluids and power blocks. Some plants have several towers that feed one power block. Examples of commercial power tower plants currently in operation are Abengoa's PS10 (11 MWe) and PS20 (20 MWe) steam towers in Spain and eSolar's Sierra Sun Tower (5 MWe) steam towers in California. Other plants under construction include Bright Source Energy's Ivanpah (392 MWe) steam towers in California and Torresol Energy's (SENER and Masdar) Gemasolar (17 MWe) molten-salt tower in Spain.

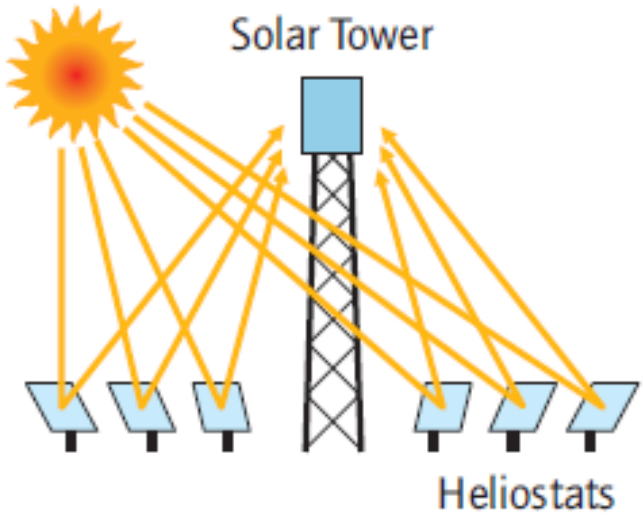

Figure 2.7: Power tower system [84].

2.3.3 Concentrating Dish

Dish technology is used to convert thermal energy to electricity by using a parabolic dish mirror concentrating the solar radiation on the receiver of an engine generator placed on the focal point of the reflector. The engine is usually a Stirling engine; however, the use of a gas turbine instead of the Stirling engine is being studied. The technology is appropriate for decentralized power supply and remote locations. It can achieve high concentration ratio and temperatures of the working fluid up to 1480°C [85]. Figure 2.8 shows a parabolic dish/Stirling solar system; Stirling engines are a leading candidate for dish technologies not only due to their high efficiency but also due to their adequacy to external heating. In addition, the Stirling engine has the advantage of not requiring water for cooling as other CSP technologies do. The drawback of the Stirling dish technology results from its incompatibility with thermal storage. The only form of energy storage that is viable with this technology is electrical storage, which still is expensive.

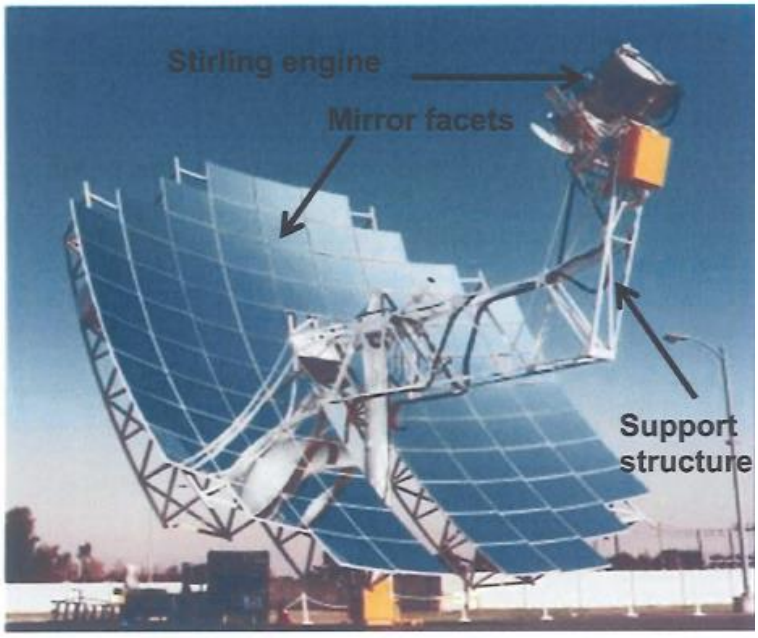

Figure 2.8: Dish / Stirling technology [86].

2.3.4 Linear Fresnel

The Linear Fresnel technology is a line-focusing system of CSP which is based on arrays of Fresnel reflectors which reflect the Sun radiation to the tubular absorber (receiver) to boil the water inside the absorber tubes generating steam. The steam is then used to drive a steam turbine to generate electricity as shown in Figure 2.9.

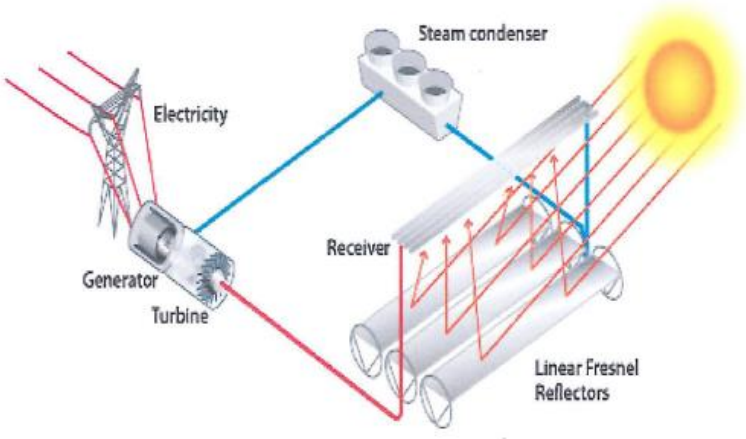

Figure 2.9: The Linear Fresnel power generation system [86].

The main advantage of this system is using water as the HTF, eliminating in this way the need of, in general, hazardous heat transfer fluids and of HTF/water heat exchanging equipment. In fact this system is the least expensive in terms of installed power among CSP systems. However, this technology is very much in its infancy. A considerable shortcoming, so far not resolved, is the relatively low steam temperatures that can be achieved yielding relatively unattractive cycle efficiencies.

Chapter 3

Modeling and Simulation of Parabolic Trough-CSP Plants

3.1 Introduction

In this chapter a performance analysis is conducted for a concentrating solar power (CSP) plant with the parabolic trough technology. The analysis, although it aims a particular type of CSP plant - 50 MW parabolic trough-CSP plant, is sufficiently general to be applied to other configurations where the major differences are associated to the modeling of the heat transfer mechanism as compared to the power tower and linear Fresnel technologies. Moreover, by taking into consideration the Libyan territory for its implementation, the analysis will serve as the first step to evaluate the technical viability of this project. The Tripoli region was selected as the specific location of the CSP plant – the decision was made based on the region's high solar irradiation, consumer proximity and density, and condenser cooling water availability. In the Tripoli region it prevails a large-scale Mediterranean climate, where the average annual levels of irradiation are very favorable to practical applications [11,87,88].

The analysis of the plant under study encompasses two modeling components: the first one addresses the power cycle, which is the reheating Rankine cycle, while the second one aims at the solar field, which essentially consists of mirror receivers

and tube absorbers. The thermodynamic characterization of the power cycle was conducted along with the thermodynamic properties (P, T, v, x, h, s), which are determined for the operating state points of the cycle. The flow through the components associated with the power cycle (boiler, turbine, condenser and pump) is assumed to be steady-state and steady-flow; a computer model was developed for the analysis of the selected plant and it is based on algebraic equations describing the power cycle and the solar field. The resulting system of equations describing the model is solved using the Engineering Equation Solver (EES) software [68]. The computer model is designed to define the properties at each state point of the cycle and then, sequentially, to determine energy, efficiency and irreversibility for each power cycle component. The solar field model is based on the simplified methodology proposed by Forristall [69]; the heat transfer model for the heat collection is one-dimensional and steady-state and it is based on a thermal resistance analysis. The main goal of this model is the determination of the temperature of the heat transfer fluid (HTF) leaving the solar field. The thermal performance and energy gained by the HTF can be calculated under different meteorological conditions, in addition to different configurations and HTFs, where the geometry and thermal properties, respectively, are predefined.

The developed model has the potential of becoming a useful tool for the preliminary design of CSPs and, in particular, for the configuration of the solar field using existing commercial plants. Moreover, it has the ability of analyzing the energetic performance feasibility of using CSPs in different regions of the world, which is being illustrated for a particular region of Libya.

3.2 Power Cycle

In order to generate electricity from the concentrated solar power systems, the thermal energy received at the solar field is required to be converted by an appropriate power cycle; in the present study, the reheat Rankine cycle was selected

as power cycle as depicted in Figure 3.1, due to its proven record and widespread utilization. The cycle includes boiler, steam turbine stages (high and low pressure stages), condenser, and feedwater pump. It is assumed that no subcooling of the working fluid occurs at the condenser outlet, i.e., saturated liquid prevails. The analysis of each component was conducted in terms of energy and mass balances under steady state conditions. The HTF coming from the solar field transfers heat to the working fluid through the boiler [18,89]. The boiler consists of a feedwater preheater, a steam generator and a superheater in series and a reheater in parallel with them. The reheating prevents the steam from condensing during its expansion in the low stages of the turbine, in this way avoiding damage of the turbine blades and, in addition, it increases the overall efficiency of the Rankine cycle [75].

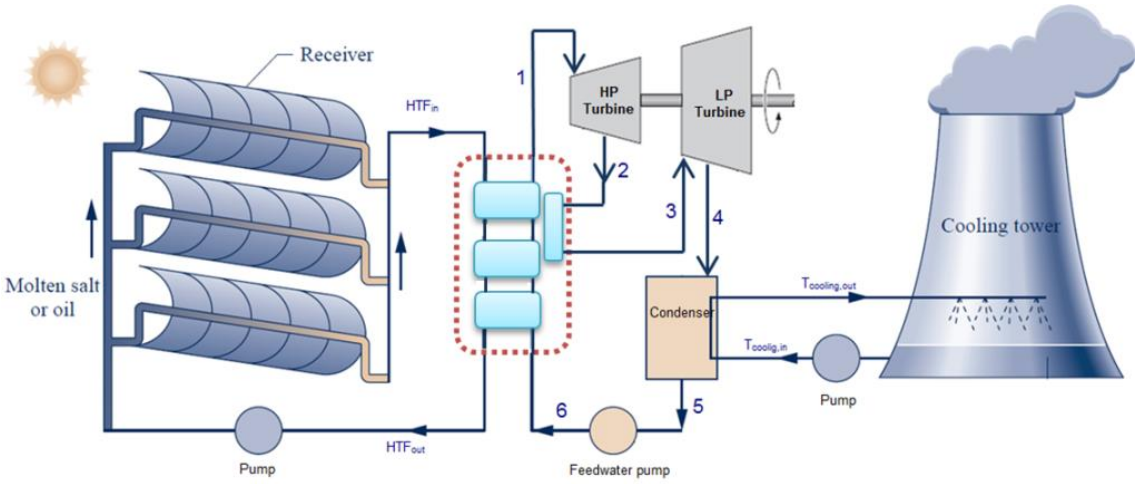

Figure 3.1: Parabolic trough power plant [90].

The HTF is also used to preheat the feedwater and finally to generate dry steam at high pressure and temperature. After the steam passes through the HP-turbine, it re-enters the boiler and is reheated before passing through a LP-turbine. The reheat temperature is approximately equal to the inlet temperature. The expansion of the steam in the turbines converts the thermal energy to mechanical energy. The mechanical power generated with the rotating shaft is converted to electrical power through a power generator.

3.2.1 Modeling of the Power Cycle

The thermodynamic analysis of the power cycle uses the net output thermal capacity as the objective function in the optimization process. As mentioned, the components associated with the cycle were analyzed under the assumption of steady-flow, and actual efficiencies are considered for the pump and turbine. The model is structured to define the properties at each state point of the cycle and then, sequentially, to determine energy, efficiency and irreversibility for each power cycle component. The thermodynamic properties of water and steam are implemented in the EES environment where they are considered in SI units with T in °C, P in kPa, energy units in kJ and specific property values in their customary units on a mass basis. The analysis of the power cycle key components is presented in the following sections.

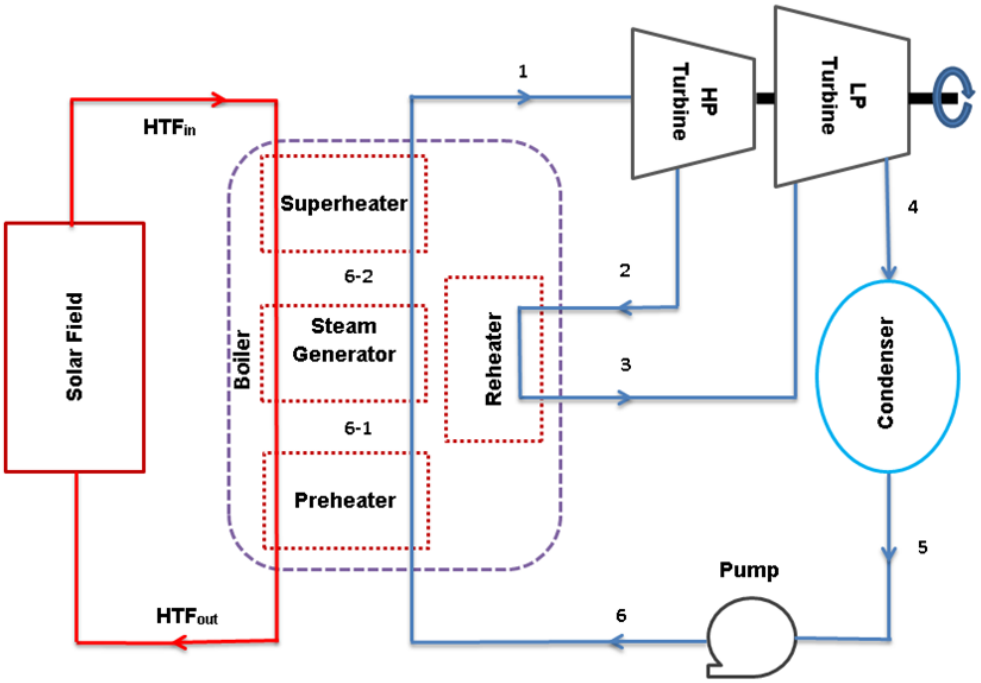

Figure 3.2: Parabolic trough power cycle under study.

3.2.1.1 Train Heat Exchanger (boiler)

The boiler consists of a feedwater preheater, a steam generator and a superheater in series and a reheater in parallel with them. The flow is separated into two parallel heat exchanger elements: the steam train and the reheater. The steam train is a term used to describe the heat exchangers that heat the working fluid, highly pressurized water, from a compressed liquid state into a superheated vapor state.

$$\dot{Q}_{in,boiler} = \dot{m}.(h_1 - h_6) + \dot{m}.(h_3 - h_2) - Loss_{boiler} \quad 3.1$$

$$\eta_I = \frac{\dot{m}(h1-h6)+\dot{m}(h3-h2)}{\dot{Q}_{in,boiler}} \quad 3.2$$

$$\dot{I} = T_0.S_{gen} \quad 3.3$$

$$\dot{I} = [\dot{m}_{HTF}(h_{HTF,in} - h_{HTF,out}) - \dot{m}(h1 - h6) - \dot{m}(h3 - h2)] - T_O[\dot{m}_{HTF}(s_{HTF,in} - s_{HTF,out}) - \dot{m}(s1 - s6) - \dot{m}(s3 - s2)] \quad 3.4$$

$$\eta_{II} = \frac{[\dot{m}(h1-h6)+\dot{m}(h3-h2)]-\dot{m}\dot{T}_0[(s1-s6)+\dot{m}(s3-s2)]}{\dot{m}_{HTF}.(h_{HTF,in}-h_{HTF,out})-T_O.\dot{m}_{HTF}.(s_{HTF,in}-s_{HTF,out})} \quad 3.5$$

Where Q is the amount of heat transfer, ṁ is the working fluid mass flow rate, İ irreversibility and S_{gen} is the entropy generation, which measures the irreversibilities generated during a process. Equations for modeling the boiler, which are used for the calculations of all relevant parameters including temperatures, mass flow rates, and heat transfers of the power cycle working fluid (steam) and HTF, in addition to the effectiveness of each element, are presented below. It is assumed for each heat exchanger that heat transfer losses to the ambient are negligible and there is no heat generation in the heat exchangers. The enthalpy of the HTF is given by [91]:

$$h_{HTF} = 1.498T_{HTF} - 18.34 + 0.001377T_{HTF}^2 \quad 3.6$$

Where the temperature is in °C and the enthalpy is returned in kJ/kg. The amount of heat supplied to the power cycle can be calculated as:

$$\dot{Q}_{in,boiler} = \dot{m}_{HTF}\left(h_{HTF,i} - h_{HTF,o}\right) \quad 3.7$$

The number of transfer units (NTU) and dimensionless capacity ratio (C_r) are defined by the following relations:

$$NTU = \frac{UA}{C_{min}} \quad 3.8$$

$$C_r = C_{min}/C_{max} \quad 3.9$$

Where UA is the overall heat transfer coefficient and C indicates the heat capacity rate.

3.2.1.1.1 Reheater and Superheater

Superheater and reheater both increase the temperature of the saturated steam with the purpose of increasing the thermodynamic efficiency of the cycle [75]. They are shell-and-tube heat exchangers whose main difference is the operating pressure. In the superheater, thermal energy is added to the steam coming from the steam generation to pass it to superheated conditions. While in the reheater, steam coming from the HP turbine is reheated to avoid problems with the steam quality leaving the low pressure turbine and to increase the overall efficiency of the Rankine cycle [75]. The heat transfer effectiveness is dependent on the geometry of the heat exchanger and the flow arrangement [92]; for the counter flow heat exchanger, it related to the number of transfer units (NTU) and capacitance ratio as given by:

$$\varepsilon = Q_{actual}/Q_{max} \quad 3.10$$

$$\varepsilon = \frac{1-e^{[-NTU(1-C_r)]}}{1-C_r e^{[-NTU(1-C_r)]}} \quad 3.11$$

Where Q_{actual} is the actual heat transfer rate between the HTF and the power cycle working fluid, and it can be obtained by performing a simple energy balance. The pressure drop is determined using the following relation:

$$P_{out} = P_{in} - k_{steam}\dot{m}^2 \quad 3.12$$

The pressure drop coefficient k_{steam} was defined by Pantnode [91], as 0.0023 bar-s^2/kg^2 for the superheater and as 0.001 bar-s^2/kg^2 for the reheater.

1. Superheater

The energy balance equation for the superheater is given by:

$$\dot{Q}_{superheater} = \dot{m}(h_1 - h_{6\_2}) \quad 3.13$$

The fluid with the smaller heat capacity rate will reach the larger temperature difference; therefore, the maximum possible heat transfer rate in the superheated is given by:

$$\dot{Q}_{superheater,max} = C_{min}\left(T_{HTF,i} - T_{6\_2,steam}\right) \quad 3.14$$

and,

$$C_{steam} = \dot{m}\ \frac{h_1 - h_{6\_2,steam}}{T_1 - T_{6\_2,steam}} \quad 3.15$$

$$C_{HTF} = \dot{m}_{HTF}\frac{h_{6\_2,HTF} - h_{HTF\_i}}{T_{6\_2,HTF} - T_{HTF\_i}} \quad 3.16$$

Then, once the effectiveness of the heat exchanger is known, the actual rate of heat transfer can be obtained from equation 3.10.

2. Reheater

The equations are similar to those of the superheater, and the balance equation of the reheater is given by:

$$\dot{Q}_{reheater} = \dot{m}(h_3 - h_2) \quad 3.17$$

$$\dot{m}_{HTF,reheater} = \dot{m}\ \frac{h_3 - h_2}{h_{HTF,i} - h_{HTF,o}} \quad 3.18$$

$$C_{steam} = \dot{m}\ \frac{h_3 - h_2}{T_3 - T_2} \quad 3.19$$

$$C_{HTF} = \dot{m}_{HTF,reheater}\frac{h_{HTF,i} - h_{HTF\_o}}{T_{HTF,i} - T_{HTF\_o}} \quad 3.20$$

$$\dot{Q}_{reheater,max} = C_{min}\left(T_{HTF,i} - T_2\right) \quad 3.21$$

3.2.1.1.2 Preheater

The main purpose of the preheater is to bring the entering feedwater to saturated liquid conditions [91]. The heat transfer effectiveness is defined using relations similar to those for the reheater and superheater 3.10 and 3.11.

$$\dot{Q}_{preheater} = \dot{m}(h_{6\_1} - h_6) \quad 3.22$$

$$C_{steam} = \dot{m}\ \frac{h_{6\_1} - h_{6,water}}{T_{6\_1} - T_{6,water}} \quad 3.23$$

$$C_{HTF} = \dot{m}_{HTF}\frac{h_{6\_1,HTF} - h_{HTF\_o}}{T_{6\_1,HTF} - T_{HTF\_o}} \quad 3.24$$

$$\dot{Q}_{preheater,max} = C_{min}\left(T_{HTF,6\_1} - T_{6,water}\right) \quad 3.25$$

3.2.1.1.3 Steam Generator

The steam generator is a heat exchanger in which the feedwater changes phase from liquid to vapor at constant temperature and pressure [92]. The following assumptions are used to conduct the analysis, where the entering feedwater stream is at saturated liquid conditions. The feedwater coming from the preheater absorbs a large amount of heat at constant temperature during the phase-change process. The heat capacity rate of the steam during the phase-change process approaches infinity since the temperature change is zero [92]. Therefore, the minimum heat capacity rate is obtained from the HTF.

$$\dot{Q}_{staem,generator} = \dot{m}(h_{6\_2} - h_{6\_1}) \quad 3.26$$

$$C_{HTF} = \dot{m}\ _{HTF}\frac{h_{HTF,6\_1} - h_{HTF,6\_2}}{T_{HTF,6\_1} - T_{HTF,6\_2}} \quad 3.27$$

$$\dot{Q}_{steamgenerator,max} = C_{HTF}\left(T_{HTF,6\_2} - T_{6\_1,water}\right) \quad 3.28$$

$$\varepsilon = Q_{steam,generator}/Q_{steamgenerator,max} \quad 3.29$$

$$\varepsilon = 1 - e^{-NTU} \quad 3.30$$

$$NTU = \frac{UA}{C_{HTF}} \quad 3.31$$

3.2.1.2 Turbine

The selected Rankine cycle uses a two-stage turbine with high (HP) and low pressure (LP) stages. Reheat is applied between the high pressure stage and the low pressure stage of the turbine. The reheat pressure is selected based on the optimization analysis carried by Habib et al. [93]. The performance of the turbines considered in this study is defined by the isentropic efficiency, which is the ratio of the change in enthalpy of the actual process and that of the isentropic (reversible) process, where $s_{in} = s_{out}$ [94]:

$$\eta_s = \frac{h_{in} - h_{out}}{h_{in} - h_{out,s}} \quad 3.32$$

Where $h_{out,s}$ is the enthalpy at the outlet of the turbine at isentropic process. This ideal enthalpy is evaluated using the outlet pressure and inlet entropy of the fluid. The mathematical model for the turbine stages is given as follows:

3.2.1.2.1 HP-Turbine Stage

$$W_{HPT} = \dot{m}.(h_1 - h_2) - Loss_{HPT} \quad 3.33$$

$$\dot{I} = T_O.\dot{m}.(s_2 - s_1) \quad 3.34$$

$$W_{HPT} = [\dot{m}(h1 - h2) - \dot{m}To(s1 - s2)] - \dot{I} \quad 3.35$$

$$\eta_{II} = \frac{\dot{W}_{HPT}}{\dot{m}[(h1-h2)-To(s2-s1)]} = 1 - \frac{\dot{I}}{\dot{m}[(h1-h2)-To(s2-s1)]} \quad 3.36$$

3.2.1.2.2 LP-Turbine Stage

The governing equations for the low pressure stage of the turbine are given by:

$$W_{LPT} = \dot{m}.(h_3 - h_4) - Loss_{LPT} \quad 3.37$$

$$\dot{I} = T_O.\dot{m}.(s_4 - s_3) \quad 3.38$$

$$\dot{W}_{LPT} = [\dot{m}(h3 - h4) - \dot{m}.To.(s3 - s4)] - \dot{I} \quad 3.39$$

$$\eta_{II} = \frac{\dot{W}_{LPT}}{\dot{m}[(h3-h4)-To(s3-s4)]} = 1 - \frac{\dot{I}}{\dot{m}[(h3-h4)-To(s3-s4)]} \quad 3.40$$

3.2.1.3 Condenser

In the condenser, the heat is transferred from the working fluid (the vapor exhausting from the turbine) to the cooling water flowing in a separate stream. The working fluid condenses and the temperature of the cooling water increases. At steady state, mass and energy rate balances for a control volume enclosing the condensing side of the heat exchanger are:

$$\dot{Q}_{condenser} = \dot{m}(h_4 - h_5) \quad 3.41$$

$$\dot{I} = [\dot{m}.(h_4 - h_4) - T_o.\dot{m}.(s_4 - s_5)] - \left(1 - \frac{T_o}{T_{Cond.}}\right).\dot{Q}_{condensor} \quad 3.42$$

$$\eta_{II} = 1 - \frac{\dot{I}}{\dot{m}.(h_4-h_4)-T_o.\dot{m}.(s_4-s_5)} \quad 3.43$$

Where $Q_{condenser}$ is the rate at which energy is transferred in the form of heat from the working fluid to the circulating cooling water in the condenser. In general, it is assumed that negligible pressure drop occurs across the condenser. Moreover, the assumption of no sub-cooling of the working fluid occurs in the condenser outlet is made, i.e., saturated liquid prevails and the condensate pressure is determined by the coolant temperature. Equations for the condenser modeling are as follows:

$$\dot{m}(h_4 - h_5) = \dot{m}_{cooling} c_w \left(T_{cooling,out} - T_{cooling,out}\right) \quad 3.44$$

$$\dot{Q}_{condenser,max} = \dot{m}_{cooling} c_w \left(T_4 - T_{cooling,in}\right) \quad 3.45$$

$$\varepsilon = Q_{condenser}/Q_{condenser,max} = 1 - e^{-NTU} \quad 3.46$$

$$NTU = \frac{UA}{\dot{m}_{cooling} c_w} \quad 3.47$$

3.2.1.4 Pumps

The pumps in the cycle serve to increase the pressure of the working fluid; and the pump performance is characterized by its isentropic efficiency.

$$\dot{W}_{Pump} = \dot{m}(h_6 - h_5) \quad 3.48$$

$$\dot{I} = [\dot{m}(h_6 - h_5) - \dot{m}To(s_6 - s_5)] + \dot{W}_{Pump} \quad 3.49$$

$$\eta_{II} = \frac{\dot{m}[(h_6 - h_5) - To(s_6 - s_5)]}{\dot{W}_{Pump}} = 1 - \frac{\dot{I}}{\dot{W}_{Pump}} \quad 3.50$$

3.2.1.5 Power Generation and Cycle Efficiency

The thermal efficiency gauges the extent to which the energy input to the working fluid passing through the boiler is converted to mechanical output. Its determination is calculated as follows:

$$\dot{Q}_{out,boiler} = \dot{m}[(h_1 - h_6) + (h_3 - h_2)] \quad 3.51$$

$$\eta_{I,boiler} = \frac{Q_{out,boiler}}{Q_{in,boiler}} \quad 3.52$$

Where $Q_{out,boiler}$ is the rate of heat transfer from the energy source in the working fluid passing through the boiler. The gross power out of the high and low pressure turbines equals the mass flow rate through each turbine section, multiplied by the specific work for that section. The sum of the power out of each turbine section equals the gross power output of the cycle [95]. The working relations, by neglecting changes of potential and kinetic energy, are:

$$\dot{W}_{HPT} = \dot{m}(h_1 - h_2) \quad 3.53$$

$$\dot{W}_{LPT} = \dot{m}(h_3 - h_4) \quad 3.54$$

The total turbine work is found as follows:

$$\dot{W}_{Turbine} = \dot{W}_{HPT} + \dot{W}_{LPT} \quad 3.55$$

The pump work given by:

$$\dot{W}_{pump} = \dot{m}(h_6 - h_5) = {\dot{m}\Delta P}/{\rho_w} \quad 3.56$$

The power output is multiplied by the efficiency of the generator to give the gross electric power output of the cycle [91]. The generator efficiency is dependent on the fraction of the load at which the plant operates as defined by Patnode [91] for the SEGS VI; the generator efficiency correlation with load is given as:

$$\eta_{generation} = 0.9 + 0.258\,Load - 0.3Load^2 + 0.12Load^3 \quad 3.57$$

Where:

$$Load = \frac{\dot{W}_{Turbine}}{\dot{W}_{Ref}} \quad 3.58$$

and,

$\dot{W}_{Ref}$ is assumed in this study to be 50 MW and the work output is calculated as follows:

$$\dot{W}_{net} = \dot{W}_{Turbine} - \dot{W}_{Pump} \quad 3.59$$

The thermal efficiency of the cycle and the gross power output are given by:

$$\eta_{cycle} = \frac{\Sigma\dot{W}_{turbines} - \Sigma\dot{W}_{pumps}}{\dot{Q}_{in,boiler}} \quad 3.60$$

$$\dot{W}_e = \dot{W}_{Turbine} \cdot \eta_{genenration} \quad 3.61$$

$$\eta_{cycle,gross} = \frac{\dot{W}_e}{\dot{Q}_{in,boiler}} \quad 3.62$$

3.3 Heat Transfer Analysis of the Collector

The parabolic trough collector still presents the most mature technology for solar thermal power generation and the one with the widest usage. The principle is simple: the collectors concentrate energy from the radiation of the sun onto receivers, then, this concentrated energy is transferred to the power block. It converts the radiant

energy into useful thermal energy in the heat transfer fluid that circulates through the solar field. The parabolic trough systems use mirrors which are shaped as array parabolas to reflect the sun's rays to the absorbing tube placed at the center of the arc of the trough. The heat receiving tube, in general, is made of steel, and it is encapsulated by an evacuated glass tube to reduce the heat loss by convection; the heat receiving tube must be capable of sustaining very high temperatures (~700 K). The absorptivity of the absorbing tube is absolutely critical in the performance of the device. A recently developed coating can achieve an absorption rate of 95% at a temperature of 700 K. To increase the irradiation collection, usually, the parabolic troughs are arrayed to track the sun path. The solar collector field would be modeled as a component and the temperature of the thermal fluid leaving the solar field will be calculated. The required inputs to the solar field model are:

- The Direct Normal Irradiation (DNI) [W/m²]
- The ambient air temperature [°C]
- The wind speed [m/s].

Solar thermal power plants are best suited to those areas of the world with high levels of solar irradiation. In Libya most areas, which are located along the coastline and in the southern Sahara have these characteristics and they are dominated by a large-scale Mediterranean climate with average annual levels of irradiation of (1600–1800 kWh/m²) [11], which are highly suitable for practical applications. The maximum and minimum annual solar days for the location of Tripoli (Latitude 32.667° N, Longitude 13.15° E) are investigated in this analysis. The database for this location is collected within the Meteonorm7 software [71], and the results are reported further on in this thesis. Figure 3.3 reports the daily global horizontal irradiation and normal direct irradiation; the maximum radiation occurs during July, while the minimum occurs in December. Figure 3.4 reports the daily maximum and minimum temperatures during the year, where the approximate maximum and minimum temperatures are 45ºC and 5ºC, respectively.

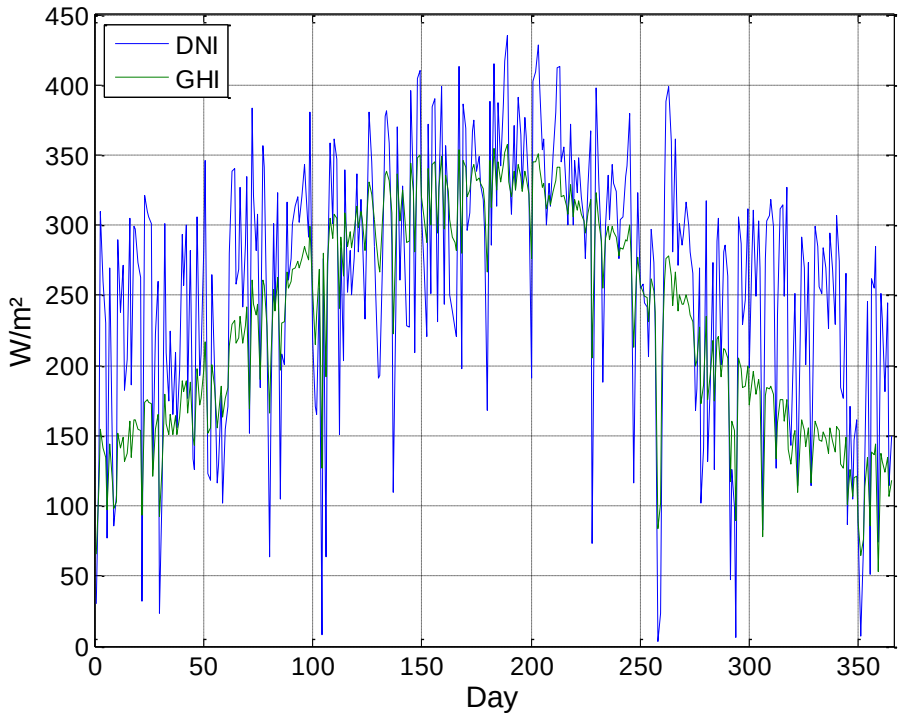

Figure 3.3: Daily global horizontal irradiation (GHI) and direct normal irradiation (DNI) of Tripoli.

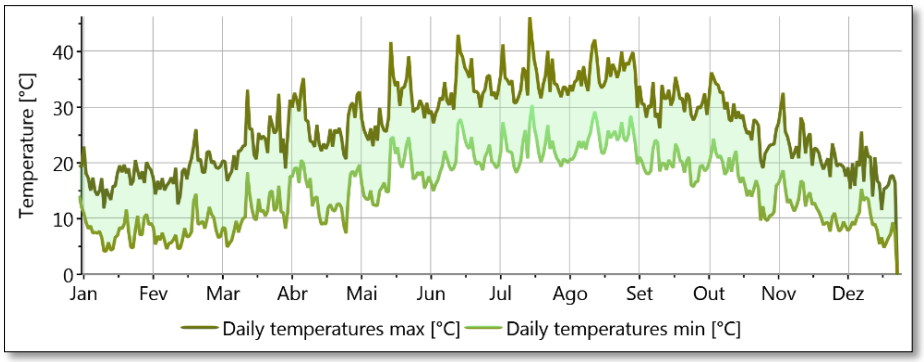

Figure 3.4: Daily maximum and minimum temperatures of Tripoli.

Figures 3.5 and 3.6 illustrate the sunshine duration of each month and daily wind speed, respectively. July is the month with the longest duration of sunshine, which is about 12 hours per day and the average annual wind speed is 3.7 m/s.

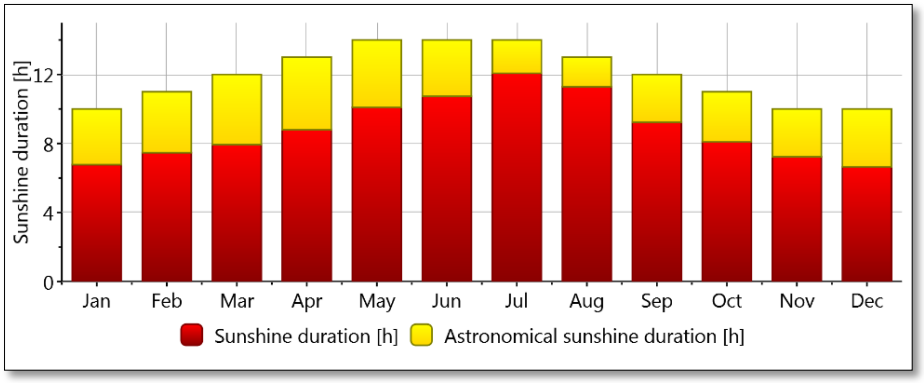

Figure 3.5: Sunshine duration of Tripoli.

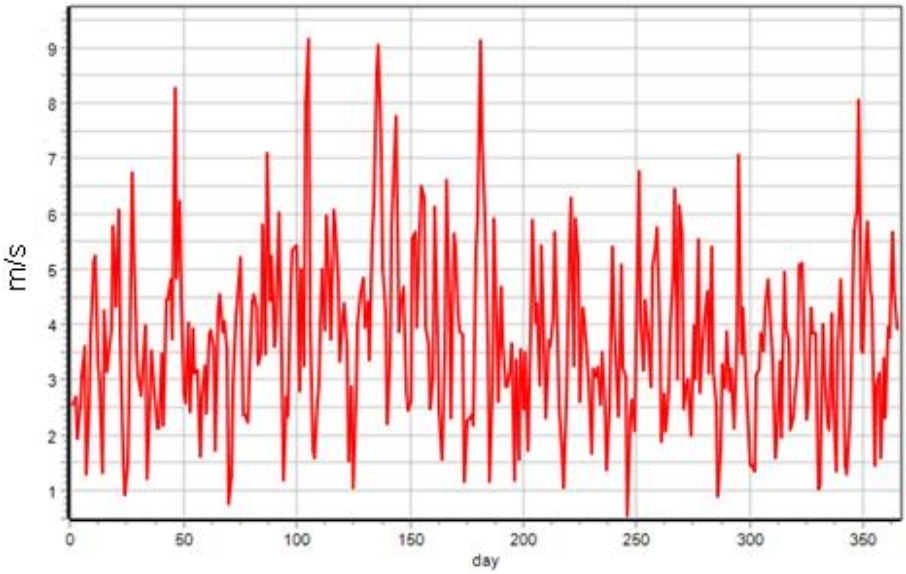

Figure 3.6: Daily average daily wind speed at Tripoli.

The thermal performance and energy gained by the HTF can be calculated under different configurations and meteorological conditions when the geometry and thermal properties are defined. The parabolic systems are typically operated at temperatures up to 400°C and, in this study, the HTF is considered to be the commonly used synthetic oil VP-1. The heat transfer analysis of the collectors is required for the calculation of thermal losses and sizing of the solar field; in addition, it allows determining the level of collector degradation. The heat transfer model for the heat collection element is one-dimensional steady-state and it is based on a thermal

resistance analysis. It is assumed that there is no thermal interaction between the neighboring surfaces (absorber-envelope, and envelope-envelope) for thermal radiation losses. Although these assumptions simplify the analysis, they tend to underestimate the radiation losses at high absorber temperatures [75].

3.3.1 Modeling of the Solar Field

3.3.1.1 Solar Irradiation Absorption

The heat transfer fluid absorbs concentrated solar radiation when passing through the heat collection elements (HCEs), located in the focal line of each parabolic trough. $Q_{absorbed}$ is the concentrated solar radiation absorbed by the collector*;* is defined as the energy from the sun that is actually absorbed by the HTF through the absorber tube. The absorbed radiation $Q_{absorbed}$ is affected by the fraction of the direct normal insolation, adjusted for incidence angle, row shading, solar field availability, collector cleanliness, and the surface properties of the collector field and HCE, and it is given by the following relation:

$$Q_{absorbed} = DNI.IAM.\cos\theta.\eta_{opt}.A_p \quad (3.63)$$

$$\eta_{opt} = \rho_{cl}\gamma\tau_e\alpha_a \quad (3.64)$$

Where τ_e is the envelope transmittance, α_a is the coating absorptance, ρ_{cl} is the clean mirror reflectance and γ is a fraction of the direct solar radiation reflected by mirrors, which does not reach the glass cover. IAM, the incidence angle modifier, is a function of incidence angle and the optical quality of the collector; it is defined by the following relation [96]:

$$IAM = min\left(1, \frac{\cos\theta + 0.000884.\theta - 0.0000537.\theta^2}{\cos\theta}\right) \quad (3.65)$$

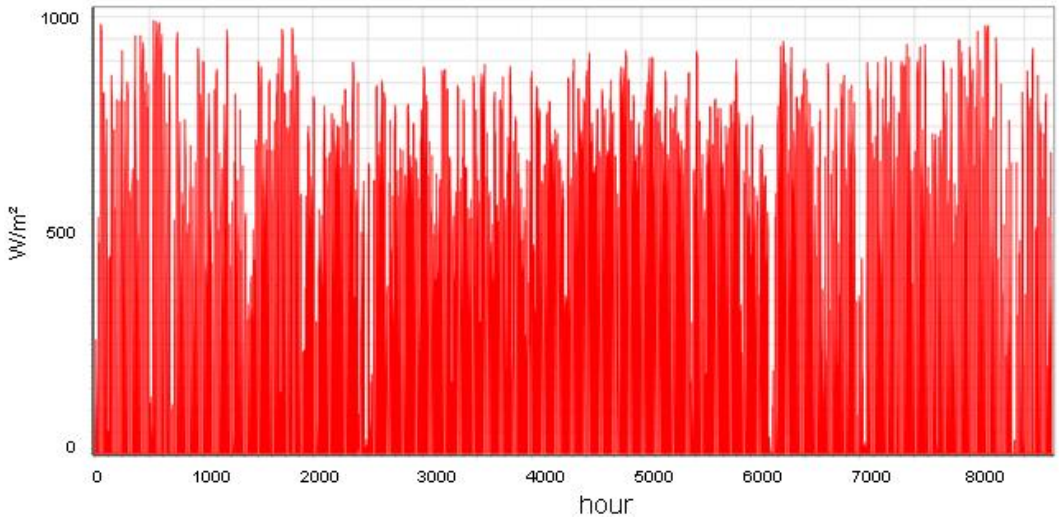

Figure 3.7: Hourly normal Irradiation for the Tripoli region.

Figure 3.8 presents the daily average of IAM for the selected location (Tripoli) over the year.

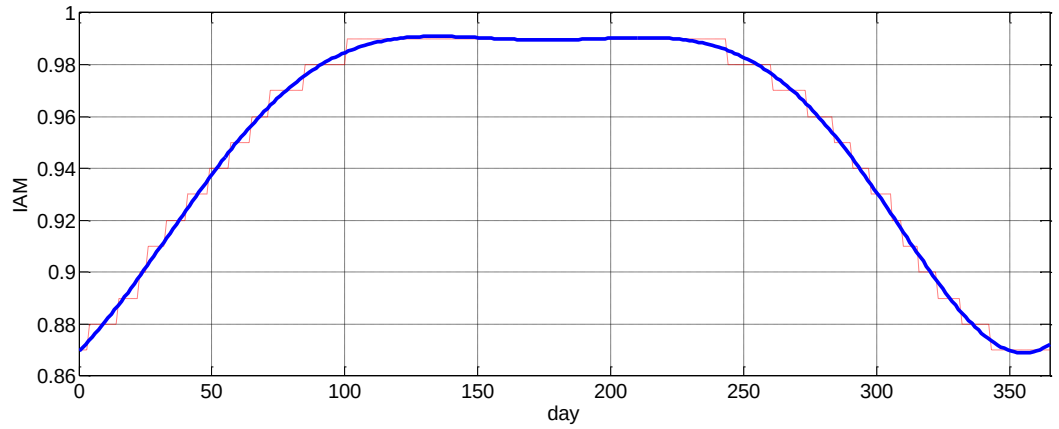

Figure 3.8: Daily incidence angle modifier (IAM) for Tripoli region.

3.3.1.2 Receiver Heat Losses

The solar energy reflected by the mirrors is absorbed by the glass envelope and the absorber surface. Part of this absorbed energy is transferred to the HTF by forced convection while the remaining energy is either transferred back to the glass envelope by radiation and natural convection or lost through the support brackets by conduction. The heat losses coming from the absorber by radiation and natural

convection pass through the glass envelope by conduction and along with the energy absorbed by the glass envelope is lost to the environment by convection and to sky by radiation [69]. The absorbed radiation is considered as a heat flux term in this analysis. Figure 3.9 illustrates the solar field for an operating parabolic trough power plant. The parabolic trough receivers, also known as heat collector elements or HCEs, are linked in series to form “loops” in the solar field. The HTF which leaves the power cycle is directed through large diameter cold header pipes and flows through a loop of collectors, where the HTF is heated by concentrating solar radiation. Finally, the heated thermal fluid flows through a “hot” header pipe which returns it to the power plant.

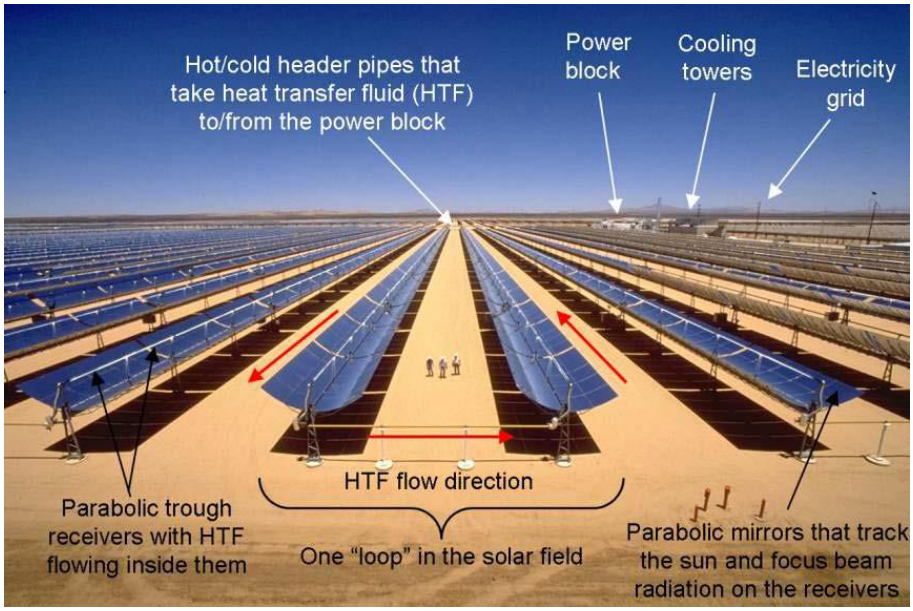

Figure 3.9: Parabolic trough receivers, mirrors, collectors, and “loops” in the solar field of a parabolic trough power plant [97].

The electricity produced by the power plant depends on the mass flow and temperature of the HTF delivered by the solar field; a large mass flow rate of HTF and/or higher temperatures yield higher potential of producing power. Figure 3.10 presents Forristall’s one-dimension HCE model simplified for heat loss in evacuated HCEs. This model involves a collector with a specified aperture. $T_{abs,i}$ and $T_{abs,o}$ are the inner and outer average absorber surface temperatures respectively. $T_{gl,i}$ and $T_{gl,o}$

are the inner and outer average glass surface temperatures respectively, and T_{HTF} is the thermal fluid temperature. T_{sky} is the sky temperature for radiation heat transfer. The diameters $r_{abs,i}$, $r_{abs,o}$, $r_{gl,i}$, and $r_{gl,o}$ are the inner absorber surface, outer absorber surface, inner glass envelope surface, and outer glass envelope surface respectively. The HCE performance model uses an energy balance between the HTF and the atmosphere, and includes all equations and correlations necessary to predict the terms in the energy balance, which depend on the collector type, HCE condition, optical properties, and ambient conditions. For the sake of clarity, the incoming solar energy and optical losses have been omitted from the resistance model shown in Figure 3.11.

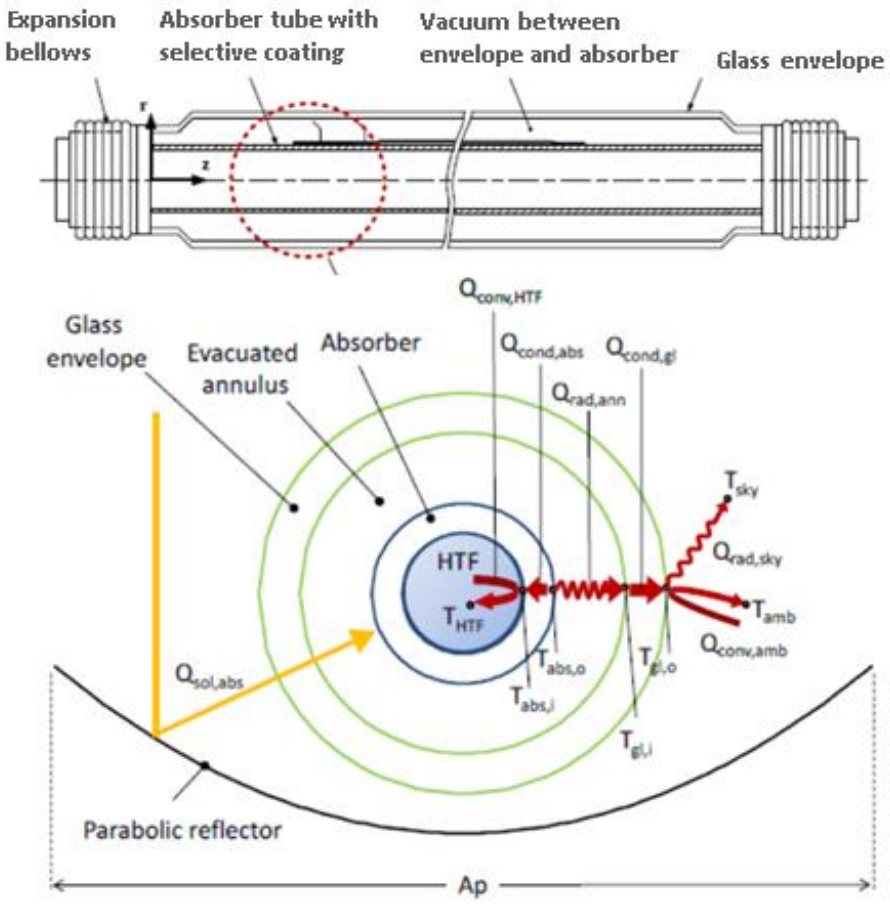

Figure 3.10: Heat collection element HCE and heat transfer analysis [97].

The optical losses are due to imperfections in the collector mirrors, tracking errors, shading, and mirror and HCE cleanliness. The effective incoming solar energy (solar energy minus optical losses) is absorbed by the glass envelope and the absorber selective coating. Some energy that is absorbed into the selective coating is conducted through the absorber and transferred to the HTF by convection; the remaining energy is transmitted back to the glass envelope by convection and radiation and lost through the HCE support bracket through conduction. The energy from the radiation and convection then passes through the glass envelope by conduction and along with the energy absorbed by the glass envelope is lost to the environment by convection and radiation. For the average of the heat loss from the HCE absorber $Q_{rad,ann}$, the calculation commonly takes into account three cases: i) the annulus is nearly evacuated and there is a small amount of air at a pressure 0.00001333 kPa, ii) with time there will be air in the annulus at 100 kPa and finally iii) where the annulus is permeated by hydrogen at 0.1333 kPa.

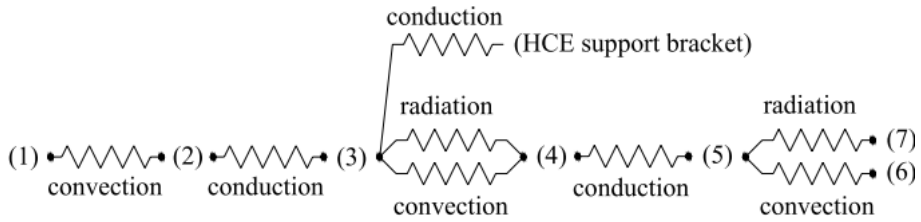

Figure 3.11: Thermal resistance model in a cross-section at the HCE [69].

The simplified calculation is divided into three parts in this study; the first, absorbed energy $Q_{absorbed}$, which was defined in the previous section 3.3.1.1. Next, heat loss through the receivers (Q_{loss}) is calculated based on the convection and radiation between the outermost HCE surface and the ambient surroundings in addition to conductive losses through receiver support brackets. Heat loss is given by

$$Q_{loss} = Q_{conv,amb} + Q_{rad,sky} + Q_{bracket} \qquad 3.66$$

where $Q_{conv,amb}$ is the heat transferred to ambient from the outer glass surface by convection, $Q_{rad,sky}$ is the heat transferred from the outer glass envelope surface to the sky by radiation, $Q_{bracket}$ is the total conductive loss through the receiver support brackets, which amounts to 1% - 4% of the total HCE thermal losses, depending on the ambient conditions and HTF temperature [69]. The energy balance shows that the difference between the absorbed energy and the receiver heat loss is the effective energy gain of the HTF, $Q_{collected}$, which is the useful energy gain to the HTF, namely:

$$Q_{collected} = Q_{absorbed} - Q_{Loss} \quad 3.67$$

Finally, based on the $Q_{collected}$, the outlet enthalpy and temperature can be determined; and the thermal efficiency of the collector and HCE system is calculated using the following relation:

$$\eta_{th,collector} = \frac{Q_{collected}}{DNI.A_p} \quad 3.68$$

As the HTF in the absorber tubes receives heat, its temperature will increase. The increase of temperature creates a temperature difference between the bulk temperature of the fluid and the temperature of the surrounding ambient air. Heat losses from the receiver tube to the glass envelope, as well as from the glass envelope to the ambient air as shown in Figure 3.11, are driven by this temperature difference. This parasitic heat loss can be correlated with the temperature of the heat transfer fluid, as described later on. The radiation heat transfer from the outer surface of the glass envelope to the atmosphere is defined by Incropera et al. [98] as:

$$\mathrm{Q_{rad,sky}} = \sigma.\varepsilon_g.2\pi.r_{gl,o}.\left(T_{gl,o}^4 - T_{Sky}^4\right) \quad 3.69$$

Where $T_{gl,o}$ is the outer glass envelope surface temperature in Kelvin and T_{sky} is the sky temperature in Kelvin. Forristall [69] reports that $Q_{rad,sky}$ is relatively insensitive to the variation of the view factor to the reflector and the temperature of the reflector, and the relation between the sky and ambient temperatures is (T_{sky}=T_{amb}-8, in °C)

[97]; σ is the Stefan-Boltzmann constant it is equal to 5.670 x10^{-8} (W/m².K^4), and ε_g is the emissivity of the glass envelop outer surface. In addition, the convection heat transfer from the outer surface of the glass envelop to the atmosphere is given by Newton's law of cooling:

$$Q_{conv,amb} = h_{amb}.2.\pi.r_{gl,o}.(T_{gl,o} - T_{amb}) \quad 3.70$$

where h_{amb} is the convective heat transfer coefficient to ambient, which is a function of wind speed and is given as:

$$h_{amb} = \frac{k_{th}}{D_{gl,o}}.Nu_{air} \quad 3.71$$

and,

$$Nu_{air} = \left\{0.6 + \frac{0.387Ra_{air}^{1/6}}{\left[1+(0.559/Pr_{air})^{9/16}\right]^{8/27}}\right\}^2 \quad 3.72$$

$$Ra_{air} = \frac{g\beta(T_{gl,o}-T_{amb})}{\alpha_{air}\nu_{air}} \quad 3.73$$

Where $Nu_{,air}$ is the average Nusselt number based on the glass envelope outer diameter, which is presented by Incropera and et al. [98]; k_{th} is the thermal conductance of the air at ($T_{gl,o}$ + T_{amb})/2, while Ra_{air} is the Rayleigh number for air based on the glass envelope outer diameter and α_{air} is the air thermal diffusivity; β is the volumetric thermal expansion coefficient (ideal gas) (1/K), ν_{air} is the kinematic viscosity of air (m²/s) and finally Pr_{air} is the Prandtl number of the air. The collected heat energy can be determined using equations 3.66 and 3.67.

3.4 Results and Discussion

The analysis was carried out for the selected 50 MW_e parabolic trough-CSP plant. The analysis was divided into two parts, the power generation cycle, which a reheating Rankine cycle and the solar field, which includes mirror receivers and tube absorbers.

3.4.1 Power Cycle Analysis

The simulation is carried out at full load and the nominal conditions, which are reported in Table 3.1. The use of reheating aims to reduce the wetness fraction at the last stages of the turbine, as the steam condensation will cause pitting of the turbine blades. The optimum high pressure (10.5 MPa), which is selected based on the optimization analysis of Reddy et al. [18]; while the reheating pressure (2.1 MPa) is selected based on the optimization analysis of Habib et al. (1999). The reheated steam is brought to 663 K before being expanded in the LP turbine to 6 kPa, while the dryness fraction is always higher than 0.88 [18] at the LP-turbine outlet/condenser inlet. The condenser pressure is defined based on the assumption of no sub-cooling of the working fluid occurring at the condenser outlet, i.e., saturated liquid prevails; the temperature of the coolant (in this particular case, sea water) is retrieved from the data concerning the location of Tripoli. The condenser steam-side outlet state is assumed to be saturated liquid (x=0) [91], and pressure is the same as the condenser pressure.

Table 3-1: Nominal parameters considered for the simulation.

Parameter	Amount	Reference
HTF	Synthetic oil (VP-1, Hitec)	[99]
HTF inlet temperature	390°C	[91]
Electric Power	50MWe	
High Pressure	105bar	[18]
Reheat pressure	20% of high pressure	[93]
Isentropic High pressure turbine efficiency	85.5%	[18]
Isentropic Low pressure turbine efficiency	89.5%	[18]
Isentropic Pump Efficiency	78%	[18]
Boiler thermal efficiency	98%	[18]
Condenser Pressure	6 KPa	
$\Delta T_{cooling}$	10°C	

The results obtained are summarized in Table 3.2 and Table 3.3 at the nominal conditions of the study. Table 3.2 reports the property data of the stream state points,

while Tables 3.3 and 3.4 summarize the results obtained through the energetic and exergetic analysis.

Table 3-2: Stream data for the power cycle.

S. ID	Working fluid	Temperature (K)	Pressure (bar)	Enthalpy (kJ/kg)	Entropy (kJ/kg K)
1 (Hp-turbine inlet)	Steam	663	105	3052	6.13
2 (Reheater Inlet)	Steam	488	21	2755	6.23
3 (LP-turbine inlet)	Steam	663	19.4	3226	7.11
4 (Condenser inlet)	Steam	309.3	0.06	2293	7.44
5 (Condenser outlet)	Water	309.3	0.06	151.5	0.52
6 (Boiler inlet)	Water	310.4	114	166.1	0.53

Table 3-3: Energetic and exergetic of the power cycle components.

Components	Energetic input kW	Energetic output kW	Exergetic input kW	Exergetic output kW
Train heat exchanger	137030	134290	66620	55824
HP Turbine	11889	10165	11417	10165
LP Turbine	37330	33411	37474	33411
Condenser	85656	-	-	-
Pump	750	586	750	626

In conclusion, the maximum steam temperature in the power cycle is nearly 643 K. The optimum high pressure is 10.5 MPa, while the reheating pressure is 2.1 MPa; the reheated steam is brought to 663 K before being expanded in the LP turbine to 6 kPa, and the mass working fluid mass flow rate is 40 kg/s; the calculated values for the energetic thermal efficiency of the power cycle is 36% and the gross power output is 48 MW, respectively (Table 3.4). The exergetic losses reach a maximum at the boiler (10796 kW), and the daily averaged amount of energy needed to be delivered to the train exchanger is 3289 MWh. In addition, Table 3.5 presents the UA, NTU and effectiveness for all heat exchangers; the effectiveness of the condenser is approximately 88%.

Table 3-4: Cycle parameters obtained at nominal conditions.

Variables	Amount	Units
$\dot{W}_e$	48	MW
$\dot{m}_{steam}$	40	kg/s
$\dot{m}_{HTF}$	561.6	kg/s
$\dot{m}_{steam,Reheater}$	78.8	kg/s
η_{cycle}	36	%

Table 3-5: Effectiveness, UA and NTU values for heat exchangers.

	ε	UA (W/K)	NTU
Preheater	0.92	499.8	2.73
Steam generator	0.98	1214	0.87
Superheater	0.58	968.4	4.78
Reheater	0.99	1067	9.9
Condenser	0.88	18420	2.15

3.4.2 Solar Field Analysis

The solar field model is based on the simplified model proposed by Forristall. Table 3.6 summarizes the nominal parameters of the solar field analysis. The effect of wind speed is not taken into account in this analysis; the loss through the receiver support brackets is assumed to be 4% of the total HCE thermal losses. Based on the energy balance using the thermal resistance model with the iterative calculation, temperatures at each surface of the heat collection element (HCE) are calculated, and then the heat flows are determined. The investigation is carried out for two different weather database days, the middle of December and the middle of July at noon hour. Table 3.7 summarizes the obtained results for the solar field, where it is considered the third generation parabolic trough design developed by Luz industries LS3.

Table 3-6: Specifications used for the heat loss model.

Solar collector [89]			LS3
inner absorber diameter, $r_{abs,i}$,			0.0325m
outer absorber diameter, $r_{abs,o}$			0.035m
inner glass envelope diameter, $r_{gl,i}$			0.0457m
outer glass envelope diameter, $r_{gl,o}$			0.0525m
parabolic reflector aperture, A_p			5.75m
Testing time: Solar noon			
	DNI	Ambient Temperature	
15th of December	1200W/m²	30°C	
15th of July	450W/m²	15°C	
Heat Transfer Fluid			VP-1
Atmospheric Air Pressure			1 atm
Location			Tripoli

As expected, it can be observed that the effect of DNI and IAM on the heat collected by the HTF is rather important. As a consequence, the collected heat is approximately 1267 W/m in the middle of December and 4833 W/m in the middle of July. In addition, the impact of the ambient temperature is also significant; the efficiency of the collector is approximately 50% in the middle of December when the average ambient temperature is 15°C, and 70% on 1st of July, when the average ambient temperature is 30°C.

Table 3-7: Solar field results.

	IAM	$Q_{absorbed}$ (W/m)	Q_{loss} (W/m)	$Q_{collected}$ (W/m)	$\eta_{th,collector}$
15 of December	0.65	1420	153.3	1266.7	0.5
15 of July	0.98	4948	115	4833	0.7

This model has the potential of becoming a useful tool for the preliminary design of CSPs. In addition, it has the ability of analyzing the performance feasibility of operating CSPs in different locations of the world.

3.4.3 Partial Load Analysis

The previous calculations were carried out under the nominal conditions (full load); however, in fact, the solar conditions are not constant due to the fluctuation in availability of the solar radiation over the year or during a day from hour to hour and day to day. Therefore, particular variable load conditions are required to be assumed for the solar only operation of the plant. This analysis aims to carry out some other scenarios at hypothetical variable load conditions. The purpose is to present the effect of this variability on the efficiency of the plant and its components. The partial load conditions are present during the day due to the intermittent energy absorbed by the solar field. These conditions affect the temperature and mass flow rate of the HTF entering the power block. Figure 3.12 reports the variation of collected energy per meter and efficiency of the solar field with the normal direct irradiation, where the remaining parameters are kept constant. It is clear that the efficiency and collected heat energy increase with increasing DNI. In addition, the resultant solar field outlet temperature variations with DNI at different values of the solar field flow rates in each loop are shown in Figure 3.13. As expected, the outlet temperature increases with increasing DNI while decreasing with increasing HTF flow rate in each loop.

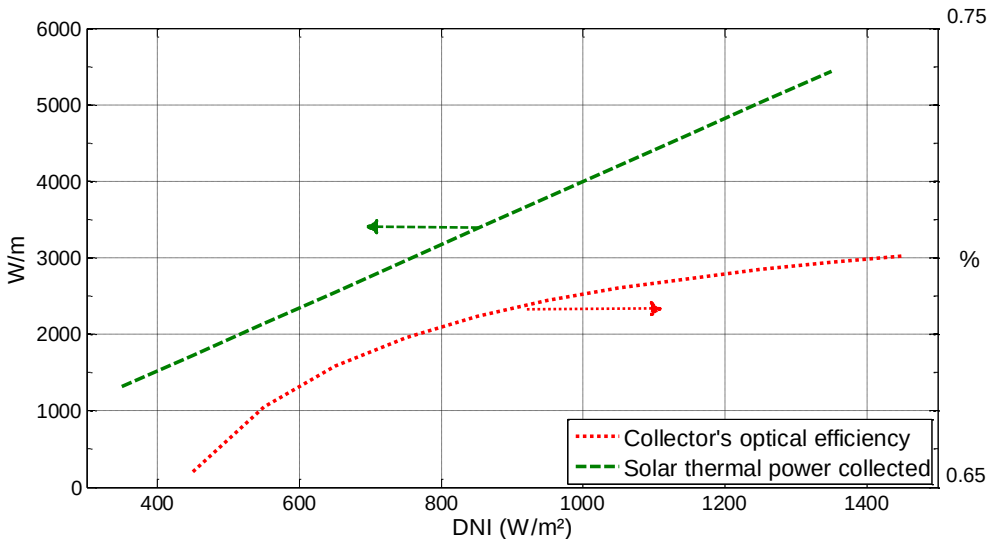

Figure 3.12: Variation of heat collected and collector's efficiency with DNI.

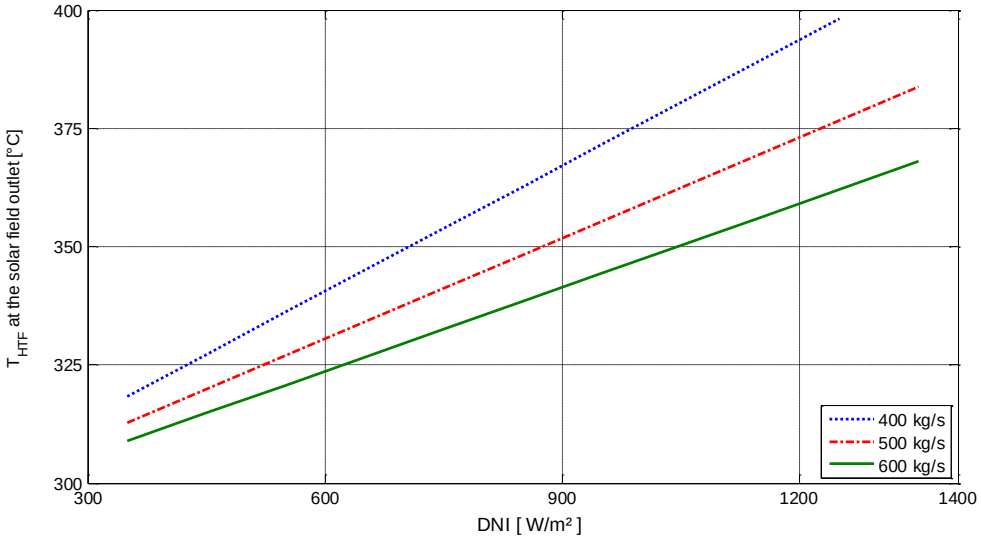

Figure 3.13: Variation of the HTF temperature leaving the solar field with DNI and mass flow rate.

However, for the selection of the optimum HTF flow rate it should be considered its dependence on the energy balance in the train heat exchanger. Figure 3.14 illustrates the variation of the heat energy collected and solar collector's efficiency with the ambient temperature while other parameters are kept constant. It can be observed that the solar field efficiency is only slightly impacted by the ambient temperature. This impact is mostly due to the thermal loss due to the heat transfer between the surrounding atmosphere and external surface of the receiver tubes.

The turbine efficiency, in general, is strongly dependent on the deviation of the operating flow $(\dot{m})$ from the design flow rate $(\dot{m}_{ref})$; the turbine efficiency is determined based on the relationship proposed by Bartlett [100] as follows:

$$\eta_{turbine} = 0.6127 + 0.2981\left(\frac{\dot{m}}{\dot{m}_{ref}}\right) - 0.1423\left(\frac{\dot{m}}{\dot{m}_{ref}}\right)^2 \qquad 3.74$$

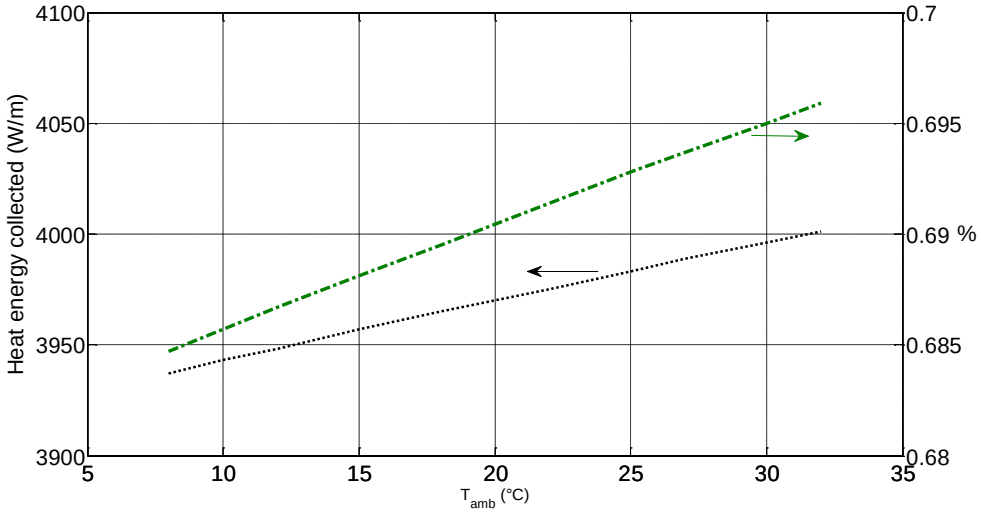

Figure 3.14: The heat energy collected and solar collector's efficiency variation with the ambient atmospheric temperature.

For the pump operating on partial load conditions, the pump efficiency is determined based on the correlation proposed by Lippke [17]:

$$\eta_{pump} = 2\eta_{Ref}\left(\frac{\dot{m}}{\dot{m}_{ref}}\right) - \eta_{Ref}\left(\frac{\dot{m}}{\dot{m}_{ref}}\right)^2 \qquad 3.75$$

In equations 3.74 and 3.75 the subscript "*ref*" designates values at design conditions; for both correlations the design flow rate, $\dot{m}_{ref}$ is 40 kg/s. Figure 3.15 reports the performance of the turbines and pump, respectively, at part load conditions. The mass flow rate has a significant impact on the pump performance, while its influence on the turbine performance is comparatively small where the turbine efficiency is 61.27% at $\dot{m}_{ref} = \dot{m}$; and the effective flow rate considered was in the range of 35 to 45 kg/s.

Figure 3.16 presents the gross electric power output, which is a function of the efficiency of the generator. It can be seen that the gross electric power output increases with the generation efficiency, which is a function of the load as indicated by equation 3.57. The value of the load depends on the net turbine work. At the full

load the gross electric power output is equal to 48137 kW and the cycle gross efficiency is 0.36.

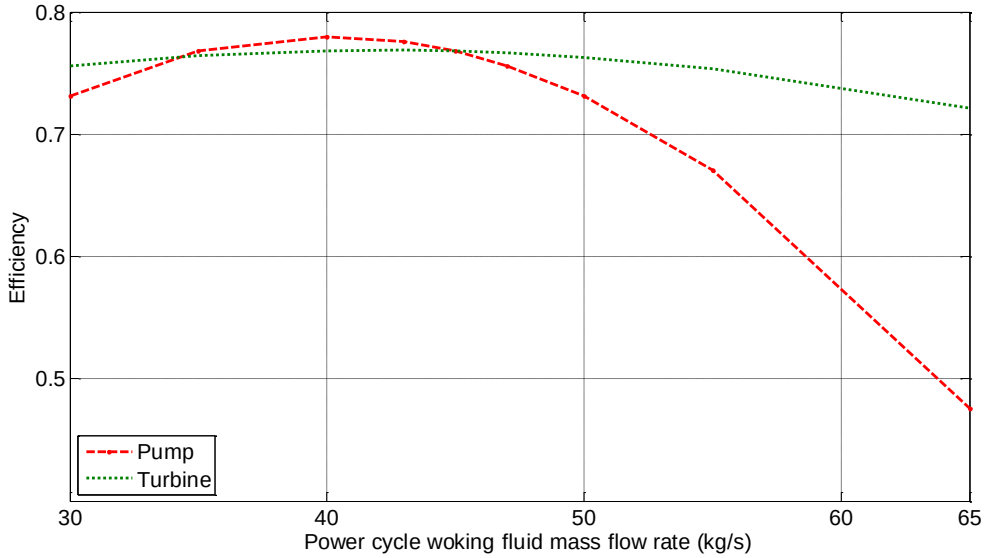

Figure 3.15: Turbine and pump efficiency variation with mass flow rate.

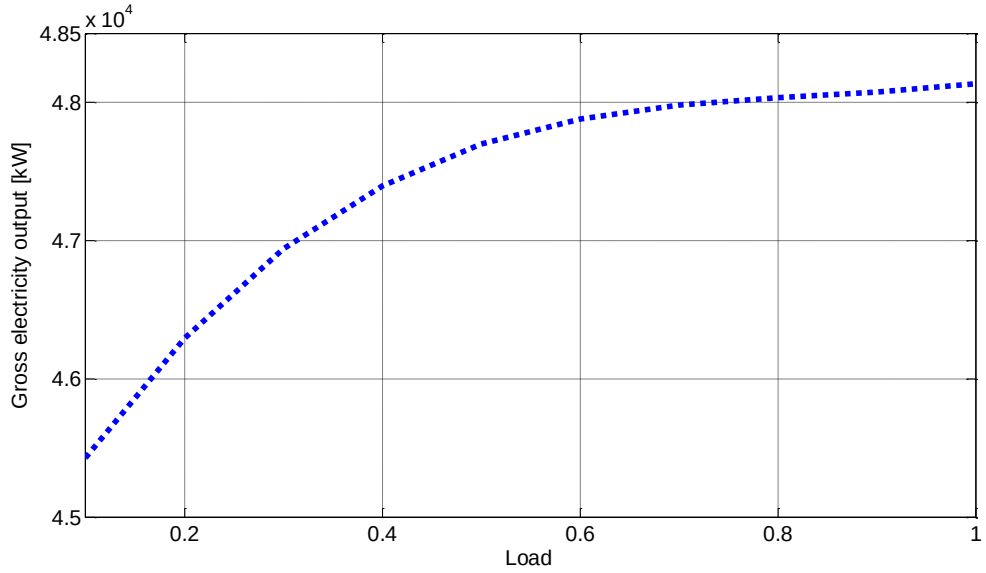

Figure 3.16: The gross electrical power output variation with the load.

The variable load conditions analysis only reflects part of the reality, since a few parameters were kept constant. A better-suited indicator of the behavior and

performance of the solar thermal power plants is to conduct the analysis on an annualized basis. Therefore, in the following chapter, the overall energy scenario for the CSP will be presented. This scenario will be obtained in terms of the behavior and performance of its components by conducting an analysis on an annual basis at intervals of an hour.

3.5 Chapter Summary

The maximum and minimum annual solar days at noon hour for the CSP plant location, as indicated by the present study, are highly attractive. The developed model has the potential of becoming a useful tool for the preliminary design of CSPs and, in particular, for the configuration of the solar field using existing commercial plants. Moreover, it has the ability of analyzing the performance feasibility of using CSPs in different regions of the world, as it was illustrated for the Tripoli region (Libya).

The reheated steam was brought to 663 K before being expanded in the LP turbine to 6 kPa, while the dryness fraction was always higher than 0.88 [18] at the LP-turbine outlet/condenser inlet. The condenser pressure was defined based on the temperature of the coolant, in the present case seawater. The working fluid at the condenser outlet state was assumed to be saturated liquid [91]. The maximum steam temperature in the power cycle was nearly 663 K and the mass working fluid flow rate is 40 kg/s. The energetic thermal efficiency of the power cycle is approximately 36% and the gross power output is 48 MW. The exergetic losses reach a maximum at the boiler (10796 kW). The daily averaged amount of energy needed to be delivered to the train heat exchanger is 3289 MWh and the effectiveness of the condenser is approximately 88%. The collected heat at the collector is 1267 W/m and the collector efficiency 70% in the middle of July; while they are 4833 W/m and 50% in the middle of December, respectively.

Chapter 4

Annual Energetic and Economic Analysis of 50MW Parabolic Trough-CSP Plant

4.1 Introduction

For an accurate and comprehensive study of the performance and behavior of solar energy systems and its components, it is required to conduct an hourly analysis on an annual basis. This analysis allows the comparison of different systems and, eventually, the selection of a particular one, and it includes both the economic and energetic components, which are simulated within the "greenius" software [70]; the climate database is collected using the Meteonorm7 software [71]. The analysis takes into consideration different locations in Libya for the standard plant selected for the present work; in addition, it considers the impact of project financing and incentives on the cost of energy. The cost reduction potential through eventual system enhancements is also evaluated within this analysis, as cost reduction is a crucial requirement for electricity generation from concentrating solar power plants to be cost competitive when compared to that of fossil-fired plants. Therefore, the levelized cost of electricity (LCE) is used as the primary metric of the financial performance to express the selling price of the energy. In addition, this analysis would be used to validate the model that was developed in Chapter 3. The idea of this analysis is to simulate the same configuration and size of the Andasol plant for the

region of Libya; to assess the advantage of Libya as a CSP location in comparison with Southern Spain, where already are installed several CSPs. The input parameters required for the simulation are based on the results obtained in Chapter 3. For the economic simulation of the CSP plant in Libya, to a great extent, the Spanish economic input parameters were used due to the lack of information on some of the required data for Libya.

The “greenius” software was developed at the German Aerospace Centre (DLR) [70] and is a free source software and powerful simulation environment for the calculation and analysis of renewable power systems such as solar thermal power plants, photovoltaic systems, wind parks or Dish/Stirling plants. It offers a unique combination of detailed technical and economic calculations as they are needed for planning and installation of renewable power systems. In addition, greenius has a good user interface for the analysis of solar thermal power plants. It distinguishes itself by numerous export possibilities for intermediate and final results.

The present analysis reports on the current cost of energy and the potential for reducing the cost of energy derived from parabolic trough-CSP plant. It interesting to note that in the present study it is found the operation in Libya offers higher performance and lower LCE than that in Southern Spain. Therefore, Libya has the potential of becoming attractive for establishing CSPs in its territory and, in this way, to facilitate the target of several European initiatives that aim to import electricity generated by renewable sources from North African and Middle East countries.

4.2 Methodology of the greenius

The model of the selected standard plant is based on the exchange of heat flows and electrical power as shown in Figure 4.1 where, the useful heat flows are illustrated in red and heat losses in blue. The useful electric power is marked brown and the parasitic power losses in green.

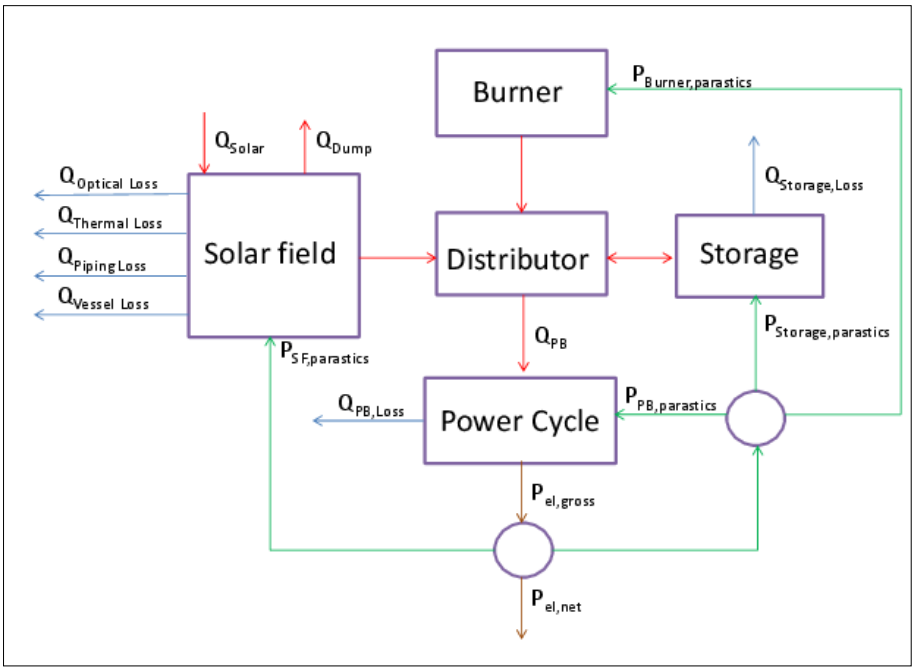

Figure 4.1: The greenius operation strategy for solar thermal power plants [101].

By controlling the heat flows to and from the distributor, the operating state of the plant can be adapted to several requirements such as achieving the highest yield. For the determination of individual heat flows, greenius follows the flow diagram shown in Figure 4.2. Initially, the heat demand is calculated and the load curve should be defined for the specified demand. Essentially the software distinguishes the situation of the solar field (SF), minus losses, delivering or not the required energy. In addition, the software takes into consideration if the storage has free capacity and the operating parameters allow for charging the storage system. However, when the SF does not deliver sufficient energy to fulfill the demand, other options may be available such as auxiliary firing systems; depending on the charging state and the storage control parameters, the storage could be discharged or charged. In the following step, the storage is loaded to its buffer level in a privileged manner if the specified parameter is set.

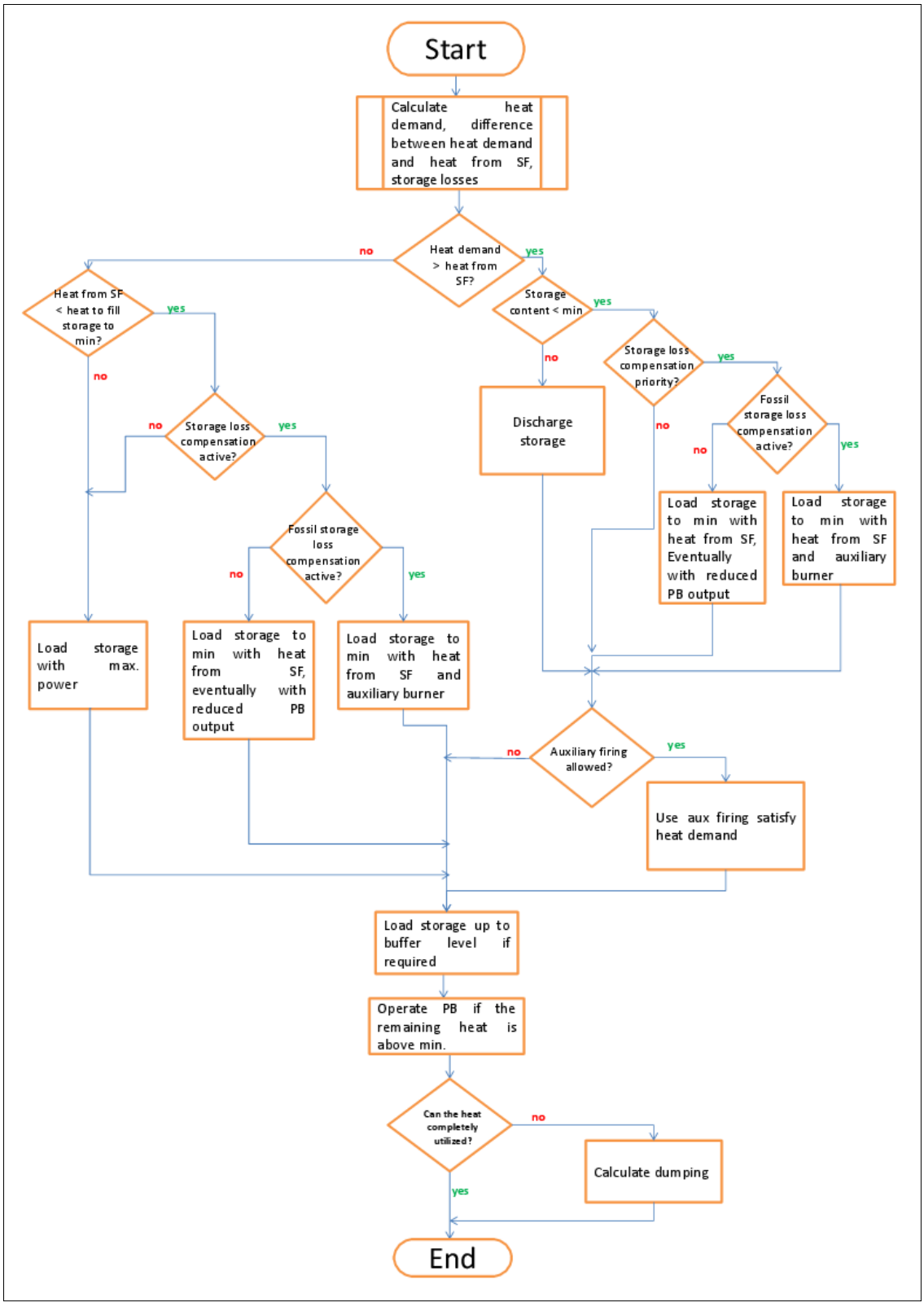

Figure 4.2: Flow chart of the determination of individual heat flows [101].

As long as the storage is loaded to its buffer level, the power block is not operated. In the next step the power block load is set to zero, when the usable heat to the power block falls below its minimum input. The last step is to dump the solar energy which cannot be used by the storage or the power block. In this analysis solar only scenario is conducted since the Solar-Only is the reference strategy for CSP plants.

In the present case, whenever there is not enough solar energy available, the power cycle will be operated with the assistance of the storage system, depending on its availability. This operating strategy ensures the utilization of the maximum amount of solar energy. The surplus energy is dumped and only the compensation of the storage system loss has higher priority than serving the power cycle. In case of storage systems using phase-change materials, this action helps to prevent the stored content from eventually solidifying, which would result in a damaged storage. It should be mentioned the plant may operate at part load for many hours; therefore, the thermal efficiency of the power cycle might not be optimal. The components of the plant being studied are defined in the following sections.

4.2.1 Solar Field

The field size and nominal thermal output are calculated from the input values. This allows a step-by-step change of the parameters of the field. The thermal field output considered in this analysis is calculated using the characteristics and dimensions of the solar field of the Andasol power plant. Data about Andasol power plant are presented in Table 4.1. The input parameter reference irradiation is used to calculate the nominal thermal output of the solar field and, consequently, is a design value – it should be noted that for parabolic troughs there is no standard reference irradiation. The heat losses and fluid properties are temperature dependent; therefore, an iterative procedure is necessary to solve the collector balance equations and the heat losses. This procedure implies that fluid properties should be calculated

simultaneously and also based on temperatures of the preceding time step; in this way, and to minimize errors each hour is subdivided into up to 30 time steps whenever large temperature gradients do occur. This ensures that the temperatures that are used to calculate heat loss and fluid properties can be determined with improved accuracy. The temperatures, and in particular those for the field inlet and outlet, and for power cycle, are important for the performance calculation since they have a large impact on thermal losses and start-up times. As long as the outlet temperature is lower than the power cycle starting temperature, the software "greenius" assumes that the solar field is in heat up mode and the power cycle is not operating.

Table 4-1: Andasol power plant general data [102].

Technology	Parabolic trough
Region	Granada - Spain
Land Area	200 hectares
Electricity Generation	158,000 MWh/yr (Expected/Planned)
SCA Manufacturer (Model)	UTE CT Andasol-1 (SKAL-ET)
Mirror Manufacturer (Model)	Flabeg (RP3)
HCE Manufacturer (Model)	Schott (PTR70)
HCE Manufacturer (Model)	Solel (UVAC 2008)
Heat-Transfer Fluid Type	Dowtherm A
Turbine Capacity (Gross)	50.0 MW
Turbine Capacity (Net)	49.9 MW
Turbine Manufacturer	Siemens (Germany)
Output Type	Steam Rankine
Storage Type	2-tank indirect - 7.5 hour(s)

4.2.2 Power Cycle

The power block input form contains only the main nominal values of this part of the plant; and the parameters can be adapted in order to modify the power cycle size and/or efficiency. The three modifiers intervene as follows:

- The scale factor changes all values from the lookup tables like heat input, electrical output, parasitics etc. by the same factor;
- The turbine efficiency modifier changes the generator output, leaving heat input and parasitics unchanged; and
- The parasitics losses modifier only affects the parasitics and leaves the heat input and gross electrical output at their original values.

Heat balance calculations obtained in the previous chapter can be used as input parameters to operate the power cycle in greenius, where the costs are defined separately from the solar field costs.

4.2.3 Storage System

There are two different storage models available in greenius: single tank (thermocline) and the two-tank molten salt, which is considered in this analysis. The main difference between the two models is the treatment of the thermal losses. While the thermal losses of 2-tank molten salt storage system are constant, they depend on the storage content for the singe tank storage model. The main parameters which have to be defined are capacity, and heat and pumping losses. The number of possible full load hours and the field excess are calculated automatically depending on the collector field parameters.

The Andasol power plant uses the two-tank molten salt storage type with a hot salt tank at temperatures of about 380°C and a cold storage tank at about 290°C. The heat is stored by cycling the molten salt between both tanks and a series of heat exchangers is used to transfer the sensible heat from the HTF to the salt during the charging period and back to the HTF during the discharging period. Since the salt mixture used in these tanks solidifies at about 220°C both tanks must always be kept hot, which is the reason why the heat losses are almost constant [103].

The net storage capacity and the maximum charging and discharging power will be specified, and they may be different since the salt pumps have a volume flow rate limit and the usable temperature difference is typically lower at the discharging mode. In addition, thermal losses must be defined by giving a value of fractional losses for 24 hours of the net storage capacity. For large thermal storage tanks, the assumption of 1% for each 24 hours is a reasonable estimate in greenius for the Andasol power plant; however, relative losses tend to increase with decreasing storage volume. Temperature differences for charging and discharging and pumping parasitics will be specified as electrical power per thermal power. The molten salt storage model needs the minimal storage content for the simulation. The actual value of this parameter has no significant impact on the simulation results and so it may be set more or less arbitrarily; therefore, 10 to 20% of the net storage capacity would be a reasonable estimate for the minimal storage content. The minimal storage content is only important to account for the constant thermal losses even in times when the storage is “empty”. Normally at the load curve/solar driven operating strategy the storage is only loaded if the field produces excess heat above the demand. In fact, molten salt storage has constant heat losses which might cause the storage content to fall below the minimal content, particularly during the cold season, when the solar field does not deliver excess heat over longer time periods. The implemented operation strategy for the molten salt storage in greenius is: charging the storage up to the minimal content has the highest priority among all options, since freezing must be prevented. This energy cannot be used for electricity production; however, it can be dissipated to the environment. The implementation strategy for parabolic trough plants with storage is as follows: if the solar field cannot cover the demand, namely the rated power, heat is taken from the storage. If this heat is not sufficient, the power block uses the parallel fossil fired heater if the plant has such a device.

4.2.4 Location and Meteorological Data

The location in greenius contains geographical data and ground structure data for the project site. Latitude, longitude and time zone are the reference for all sun position calculations. The location window contains also calculation options for sunrise, sunset and solar noon for each defined day.

Meteorological data are the basis for nearly all simulations that greenius can carry out. The software contains a small number of meteorological data files. Powerful import filters can also import and read meteorological data from other sources. For instance, with the use of the Meteonorm software, meteorological data files for every site at the Earth can be generated. A complete greenius meteorological data set contains for all time steps of a reference year the eight critical values, which are: ambient temperature, air pressure, relative humidity, global irradiance, direct normal irradiance, diffuse irradiance, wind direction and wind speed. The software “greenius” has extensive functions for the presentation and processing of the meteorological data. Latitude, longitude and time zone represent the measurement point of the meteorological data.

Since the meteorological data files give mean values for the respective hour, it may occur that the meteorological file contains significant DNI values while the sun position algorithm calculates a sun position below the horizon for early morning or late afternoon hours. That means the sunrise is in the second half or sunset is in the first half of that individual hour. In these cases, greenius does not use the sun position for the center, but rather for the edge of that hour.

4.2.5 Economics

The first step is to specify the project-specific costs as presented in Figure 4.3. The economics section of greenius includes costs of conventional and non-conventional components, where the solar field is the non-conventional component

and the power block is the conventional one. The costs are subdivided into investment costs and operating and maintenance costs (O&M).

There are limited resources in the literature that provide cost breakdown for parabolic trough power plants. In addition, currently, it is not possible to get the cost of the plant from local sources in Libya due to the lack of relevant experience. The input parameters relative to financial and economic calculations are selected from the default data of Andasol plant, which are available in greenius.

To compute the total investment costs, initial capital investment for all components of the plant are summed. The solar field costs are determined as:

$$SF_{costs} = A_{mir} \cdot c_{SF} \quad 4.1$$

Where A_{mir} is the solar field aperture area in m² and c_{SF} is the specific solar field costs, including HTF system in €/m². The power block costs are calculated as:

$$PB_{costs} = P_{PB} . c_{PB} \quad 4.2$$

Where P_{PB} is the net installed capacity of power block in kW, c_{PB} is the specific costs of power block, including turbine and generator given in €/kW. The storage costs are determined as:

$$Storage_{costs} = P_{ts} \cdot c_{ts} \quad 4.3$$

Where P_{ts} is the thermal storage size in MWh and c_{ts} is the specific costs of thermal storage in €/MWh. Then the total investment costs are given as:

$$C_i = A_{mir} . c_{SF} + P_{PB} . c_{PB} + P_{ts.} c_{ts} + [A_{SF} + A_{PB}] . c_{land} \quad 4.4$$

Where the term $[\mathrm{A_{SF}} + \mathrm{A_{PB}}] . \mathrm{c_{land}}$ refers to the cost of the land area occupied by the

solar field (A_{SF}) and by the power block (A_{PB}); c_{land} is the specific cost of the land.

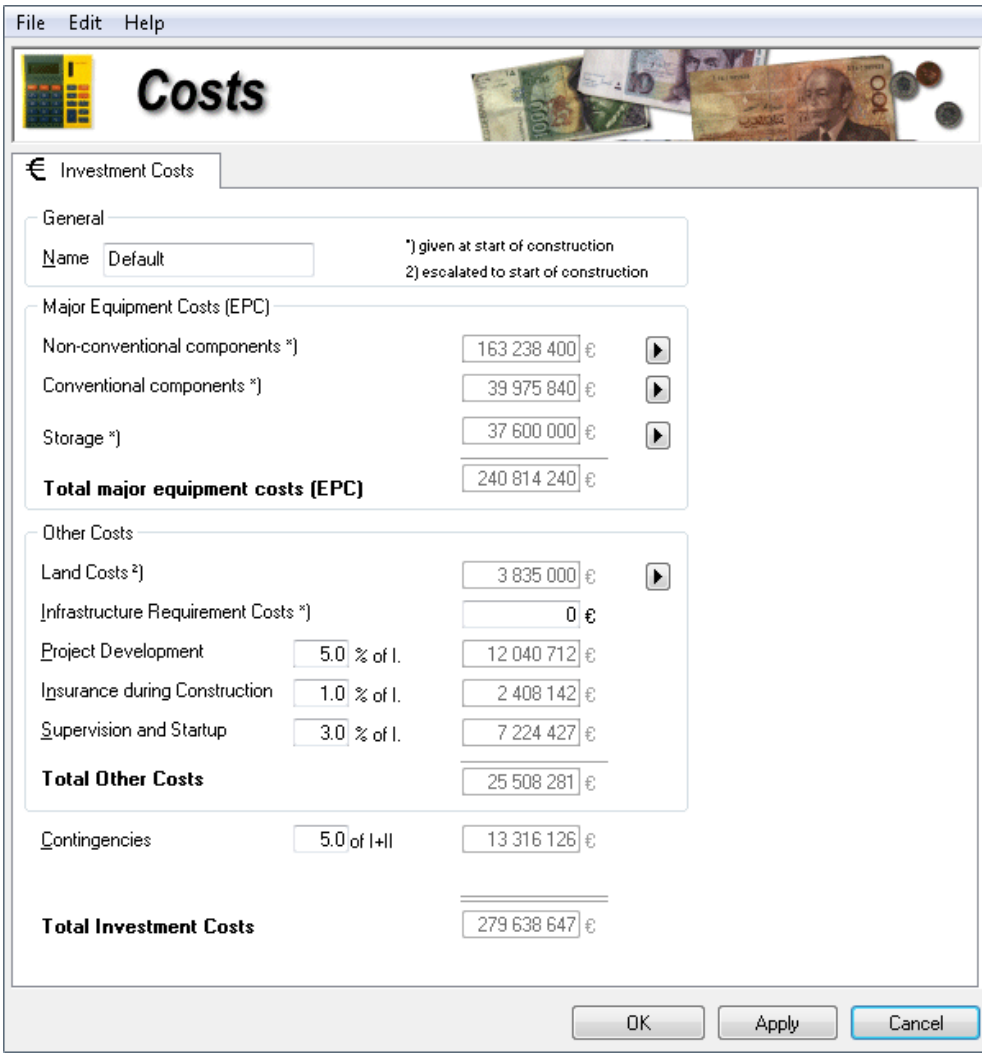

Figure 4.3. Cost parameters of greenius.

The O&M costs are subdivided into general O&M costs (including labor), replacement costs and insurance costs. Further costs are land costs that are calculated from specific land costs and the area demand and absolute costs for infrastructure. Costs for project development, insurance during construction, supervision and set up and contingencies can be defined as well. The sum of the costs is calculated automatically and is the base for all further simulations. The start of the project and the operation period are also defined. The costs of the construction

period can be split into half-year periods. The end of the construction and the start of operation are calculated automatically and refer to the first operational year. The most important financing parameters such as general information about grants, the share of equity and loans for the remaining capital requirements are also needed. The minimum required internal rate of return (IRR) can be defined as well. This value is needed for further calculation of the required tariff to meet this IRR.

The economics of CSP and other renewable technologies are, with the exception of biomass, substantially different from that of fossil fuel power technologies. Renewables have, in general, high upfront investment costs, modest O&M costs and very low or no fuel costs. Conventional fossil fuel power tends to have lower upfront costs and high (if not dominant) fuel costs, which are very sensitive to the price volatility of the fossil fuel markets. In contrast, renewable technologies are more sensitive to change in the cost of capital and financing conditions. Solar tower projects are currently considered higher risk by financiers due to their less mature status. However, in the longer-term, greater experience with solar towers will reduce this risk premium and convergence is likely to occur in financing costs. The analysis presented here assumes a standard 10% cost of capital for all the technologies evaluated. The LCE of CSPs from a developer's perspective will therefore differ from that presented here, due to differences in local conditions and developers' and lenders' perception of risk. The levelized cost of electricity (LCE) is used as the primary metric of the financial performance to expresses the selling price of the energy. The most important parameters that determine the LCE of CSPs are [79]:

- The initial investment cost, including site development, components and system costs, assembly, grid connection and financing costs;
- The plant's capacity factor and efficiency;
- The local DNI at the plant site;
- The O&M costs (including insurance) costs; and
- The cost of capital, economic lifetime, among others.

The LCE of renewable energy technologies varies by technology, country and project based on the renewable energy resource, capital and operating costs, and the efficiency / performance of the technology. The approach used in the analysis presented here is based on a discounted cash flow (DCF) analysis. This method of calculating the cost of renewable energy technologies is based on discounting financial flows (annual, quarterly or monthly) to a common basis, taking into consideration the time value of money. Given the capital intensive nature of most renewable power generation technologies and the fact that fuel costs are low, or often zero, the weighted average cost of capital (WACC), often also referred to as the discount rate, used to evaluate the project has a critical impact on the LCE. The formula used for calculating the LCE of renewable energy technologies is [79]:

$$LCE = \sum_{t=1}^{n} \frac{I_t + M_t + F_t}{(1+r)^t} \Big/ \sum_{t=1}^{n} \frac{E_t}{(1+r)^t} \qquad 4.5$$

Where:

I_t: investment expenditures in the year t

M_t: operations and maintenance expenditures in the year t

F_t: fuel expenditures in the year t

E_t: electricity generation in the year t

r: discount rate

n: expected lifetime of the system.

4.3 Results and Discussion

The plant size and configuration of Andasol power plant and the location of Tripoli are selected in this analysis. The meteorological data and site position are summarized in Table 4.2, while the dimension of the plant is reported in Table 4.3. For solar thermal trough power plants, the load curve is mandatory, because the simulation tries to cover the load with the solar power plant. During the periods for

which heat from solar field is higher than the heat demand of the power block to produce the required net electricity output, the surplus heat is used to charge the storage system. If the heat from solar field is not sufficient, it will be supplemented by heat from storage or auxiliary fossil heater. In case that all three heat sources are not sufficient to deliver the required heat, there will be a gap between load demand and actual electricity production. If the heat from solar field is higher than the heat demand required to fulfil the load demand and the storage is totally filled, then parts of the solar field should be deactivated as this heat could not be used.

Table 4-2: Meteorological data and site position.

Parameters		Units
Global horizontal irradiance (GHI)	2030	kWh/(m²·a)
Direct normal irradiance (DNI)	2293	kWh/(m²·a)
Direct irradiance on collector plane (DNC)	2033	kWh/(m²·a)
Diffuse horizontal irradiance (Diff)	614	kWh/(m²·a)
Mean annual ambient temperature	21	°C
Site	Libya - Tripoli	
Latitude	33	°N
Longitude	13	°E

kWh/(m².a): kilowatt hours per square meter per year

Table 4-3: Plant dimensions.

Parameters		Units
Collector	ET 2 with Schott HCE	
Number of collectors	624	
Effective collector area	510,120	m²
Land use	1,910,000	m²
Nominal thermal output	265	MW_{th}
Nominal electrical output	50	MW_{el}

The heat, which could have been produced by the solar field but cannot be used, it is accounted as dumping. The simulation results are reported in Tables 4.4 and 4.5 and summarized in Figures 4.4 – 4.10. Table 4.4 presents the energetic

results, while Table 4.5 shows the economic results for Tripoli and Andasol (Andalucía) locations. The mean annual solar field efficiency is 44% where the mean efficiency of the total system is 14% for the location of Tripoli in the present analysis, and they compare favorably with the corresponding values of the Andalucía location 41% and 13% respectively. The low efficiency of the total system is for the solar only case considered in the analysis; in these conditions, the solar radiation is not available during the full day over the year and it can be seen in the table that the full load hours is 3699 and 3137 hours for Tripoli and Andalucía, respectively.

Table 4-4: Simulation results.

Parameters	Tripoli	Andalucía	Unit
Annual thermal field output	511,370	442,232	MWh_{th}
Solar annual net elect. output	163,804	138,385	MWh_{el}
Solar annual gross elect. output	184,970	156,846	MWh_{el}
Total annual net elect. output	163,804	138,385	MWh_{el}
Total annual gross elect. output	184,970	156,846	MWh_{el}
Specific thermal field output	1003	867	kWh_th/m²
Specific electrical output	321	271	kWh_{el}/m^2
Mean annual field efficiency	44	41	%
Mean system efficiency	14	13	%
Full load hours	3699	3137	h/a
Number of turbine starts	373	353	1/a
Number of hours with at least temporarily full storage	148	206	h/a

a: refers to annual

This occurrence can be clearly observed in Figures 4.4 - 4.6, where Figure 4.4 reports the mean daily efficiency of solar field and the total system over the year. As expected, the efficiency is a function of the availability of solar radiation; it can be noted a steady increase in efficiency over the first seven months, then a steady decrease up to the initial state. In addition, Figure 4.5 illustrates the mean daily net and gross electricity output of the plant, which presents behavior similar to that of the efficiency. Trends for mean daily thermal field output, thermal collector output, heat absorbed by collector and irradiation on collectors are presented in Figure 4.6; in

addition, hourly averages for 15th of December and 15th of July are also presented in Figures 4.7 and 4.8. These two days were selected in the previous chapter; it can be seen the disparity of the results between the two days, which is mainly due to the differences of solar hours and the amount of DNI of each day. There are also other factors that may impact, although minor, on this disparity such as ambient temperature and wind speed.

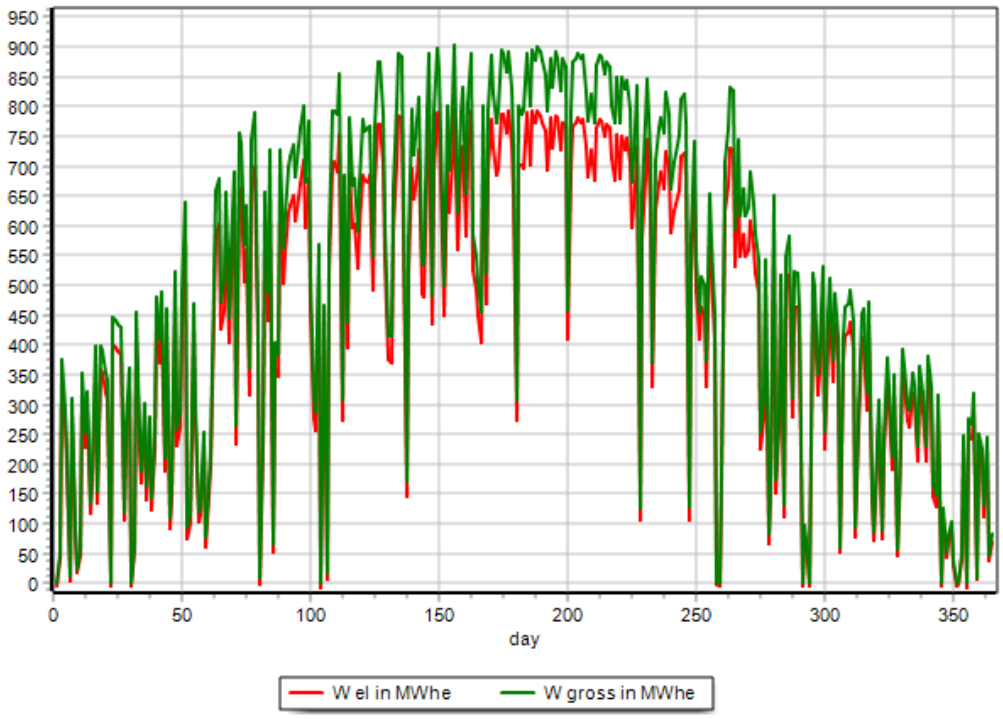

Figure 4.4: The net and gross electricity output of the plant.

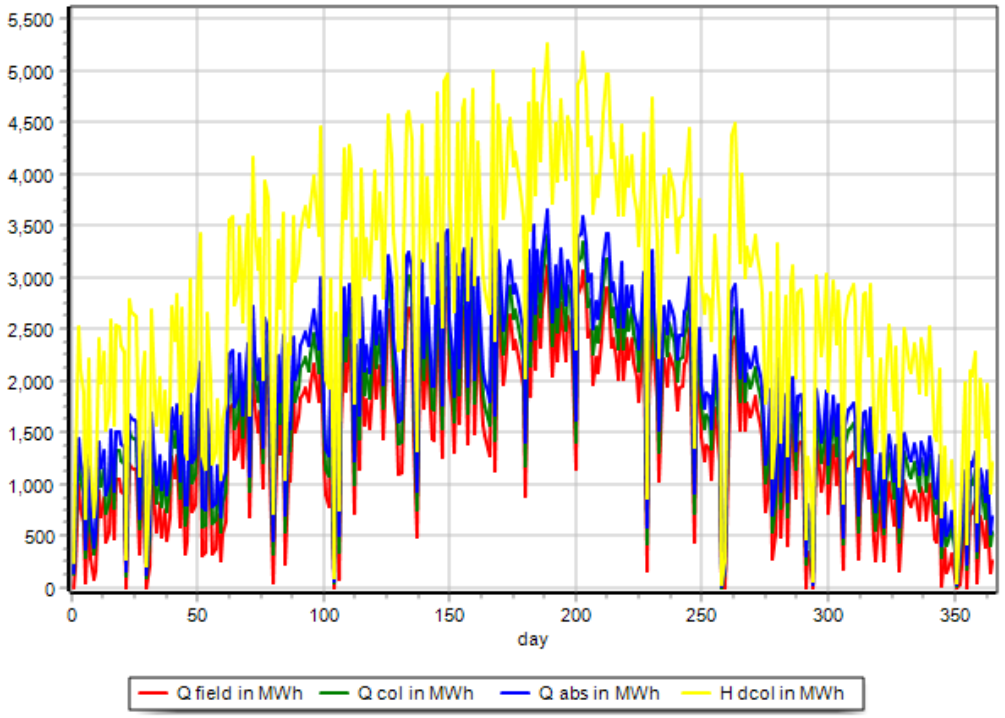

Figure 4.5: The thermal field output, thermal collector output, heat absorbed by collector and irradiation on collectors.

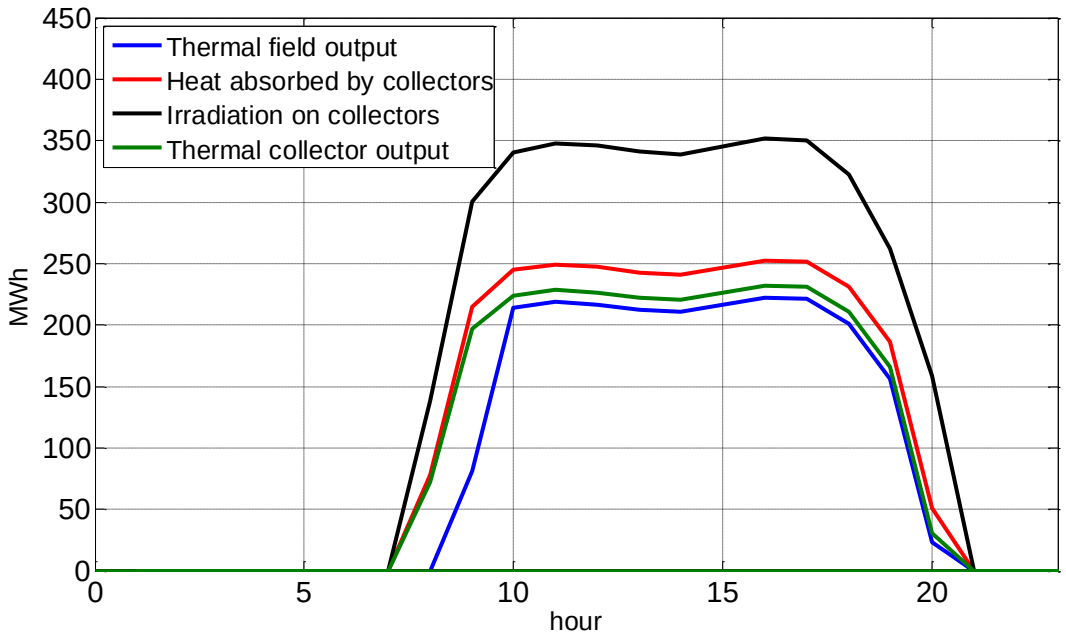

Figure 4.6: The thermal field output, thermal collector output, heat absorbed by collector and irradiation on collectors on 15th July.

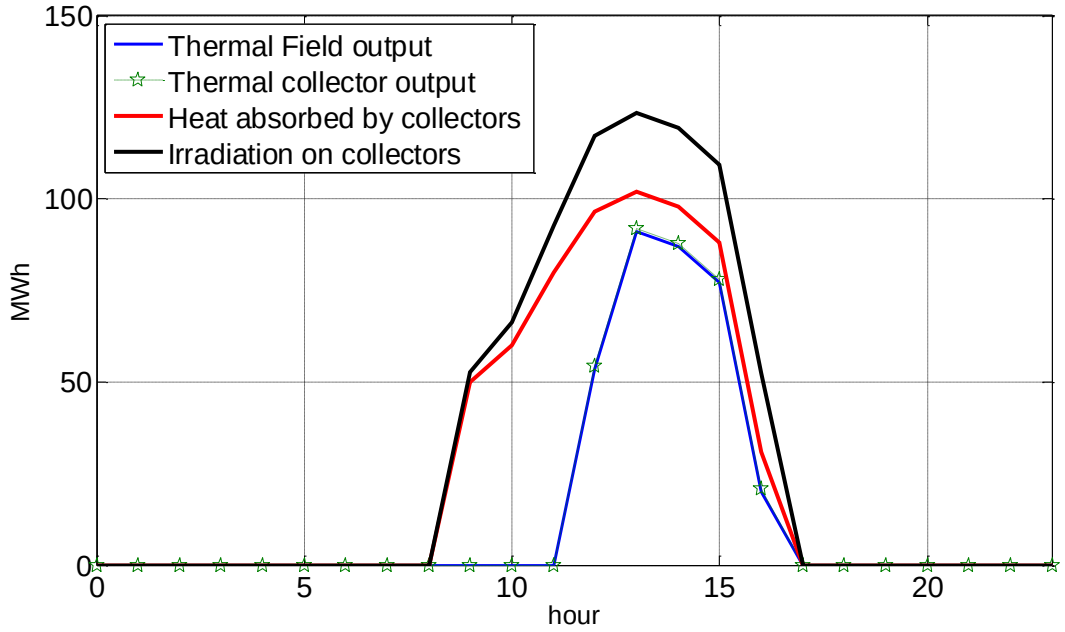

Figure 4.7: The thermal field output, thermal collector output, heat absorbed by the collector and irradiation on collectors on 15th December.

Furthermore, Figures 4.9 and 4.10 report on the electricity output and the efficiency of the plant over five days in July and December, respectively. The results indicate that it is possible the plant to produce electricity with levels higher than 40 MW over twenty hours a day in July. However, in contrast, the opportunity of operating the plant at this power output without fossil backup is practically impossible during the month of December. The benefits of integrating the storage system in the operation of the plant are clearly illustrated during the month of July. In Figure 4.10 it is reported the daily mean of storage level in MWh along the year, and its behavior, as expected, fully corresponds to the solar radiation; the full charging of the storage system can occur from March to October. However, for the other months, the solar field does not deliver sufficient excess heat to charge the storage system.

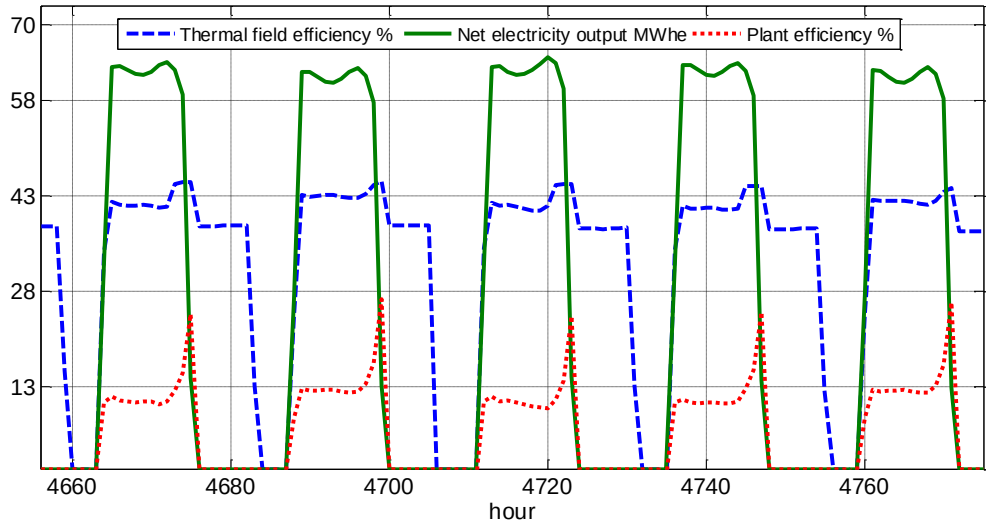

Figure 4.8: Mean hourly electricity output, solar field and total system efficiency over five days in July.

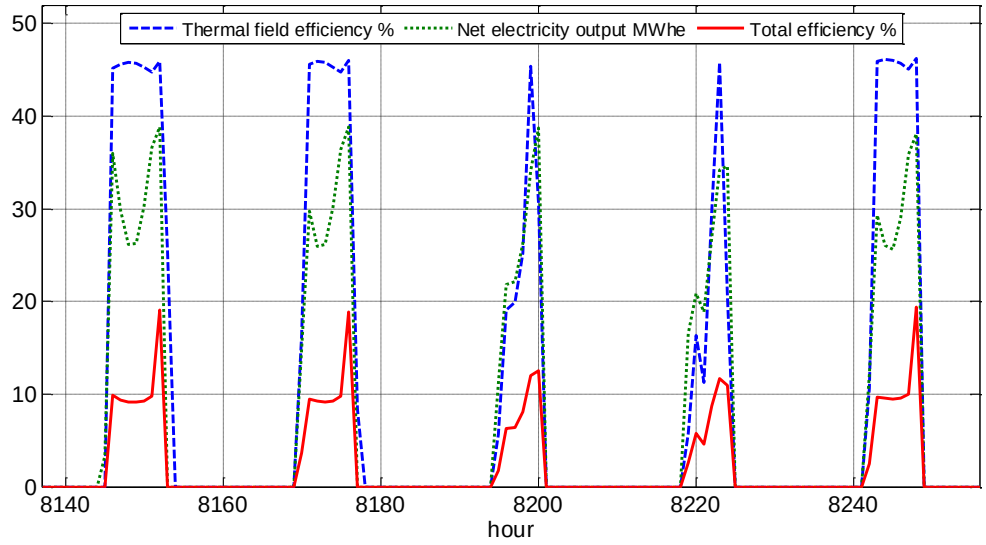

Figure 4.9: Mean hourly electricity output, solar field and total system efficiency over five days in December.

These results, to a great extent, serve to validate the model developed in Chapter 3; it is clear that the predicted results are very close to the greenius simulation predictions. For instance, it can be observed that the values for the collector efficiency agree well with the results obtained in Chapter 3, which are 49% and 70% in December and July solar hours, respectively.

Parabolic trough solar technology is the most proven and lowest cost large-scale solar power technology available today. The analysis also looks at the impact of project financing and incentives on the cost of energy. The cost reduction is a crucial requirement for electricity generation from concentrating solar power plants in order to reach cost competitiveness compared to mid-load power from fossil-fired plants. The cost reduction potential of eventual innovations is evaluated within annual performance analysis. The analysis reviews the current cost of energy and the potential for reducing the cost of energy from parabolic trough solar power plant technology. The primary metric of the financial performance is the levelized cost of electricity that represents the selling price of the energy. LCE and other financial indicators are listed in Table 4.5; the table summarizes the economic simulation result for Tripoli and Andalucía locations. Although, Spanish economic input parameters were used for the Tripoli location, it can be observed that the LEC and required tariff (LCOE) are lower for this location. This means that the performance of the plant has an important role on the improvement of LEC. The LCE was found to be 0.17 €/kWhe, which is still high, when compared to the Libyan cost of electricity, which is generated mainly by fossil fuels (natural gas and oil). However, taking into consideration the volatile prices of fossil fuels and the European CO_2 tax implementation, parabolic trough plants can contribute to the long-term energy security in Europe and, in particular, Libya.

Reduction in the LCE of the considered plant can be achieved in Libya through partial tax exemption along with lower interest rates than those that are practiced in Spain. However, more economically feasible parabolic trough plants can be realized by providing further financial incentives. Furthermore, an interesting option is having the participation of local manufacturing, in particular for the steel and glass components of the solar field, which may yield a considerable reduction in the solar field cost. To this purpose, the Libyan Iron and Steel Company (LISCO), which is the largest iron and steelmaking company operating in North Africa, can make a

significant contribution towards the reduction of the overall construction costs. In addition, the raw material for glass manufacturing is widely available.

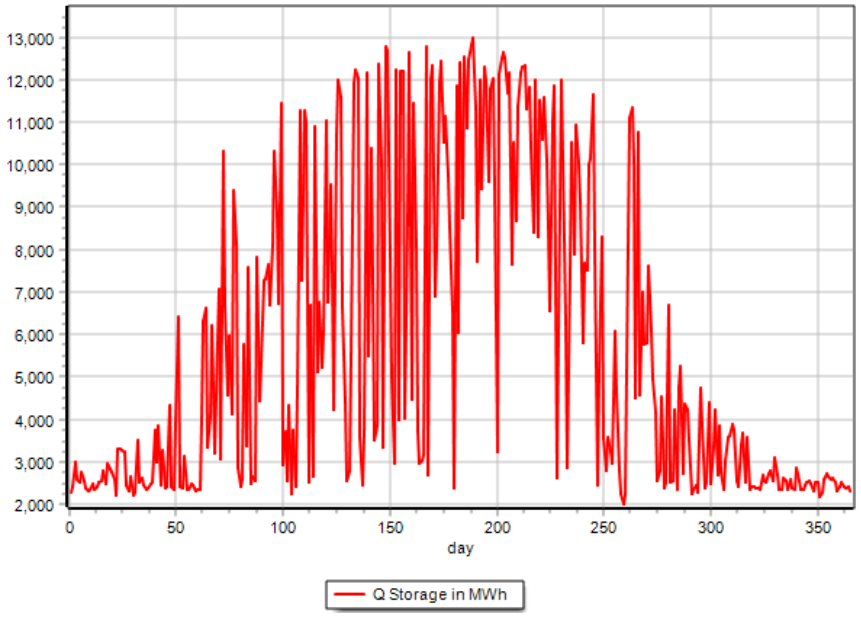

Figure 4.10: Storage level.

Table 4-5: Economic simulation results.

Parameters	Tripoli	Andalucía	Unit
Internal Rate of Return (IRR) on Equity	14	10	%
Net Present Value	116,256,770	59,030,826	€
Payback Period	10	12	yrs.
Discounted Payback Period	12	15.6	yrs.
Total Incremental Costs	251,067,407	266,236,054	€
Minimum ADSCR	1.18	1.02	
Required Tariff (LCOE)	0.25	0.30	€/kWh
Incremental LEC	0.12	0.15	€/kWhe
Levelized Electricity Costs (LEC)	0.17	0.20	€/kWhe
Total Investment Costs (IC)	279,638,648	279,638,648	€
Annuity of IC	0.08	0.08	
NPV of Running Costs (OC)	76,126,955	75,048,378	€
Annuity of OC	0.08	0.08	

Finally, in what follows, a comparative analysis is conducted for three different sites on the North (coastline), the Southwest and the Southeast of Libya; these locations are selected at the cities of Al Ugaylah, Dirj and Al Jawf, respectively. The investigation takes in consideration the same strategy, size and configuration of the plant and nominal parameters, which were used for Tripoli. The results of this simulation are reported in Table 4.6.

Table 4-6: Simulation results of three different sites in Libya.

Simulation result	Al Jawf	Dirj	Al Ugaylah	Units
Global horizontal irradiance (GHI)	2338	2279	2177	kWh/(m²·a)
Direct normal irradiance (DNI)	2760	2923	2540	kWh/(m²·a)
Mean annual ambient temperature	23	25	21	°C
Latitude	24	30	30	°N
Longitude	23	10	19	°E
Annual thermal field output	685,063	693,739	591,828	MWh_{th}
Total annual net elect. output	212,474	215,610	190,741	MWh_{el}
Total annual gross elect. output	240,276	243,726	215,248	MWh_{el}
Specific thermal field output	1343	1360	1160	kWh_{th}/m^2
Specific electrical output	417	423	374	kWh_{el}/m^2
Mean annual field efficiency	49	47	46	%
Mean system efficiency	15	13	15	%
Full load hours	4806	4875	4305	h/a
Number of hours with at least temporarily full storage	298	336	166	h/a
Total Incremental Costs	222,080,107	220,207,995	235,011,067	€
Required Tariff (LCOE)	0.20	0.19	0.22	€/kWh
Levelized Electricity Costs (LEC)	0.13	0.13	0.15	€/kWhe

To some extent, the results for the three sites are relatively close. Al Jawf presents the highest efficiency (49%) in the solar field and 15% of the plant, while Dirj presents the highest annual net output of gross electricity 244 MWhel. In addition, both locations also may have the advantage of accessing largely available land. However, Al Ugaylah has the advantage of being near to the sea, and, in this way having available the required condenser cooling water. This aspect is important in

terms of capital costs because there is no need to use cooling towers and in addition, there will be a considerable reduction in freshwater consumption.

4.4 Chapter Summary

The main technological finding of the study is the advantage of Libya in terms of higher performance and lower LCE for the location of the CSP plant as compared to Southern Europe. Therefore, Libya has the potential of becoming attractive to establish CSP plants in its territory and, in this way, to facilitate the aim of several European initiatives of importing electricity generated by renewable sources from North African and Middle East countries. The analysis is based on the current cost of energy and it offers potential opportunities for reducing the cost of energy from parabolic trough solar power plant technology.

Chapter 5

Exergetic and Environmental Life Cycle Assessment of CSP Plants

5.1 Introduction

Environmental performance has become a key issue, and in the conception and design stages of a large-scale project; ways to minimize its impact on the environment should be investigated. Life Cycle Assessment (LCA) has emerged as one of the preferred tools to assess the environmental impact of a selected product or process over its life and it encompasses all its stages, including raw materials selection, production, assembly, use and disposal.

The present research lies in the use of a state-of-the-art exergetic analysis combined with LCA for CSP plants. The integrated analysis is used to evaluate the best combination in terms of operation, capital cost, and environmental impact. The Exergetic Life Cycle Assessment (ELCA) examines the flows of exergy within a system with the purpose of the reduction of exergy destruction and consequent improvement of efficiency. ELCA analysis is the most appropriate instrument to quantify environmental impact related to the depletion of natural resources [21] and integrates exergetic considerations into the LCA framework. Its applicability is clearly the same as that of LCA; however, its implementation requires a far more

comprehensive database. In particular, it needs the exergetic values of all inputs in addition to highly detailed disaggregated data of the processes involved. Its advantages with respect to LCA are the same as those of the Cumulative Exergy Content Method with respect to energy analysis; considering exergy instead of energy allows a thermodynamically correct assessment of both the resource base and its final use.

Exergetic and environmental life cycle assessment was carried out by employing the SimaPro software [104]. The analysis is concentrated on the already-selected 50 MW parabolic trough-CSP plant; and the data for the LCA was provided for a particular region in Libyan territory. The study intends to be a supporting tool in making decisions for future CSPs designs and their construction; the novelty of the study is based on the combined use of exergy and LCA for the simultaneous analysis of environmental and economic components of CSP plants. The objectives are: i) to assess the environmental impact and cost, in terms of exergy of the life cycle of the plant; ii) to find out the weak points of the process; and iii) to verify whether solar power plants have the potential of reducing environmental impacts and the cost of electricity generation.

5.2 Life Cycle Assessment - Concept

Life cycle assessment (LCA) is an objective process to evaluate environmental loads or impacts associated with products, processes or activities, based on the identification and quantification of the energy and materials used, and the waste and pollution emitted into the environment. International Organization for Standardization (ISO 14044) [105] defines the LCA as a methodology for assessing environmental impacts of a product throughout its life cycle by evaluating resource consumption and emissions. LCA has been used over the past four decades [106], starting from late sixties and early seventies [107]. In LCA, environmental aspects of all stages from the cradle-to-grave of a product's life are to be analyzed from the extraction of raw

materials needed to make the product to its final distribution as depicted in Figure 5.1. The method helps the decision makers select the products or processes that result in the least impact to the environment. This information can be used with other factors, such as cost and performance data, to select a particular product or process.

The goal of LCA is to compare the full range of environmental and social damages assignable to products and services, and allowing the choice of the least burdensome one. As a consequence, LCA succeeds not only in accurately measuring the impacts of the technology used for delivering products, but also the whole impact of making the economic choice of using it. The term “life cycle” refers to the notion that a fair, holistic assessment requires the assessment of raw material production, manufacture, distribution, use and disposal including all intervening transportation steps necessary or caused by the product's existence. The sum of all those stages is the life cycle of the product.

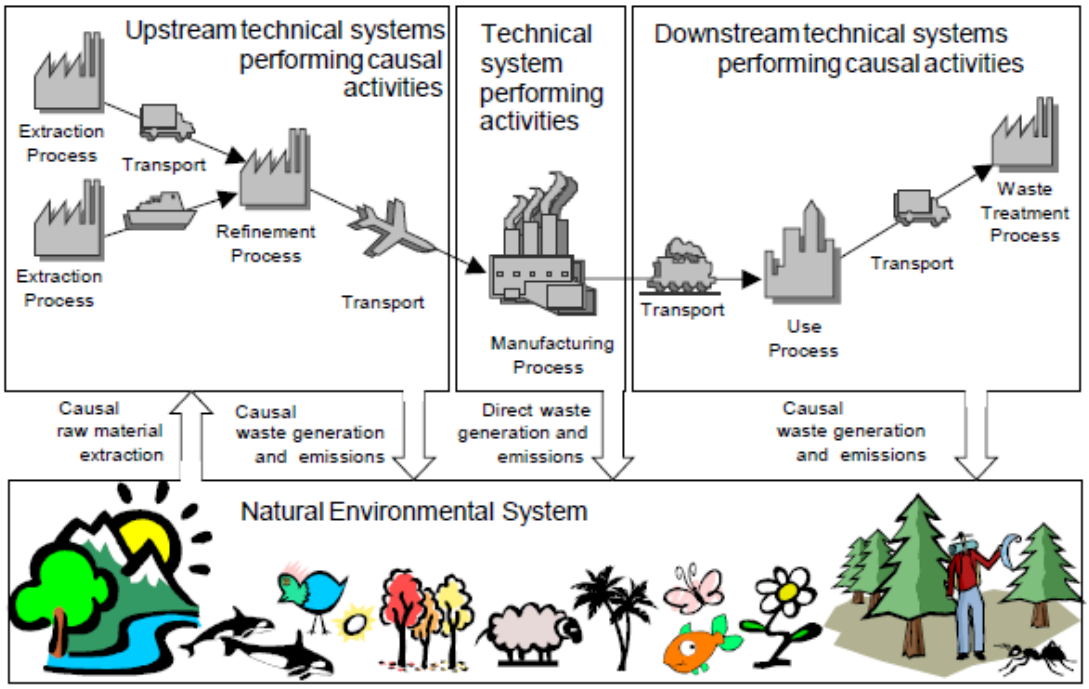

Figure 5.1: Schematic of Life Cycle Assessment stages of a product [108].

The concept also can be used to optimize the environmental performance of a single product (Eco-design) or to optimize the environmental performance of a company. Common categories of assessed damages are global warming (greenhouse gases), acidification, smog, ozone layer depletion, eutrophication, eco-toxicological and human-toxicological pollutants, habitat destruction, desertification, and land use, in addition to depletion of minerals and fossil fuels.

5.2.1 Overview of the Life Cycle Assessment Methodology

The procedures of life cycle assessment are part of the ISO-14000 environmental management standards: in ISO 14040 [109] and ISO 14044 [105] 2006, where ISO 14044 is a modified version of ISO 14041 to ISO 14043. The LCA methodology follows the ISO guidelines that standardized with the introduction of the international standards; the standard analysis contains of four interrelated steps: a) Goal and scope definition, b) Life cycle inventory (LCI) during which input and output data are collected and analyzed, c) Life cycle impact assessment (LCIA), and d) Interpretation of the results. The Life Cycle Inventory (LCI) involves tracking of all flows in and out of the system of interest – raw resources or materials, energy by type, water, emissions to air, water and land use by specific substance.

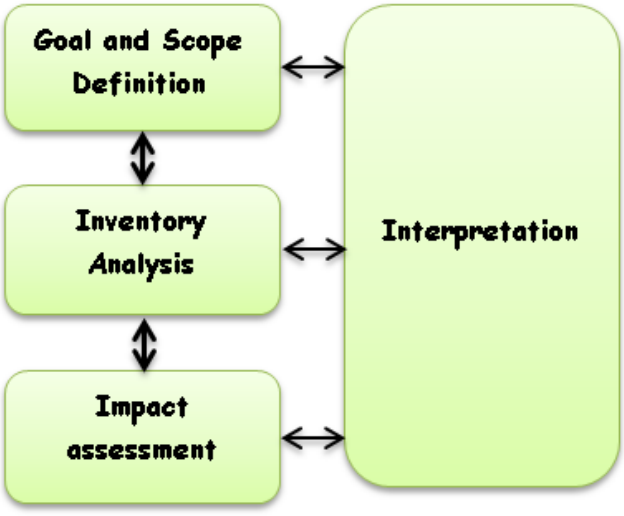

Figure 5.2: LCA analysis interrelated plan [110].

5.2.1.1 Goal and Scope Definition

Goal and scope definition is the first phase of LCA which contains goal, scope, functional unit, system boundaries, and data quality [107]. The goal defines the purpose of the study, intended use of the results, and users of the results. The scope provides the border of the assessment, providing the breadth, depth and the detail of the study. Functional unit is the foundation of an LCA which sets the scale for comparison and describe the object of study. In addition, the functional unit is defined to compare the systems on the same quantitative basis. Therefore, all the energy and mass flows in the inventory are normalized to the functional unit. Apart from describing the functional unit, the goal and scope should address the overall approach used to establish the system boundaries. The system boundary determines which unit processes are included in the LCA and must reflect the goal of the study.

5.2.1.2 Life Cycle Inventory (LCI)

The inventory stage involves data collection and modeling of the product system, as well as description and verification of data, and this is the most time consuming step. It entails identifying and quantifying resources used (including energy, raw materials, and capital), as well as waste and emissions generated at each phase of production in the entire life cycle of a product or process. A major part of any life cycle analysis is data collection of such inputs and outputs of the production cycle. This encompasses all data related to environmental such as CO_2 and technical (e.g., intermediate chemicals) quantities for all relevant unit processes within the study boundaries that compose the product system.

The inputs and outputs quantities include inputs of materials, energy, chemicals and other and outputs in the form of air emissions, water emissions or solid waste. Other types of exchanges or interventions such as radiation or land use can also be included. The data must be related to the functional unit defined in the goal and scope definition. The results of the inventory comprise the LCI, which provides

information about all inputs and outputs in the form of elementary flow to and from the environment from all the unit processes involved in the analysis.

5.2.1.3 Life Cycle Impact Assessment (LCIA)

The third step of life cycle analysis is the impact assessment, which evaluates the results of the LCI to understand their significance. The Life Cycle Impact Assessment is aimed at evaluating the contribution to impact categories, among others, global warming and acidification. It translates or converts inventory results obtained from the LCI into consequences in what could also be a qualitative or quantitative process. According to the definition, impact assessment has to be transparent and effective in terms of cost and resource use. LCIA contains four main elements: category definition, classification, characterization, and valuation [107]. Each of these elements represents a specific procedure, but all elements are not required for all applications. Impact categories describe impacts associated with a product system being considered. For instance, abiotic resources, biotic resources, land use, global warming, stratospheric ozone depletion, eco-toxicological impacts, human toxicological impacts, photochemical oxidant formation, acidification, eutrophication, and work environment are considered as impact categories [107]. The second element of LCIA is classification, which assigns the inventory input and output data to potential environmental impacts indicated above. Global impacts, regional impacts, and local impacts are three different divisions into which the impact categories are grouped. Quantification of environmental processes by scientific analysis is called characterization; it assigns the relative contribution of each input and output to the selected impact categories. As different impact categories have different units, they are plotted on a percentage scale. These quantified impact categories are weighted during valuation. There are different weighting methods available, such as proxy approach, technology abatement approach, monetarization, distance to target, and authoritative panels; each method focuses on different impacts [107].

In summary, the first step of LCIA is termed characterization. Here, impact potentials are calculated based on the LCI results. The next steps are normalization and weighting, but these are both voluntary according to the ISO standard. Normalization provides a basis for comparing different types of environmental impact categories. Weighting implies assigning a weighting factor to each impact category depending on the relative importance.

5.2.2 Interpretation of Results

The interpretation is the most important stage. According to International Organization for Standardization (ISO), interpretation is composed of specific steps: i) identification of significant environmental issues; ii) evaluation; and iii) conclusions and recommendations. These steps involve an interpretation of LCA results for communication, for process, product, or design changes, or for further purposes. Sensitivity analyses identify and check the effects of critical data on the results. They can be conducted by systematically changing input parameters.

5.3 Methodology of the Study

Two methodology tools are combined, namely, Exergetic and Environmental LCA, to evaluate the selected CSP plant. This combination allows studying thermodynamic irreversibility and its eventual reduction on a life cycle scale. The integration of these two tools leads to the use of exergy consumption as an impact category in the established LCA framework. The method used in the present study encompasses the following steps: develop LCA using Eco-indicator 99 method; perform an ELCA by using the Cumulative Exergy Demand Method. The analysis also aims to address the thermoeconomic analysis using the specific exergy costing (SPECO) method in order to evaluate the level of the cost caused by exergy destruction in each component and in the overall system. The final step is the selection of the best alternative considering the combined environmental, exergetic and economic performance.

5.3.1 Eco-Indicator 99 Method

To quantify the environmental impacts, different types of indicators are possible, categorized in two groups: problem-oriented (mid-points) and damage-oriented (end-points) [111]. The first group classifies impacts into environmental themes such as, just to name a few, global warming potential, acidification potential, ozone depletion potential. This method generates a more complete picture of the ecological impact, but requires good knowledge of the LCA to interpret the results. The second group translates environmental impacts into issues of concern such as human health, natural environment and resources. The results of the latter are easier to understand, but there is the risk of loss of transparency [112]. Eco-indicator 99 is a damage-oriented method and selected in the present work because it is widely used in LCA environment and it is supported by an extensive database. The damages are associated in three categories:

1. Human Health (HH), that sets, among others, the number of the years of life lost and the years of living disabled (DALYs), and it includes the following subcategories:
    - Carcinogens
    - Respiratory organics
    - Respiratory inorganics
    - Climate change
    - Radiation
    - Ozone layer

2. Ecosystem Quality (EQ), which takes into consideration the loss of species per area over a particular time span (species/m^2·year) includes the following subcategories:
    - Ecotoxicity
    - Acidification/eutrophication

- Land use

3. Resources (R), the coefficient of damage of the resources impact category is presented of surplus energy wanted for the new extraction in MJ, which includes:
    - Minerals
    - Fossil fuels

The categories can be combined into a single score [110]; the environmental impact is quantified in terms of increased energy needed for future extractions (MJ surplus energy). The impact categories can be added into 3 damage categories (human health, ecosystem quality and resources), weighted, and then aggregated into a Single Score, which represents the overall environmental load in points. One point (Pt) can be interpreted as one thousandth of the annual environmental load of one average European inhabitant [113]. There are three different approaches that determine the allocation of weights to the impact categories: Egalitarian perspective (HH 30%, EQ 50%, R 20%), Individual perspective (HH 55%, EQ 25%, R 20%) and Hierarchical perspective (HH 40%, EQ 40%, R 20%) [110]. The hierarchical approach is selected in the present analysis, and the results are expressed in a composite single score, which is determined on the basis of environmental impacts of each component.

In order to be able to use the weights for the three damage categories a series of complex damage models had to be developed; these models are represented in a schematic way in Figure 5.3. One of the advantages of the single score output of the Eco-indicator 99 method is that it makes it relatively easy to compare different system elements. At the same time, the subjectivity of the weighting factors is one of the main weaknesses of this method. The evaluation of each impact category is given by:

$$IMP_j = \sum_k d_{k,j} * LCI_k \qquad 5.1$$

Where IMP_j is the j impact category, $d_{k,j}$ is the coefficient of damage associated with the component k and impact j and LCI_k is the Life Cycle Inventory entry.

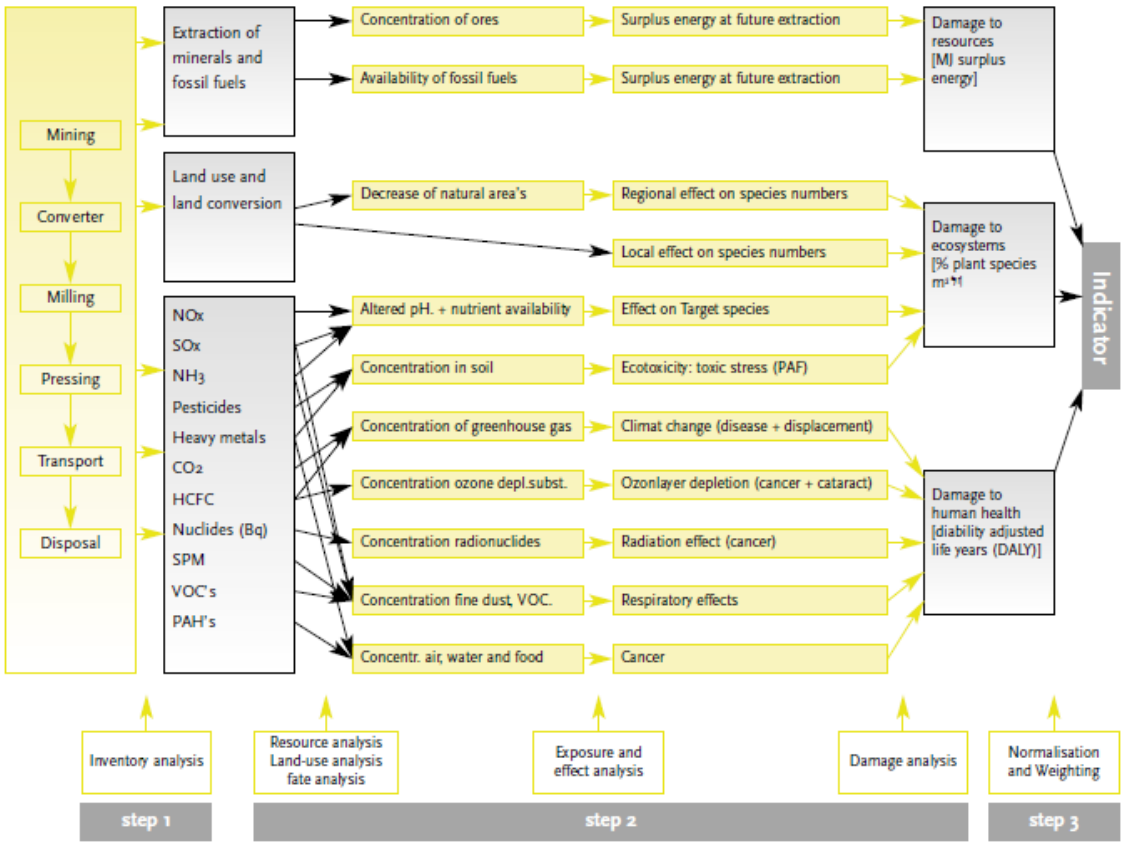

Figure 5.3: Detailed representation of the damage model [110].

5.3.2 Cumulative Exergy Demand Method

Exergy balances are determined for all unit processes by assigning specific exergy contents to all mass and energy inflows and outflows. The exergy terms comprise both physical and chemical exergy components. Combining two different perspectives within one combined method has large potential to make use of the strengths while reducing the weaknesses of the individual tools; in SimaPro environment, Cumulative Exergy Demand Method (CExD) is directly taken from Eco-invent. In this method, exergy is used as a measure of the potential loss of "useful" energy resources. CExD is a more comprehensive indicator where compared to the

Cumulative Energy Demand Method (CED) due to consideration of the quality of energy and the integration of non-energetic resources. All of the CExD categories proposed are significant contributors to Cumulative Exergy Demand in at least one of the product groups analyzed. In product or service assessments and comparative claims, careful and conscious selections of the appropriate CExD-categories are required based on the energy and resource quality demand concept to be expressed by Cumulative Exergy Demand method.

The work of Bösch et al. [22] is the basis for the implementation of the Cumulative Exergy Demand method. The CExD indicator was introduced to describe total exergy removal from nature to provide a product, summing up the exergy of all resources required. In addition, CExD assesses the quality of energy demand and includes the exergy of energy carriers in addition to non-energetic materials. The exergy concept is applied to the resources contained in the Eco-invent database, considering chemical, kinetic, hydro-potential, nuclear, solar-radiative and thermal exergies. The impact category indicator is grouped into eight resource categories fossil, nuclear, hydropower, biomass, other renewables, water, minerals, and metals. In SimaPro, the cumulative exergy demand method has ten different impact categories, which are detailed in Table 5.1. Therefore, the indicator CExD accounts for the exergy of resources that are removed from nature and, as a consequence, are not accessible anymore in future exploitation.

In comparison to the other indicators, the study of Bösch et al. [22] demonstrated that CExD provides a more differentiated and complete picture corresponding categories of CED, and resource depletion categories in CML'01 and EI'99. In this way, their work aims to present exergy scores for a large number of materials and processes and to compare the exergy scores with resource use and resource depletion scores from typical Life Cycle Assessment methods. Furthermore, the study illustrated that the exergy concept can be operationalized in product LCA.

Table 5-1: Impact categories in cumulative exergy demand as implemented in eco-invent data.

Category	Subcategory	Name
Cumulative exergy demand	Fossil	Non-renewable energy resources, fossil
	Nuclear	Non-renewable energy resources, nuclear
	Kinetic	Renewable energy resources, kinetic (in the wind), converted
	Potential	Renewable energy resources, solar, converted
	Water	Renewable energy resources, potential (in barrage water), converted
	Primary forest	Non-renewable energy resources, primary forest
	Biomass	Renewable energy resources, biomass
	Water resources	Renewable material resources, water
	Metals	Non-renewable material resources, metals
	Minerals	Non-renewable material resources, minerals

Cumulative exergy demand represents the total elimination of exergy of the nature in the generation of a system product, in this way demanding exergy from all necessary resources. The CExD is equivalent to the definition of cumulative exergy consumption [114], both quantify the total exergy required for a product. The CExD is calculated when adding the total of exergy required by a process during a period of time, and is specified in MJ equivalents to highlight that it is an impact assessment indicator and not an inventory elementary flow, namely:

$$CExD = \sum_i m_i * Ex\,(ch), i + \sum_j n_j * r_{ex-j,k} \qquad 5.2$$

Where:

m_i : The mass of resource i (kg)

$E_x(ch),i$: Exergy per kg of substance i (MJ-eq/kg)

n_j : The amount of energy from energy carrier j (MJ)

r_{ex} : The relation of exergy to energy of the carrier j (MJ-eq/MJ)

ch : Chemical exergy

k : Physical exergies (kinetic, potential, nuclear, radiative and thermal).

To compute the invested exergy, the exergy of all the inputs should be accounted for, and it is evident that the main exergy content is based on the inputs of fuels; they do not refer only to the energy directly used in the construction or disposal stage, but mainly to the energy used for production of materials.

5.3.3 Inventory Analysis

The first step in a LCA and ELCA study consists in clearly identifying the boundary of the studied plant from "the cradle to the grave". This requires specifying the production processes included in the analysis and the streams entering (input) and exiting (output) in the chosen boundary. Inside the system boundary, construction and dismantling stages are also considered. The analysis refers to the entire lifetime of the plant, which was assumed to be 25 years. Construction includes assembly of the equipment to produce the plants, considering raw materials and production processes.

In order to perform an approximate sizing of the plant under consideration, it was necessary to collect data about the different components of the equipment, weights, materials, scrap and the processes included in the manufacturing of each device in the plant. Often the only available data are referred to weights and materials. The inventory is largely selected based on Andasol-1 plant data [23,64,65, 117]. Based on the initial baseline scenario, only materials, which have relatively high contribution impact as detailed in Table 5.2, are selected. All data elements are referred to the functional unit – the CSP plant with nominal electricity production of 50 MWe. It should be noted the unit used as the reference for the detailed analysis conducted in the present work – the Andasol power plant, it is the first parabolic trough power plant in Europe and the first in the world with storage [102]. The plant consists of three main components as presented in Figure 5.4, namely:

- Parabolic trough collectors
  - Mirrors

  - Receiver tubes
  - Support structures
  - Solar tracking system

- Conventional system for generating electricity
  - Pumps
  - Steam turbine
  - Electrical power generator
  - Condenser
  - Heat exchangers

- Molten salt storage system
  - Heat exchanger
  - Pumps
  - Tow tanks (14m high and 36m in diameter)

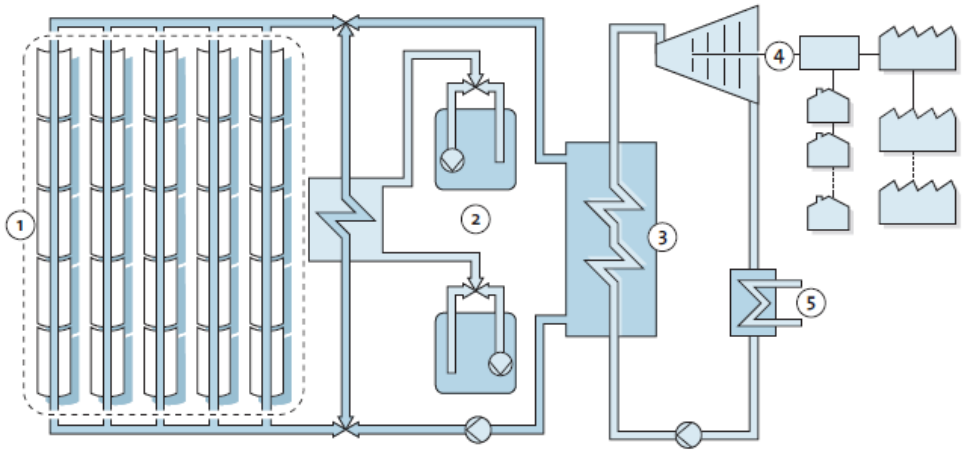

Figure 5.4: Flow diagram of Andasol 1 plant, Solar Millennium AG [102].

The power cycle is set up at the nominal production capacity of 50 MW, and the 2-tank indirect thermal storage system at the thermal capacity 1010MWh which corresponds to about 28500 tons of molten salts (60% sodium nitrate, 40% potassium nitrate) sufficient for 7.5 h electricity generation. In the balance of data for manufacturing and disposals of $NaNO_3$ in Eco-invent database, it was considered the

data for KNO_3 as a valid alternative. The correspondence between the experimental components and their processes and Eco-Invent v.3 database is summarized in Table 5.3.

Table 5-2: Life cycle inventory of Andasol power plant.

Material	Quantity			
	Solar Field	Storage System	Power Block	Total
Chromium steel [kg]	361889	112276	44050	518215
Concrete [m³]	19337.5	1628	83.6	21049.1
Synthetic oil [kg]	1995000	x	x	1995000
Flat glass coated [kg]	6148846		x	6148846
Molten salt [kg]	x	25600000	x	25600000
Reinforcing steel [kg]	15168192	386578	593258	16148028
Carbon steel [kg]	1916292	x	x	1916292

The solar field covers 510120 m², the field consists of 7488 collectors with 312 collector rows connected by tubes. The rows are set up on a north-south axis and they follow the course of the sun from east to west. Each row takes two collector units, and each collector unit has 12 collectors. Each collector has 28 mirrors and 3 absorption pipes. The heat transfer fluid HTF is synthetic oil (Therminol VP-1), type *Dowtherm A*, which is a eutectic mixture of two very stable organic compounds, biphenyl ($C_{12}H_{10}$) and diphenyl oxide ($C_{12}H_{10}O$).

Table 5.4 lists the transport stages which were considered in the present study where tKm refers to materials mass in ton multiplied by the distance in kilometers. In addition, dismantling includes disassembly of the plant and recycling or, when required, disposal of materials; a disposal scenario for the major materials is taken into consideration, as presented in Table 5.5 [27]. The present study is conducted for a particular location in Libya. However, sea transportation was assumed for materials produced in the United States and Europe; all local transportation is performed by trucks.

Table 5-3: The components in the Andasol plant as related to Eco-Invent v.3 Database.

Component	Eco-Invent V.3 equivalence	
Chromium steel	Steel, chromium steel 18/8 RER, steel production, converter, chromium steel 18/8, Alloc Def, U	
Concrete	Concrete, sole plate and foundation CH, production, Alloc Def, U	
Synthetic oil	Diphenylether-compound, RER, production, Alloc Def, U	
Flat glass coated	Flat glass, coated, RER, production, Alloc Def, U	
Molten salt	Potassium nitrate, RER, production, Alloc Def, U	
Reinforcing steel	Reinforcing steel RER, production, Alloc Def, U	
Carbon steel	Sheet rolling, steel GLO, market for, Alloc Def, U	
Chromium steel manufacturing	Metal working, average for chromium steel product manufacturing, RER, processing, Alloc Def, U	
Concrete excavation	Excavation, hydraulic digger RER, processing, Alloc Def, U	
Reinforcing steel manufacturing	Metal working, average for steel product manufacturing, RER, processing, Alloc Def, U	
Diesel burned in construction	Energy, from diesel burned in machinery/RER Energy	19.99E+6 MJ
Diesel burned in dismantling	Energy, from diesel burned in machinery/RER Energy	8.8E+5 MJ

The geographical boundaries: GLO = Global, RER = Europe and CH = Switzerland

Table 5-4: Transportation of the materials.

	Name in the database Eco-invent corresponding to the each process	Quantity [tKm]
USA	Transport, transoceanic freight ship, OCE	2.21E+08
Europe	Transport, transoceanic freight ship, OCE	9223269
Local	Transport, lorry > 16t, feet average, RER	107852.8

tKm refers to weight in ton times the distance in kilometers. OCE = Oceanic

Table 5-5: Waste fractions for calculating end of life impacts.

Materials	Eco-invent V.3 equivalence	Fraction %
Reinforced steel	Waste reinforcement steel (waste treatment) {CH}| treatment of waste reinforcement steel, recycling | Alloc Def, U	90
	Waste reinforcement steel (waste treatment) {CH}| treatment of waste reinforcement steel, collection for final disposal | Alloc Def, U	10
Concrete	Waste concrete, not reinforced (waste treatment) {CH}| treatment of, recycling | Alloc Def, U	95
	Waste concrete, not reinforced (waste treatment) {CH}| treatment of, collection for final disposal | Alloc Def, U	5
Glass	Waste glass (waste treatment) {CH}| treatment of waste glass, municipal incineration | Alloc Def, U	100
Chromium steel	Waste reinforcement steel (waste treatment) {CH}| treatment of waste reinforcement steel, recycling | Alloc Def, U	90
	Waste reinforcement steel (waste treatment) {CH}| treatment of waste reinforcement steel, collection for final disposal | Alloc Def, U	10
Molten salt	Salt tailing from potash mine (waste treatment) {CH}| treatment of, residual material landfill | Alloc Def, U	100
Synthetic oil	Waste mineral oil (waste treatment) {GLO}| market for | Alloc Def, U	100

5.3.4 Thermoeconomic Analysis

Thermoeconomic analysis combines exergy and economic principles in order to provide for more comprehensive information than that obtained using the conventional energy and economic analyses. The analysis aims to calculate separately the cost of each component, understand the cost formation process and the flow of costs in the system and, ultimately, to optimize specific variables in a single component or the overall system [118]. The specific exergetic cost (SPECO) [47,48] method is selected in the present study; and it is simplified in three steps [119], namely: define all energy and material flows that cross the control volume of each product, and determine the fuel and product exergy for each component. The third step aims to derive the exergetic cost rate balance and auxiliary equations for each component separately. The method is used in its simplest way, and in view of considerable uncertainties associated with the capital, operation and maintenance

expenses, their particular cost rate will not be considered. The cost rate of exergy destruction (€/h) for the component k ($\dot{C}_{D,k}$) is:

$$\dot{C}_{D,k} = c_k * \dot{E}_{D,k} \quad 5.3$$

Where c_k is the cost per unit exergy (€/kW h) of the component k and $\dot{E}_{D,k}$ is the rate of exergy destruction, and it is obtained by the difference between the input and output of the rate exergy:

$$\dot{E}_{D,k} = \dot{E}_{in,k} - \dot{E}_{out,k} \quad 5.4$$

The whole system cost rate of exergy destruction ($\dot{C}_{D,system}$) would be calculated as:

$$\dot{C}_{D,system} = \sum c_k * \dot{E}_{D,k} \quad 5.5$$

5.4 Results and Discussion

An exergetic and classical environmental life cycle assessment analyses of the CSP plant were carried out using the materials inventory of the Andasol power plant. The methodology used encompasses the following steps: determination of the energy consumption for the community, and LCA using Eco-indicator 99 method and ELCA in terms of the Cumulative Exergy Demand Method. The thermoeconomic analysis was conducting using specific exergy costing (SPECO) method.

5.4.1 Impact Assessment and Interpretation

The analysis includes the production of materials, and construction and disposal phases; Figure 5.5 represents only the network diagram of top-process of all life cycle stages.

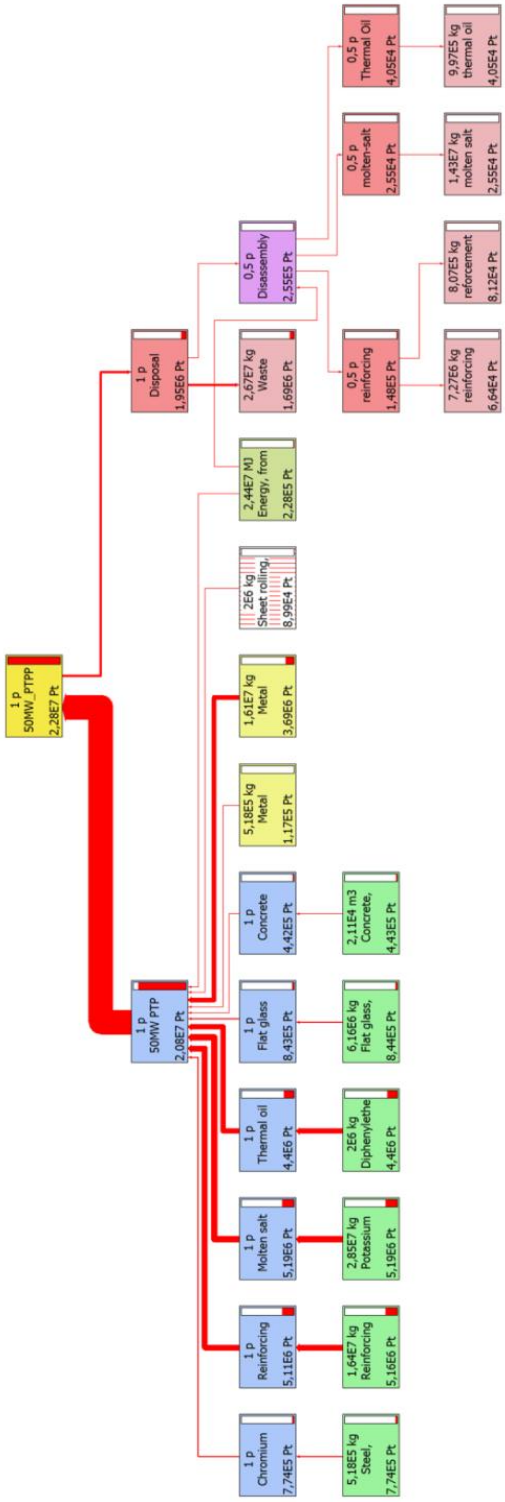

Figure 5.5: Network diagram of the top-process only performed within Simapro.

5.4.1.1 Classical Life Cycle Assessment

The results for the classical LCA are summarized in Figures 5.6 - 5.12. In the characterization indicator scale, substances that contribute to a particular impact category are multiplied by a factor that expresses their relative contribution to the category considered. The characterization result is indicated in a scale ranging from 0 to 100, as presented in Figure 5.6. The environmental damage categories are illustrated in Figure 5.7 for all components and they are represented in percentage; this allows assessing the contribution of all the unit processes to the damage categories (Human Health, Ecosystem Quality and Resources).

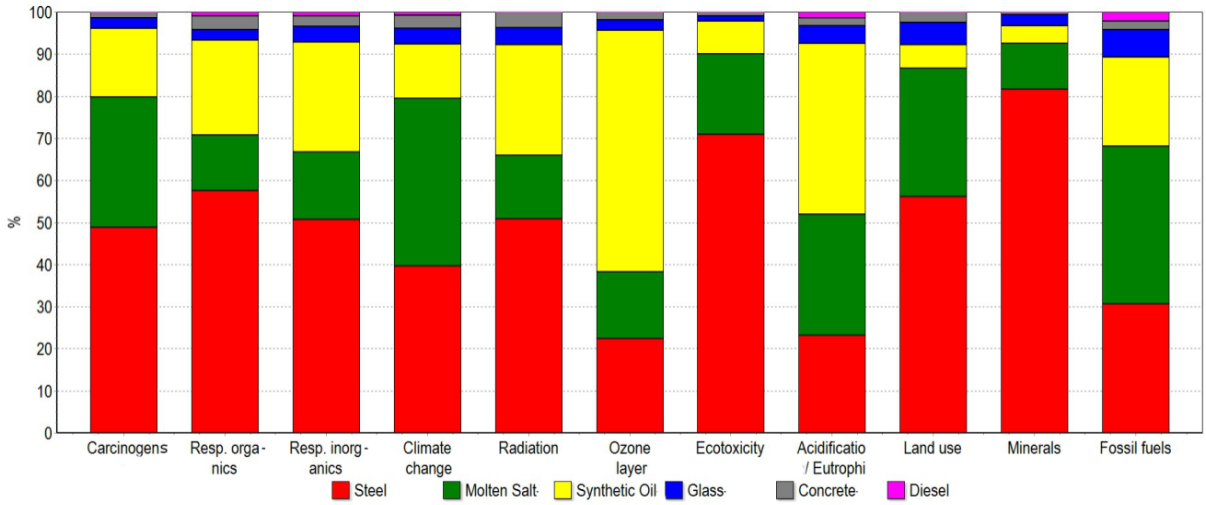

Figure 5.6: Graphical representation of the characterization phase.

Subsequently, the quantities that describe the environmental impact associated with the three macro-categories are divided by a normalization factor. Therefore, the indicators are presented in the same unit and the impact categories now can be compared; Figures 5.8 and 5.9 report the normalized results for the three damage categories and the individual impact categories respectively. In fact, the normalization is used to bring all impact categories to the same units and to indicate the relative contribution of each impact category to the normalized results.

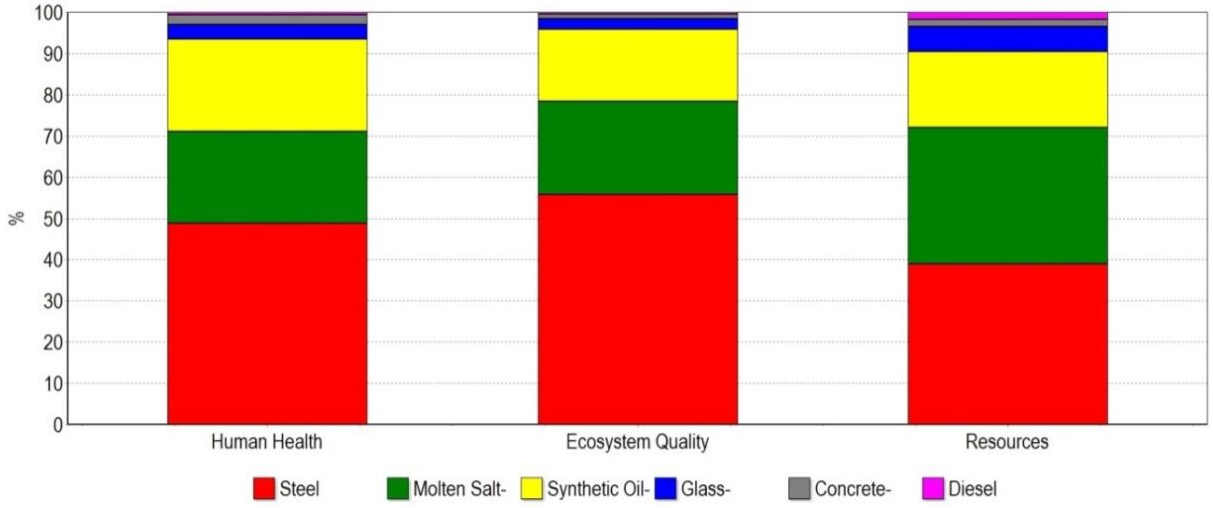

Figure 5.7: Graphical representation of the damage assessment phase.

The Human Health damage category presents the most impact with 69% followed by Resource damage category with 24% and finally Ecosystem Quality damage category with 7%; According to impact categories, the respiratory inorganics category gives the highest impact by 45.5% followed by fossil fuels with 20.4% and carcinogens impact category 14% while other categories have low impacts. The highest impacts come from steel, and then molten salt followed by synthetic oil.

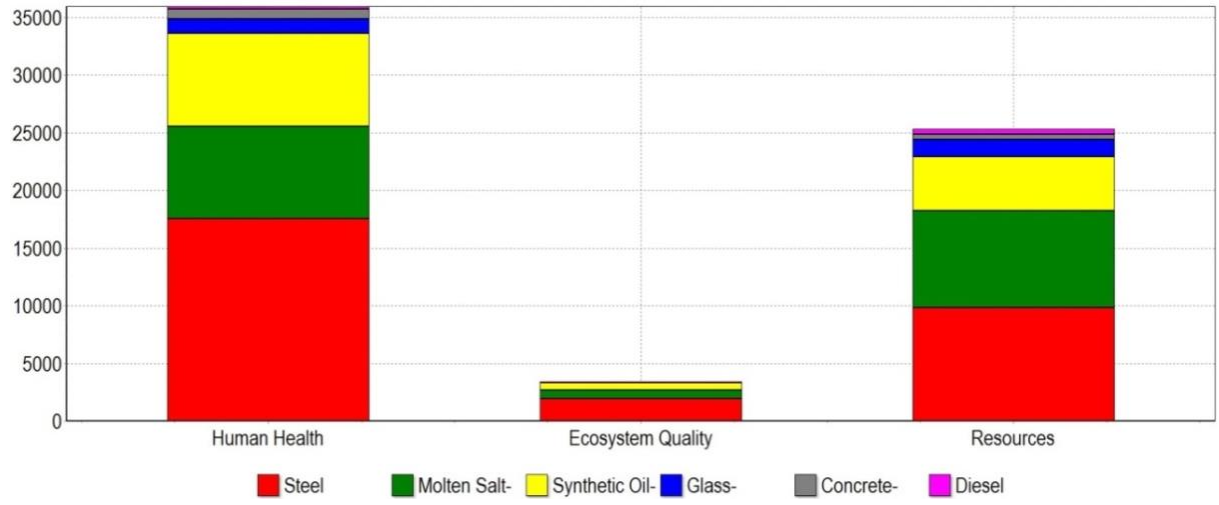

Figure 5.8: Graphical representation of the normalized results for the macro-categories.

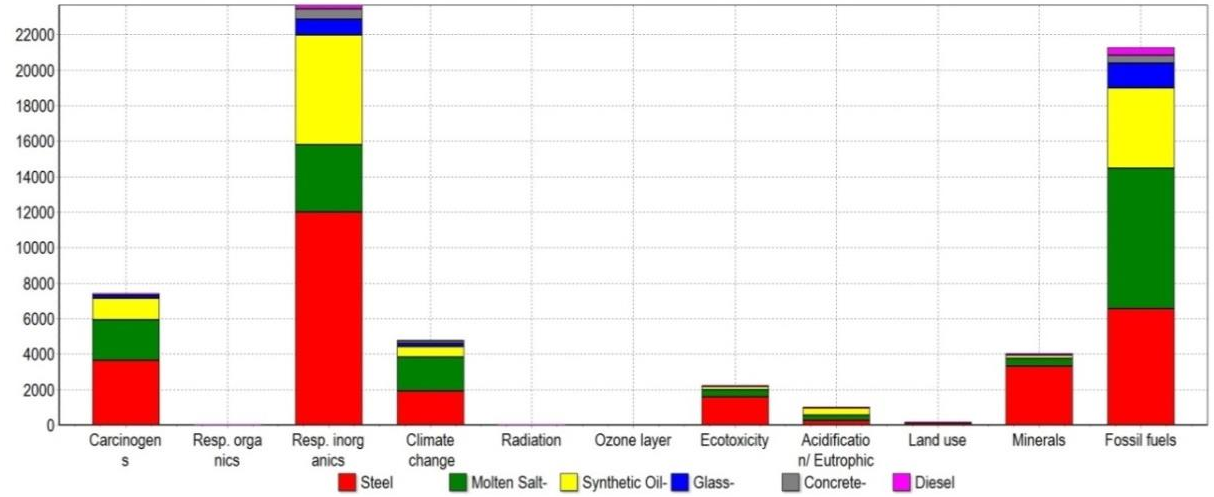

Figure 5.9: Graphical representation of normalized results for the individual impact categories.

Another scale to express the impact assessment consists of the attribution of a single score in MPt (million Pt, where Pt is a unit of measurement called the Eco-indicator Point) and it is reported in Figure 5.10.

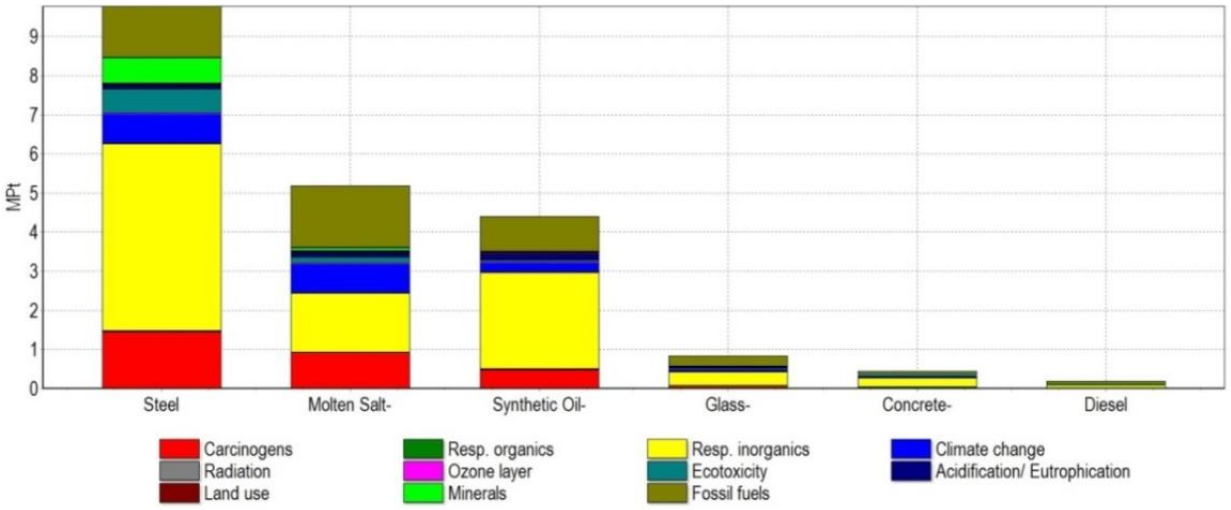

Figure 5.10: A single score result for the individual impact categories.

The steel, characterized by a total score 8.8 MPt, is the main contributor to the environmental impact; significant environmental impact is also associated with the molten salt with a score of 5.2 MPt and the synthetic oil with a score of 4.4 MPt. Then, in order of importance, they are glass, chromium steel and concrete, respectively.

The main contribution to the environmental damage is the impact on the Human Health category with a total score of 14.4 MPt followed by Resources and Ecosystem Quality with scores of 5 MPt and 1.4 MPt, respectively.

The life cycle single score of the environmental impact is compared against the result reported by Desideri et al. [11] in Pt for 1 MW h, which is presented in Table 5.6. The present study by using enhancing analysis, reports lower total impacts than that published in [1] as indicated in Table 5.6. The small differences may be attributed to the upgraded version of the materials inventory and the Eco-invent database used in the present study.

Table 5-6: Environmental impact derived from the LCA.

Impact category	Life cycle 1 MW h (Pt)	
	Desideri et al. [11]	The present study
Human Health (HH)	1.1	1.3
Ecosystem quality (EQ)	0.8	0.5
Resources (R)	0.4	0.13
Total	2.3	1.9

Figure 5.11 presents the comparison of the main subunits of the plant (solar field, storage system and power block), and also includes the transportation stage. The most important contribution impact is presented by the solar field (79%). The impact of the storage system is substantial; however, with a value approximately equal to 20.6%, it is much lower than that of the solar field. The power block and transportation impact are relatively small. This apparent disparity is due to the large amount of steel and synthetic oil used in the solar field to the quantity of the molten salt used in the storage system. The result clearly highlights that the lower damage belongs to the Ecosystem Quality category, while the higher damage contribution is related to the Human Health category, followed by the Resources category. In addition, the higher impact is associated with the respiratory inorganics, fossil fuel, carcinogens and climate change impact categories, respectively.

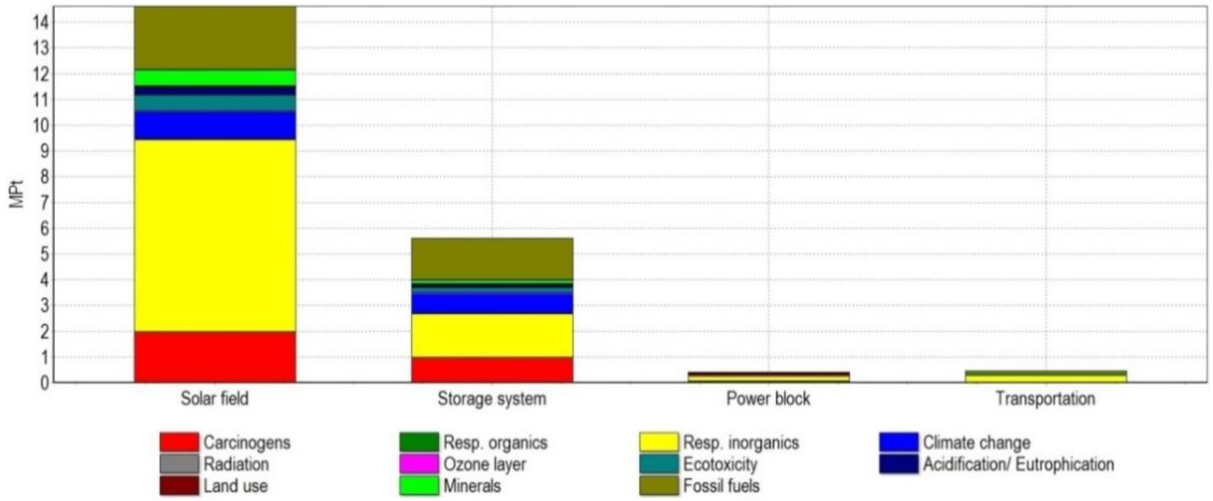

Figure 5.11: LCA comparison of three CSP plant subsystems and transportation.

Finally, a complete life cycle assessment analysis including the waste disposal and reuse of the components was carried out separately. This analysis aims to present the environmental impact caused by disposal and waste stage during the operation and at the end life of the plant. The result of this analysis is summarized in Table 5.7.

Table 5-7: Total life and disposal stages damage belonging the three categories.

Damage category	Unit	Total	Other stages	Disposal
Human Health	DALY	325	315	10.2
Ecosystem Quality	PDF*m²yr	4E+7	20E+8	2E+8
Resources	MJ surplus	2E+8	19E+8	4E+6

DALY refers to the number of year life lost and the years lived disabled

PDF.m^2.yr refers to the loss of species through a specific area and particular time

MJ surplus refers to energy demand.

In the absence of disposal requiring long term follow-up, such as radioactive or chemical waste, the impact of the disposal stage is relatively small (8.7% out of the total impacts), where the total impact is increased by 1.95 MPt. The significant increase impacts are related to the Human Health category followed by the Ecosystem category, where the damage impact of the Sources category is very small.

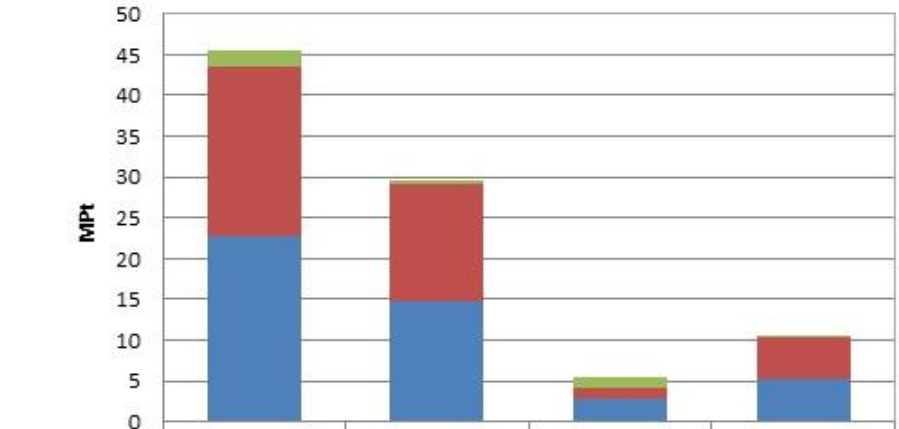

	Total	Human Health	Ecosystem Quality	Resources
Disposal	1,949000107	0,464023476	1,381425631	0,103551
Other stages	20,83172683	14,38331858	1,381948757	5,066459494
Total	22,78072694	14,84734206	2,763374388	5,170010494

Figure 5.12: Comparison the disposal stage against other stages in single score indicator.

5.4.1.2 Exergetic Life Cycle Assessment

The ELCA analysis for the plant under study was performed using the same inventory that was used for the LCA. CExD method is used in order to estimate the potential loss of useful energy resources in each alternative. The results are summarized in Figures 5.13 - 5.15; and the total CExD in the life cycle of the plant is reported in Table 5.8.

Table 5-8: The total CExD of the component of the plant.

Component	CExD [MJ]
Steel	1E+09
Molten salt	5.4E+08
Synthetic oil	4E+08
Glass	96461675
Concrete	55701623
Diesel	24026285
Total	2E+09

In the characterization scale, substances that contribute to a particular impact category are multiplied by a factor that expresses their relative contribution to each category. The characterization result is indicated in a scale ranging from 0 to 100; ten different impact categories are presented as shown in Figure 5.13. Figure 5.14 reports the exergetic demand attribution of each component and all categories. Figure 5.15 presents the weighting indicator of ECxD analysis in MJ associated with the different impact categories.

The material with highest exergy demand is steel (about 47% out of the total demand); the most important component of the exergy demand for steel is due to the non-renewable fossil fuel impact category, which has a contribution close to 82%. In addition, there is a considerable exergetic demand due to the molten salt and synthetic oil with percentages of 25% and 19%, respectively; the demand for other materials is relatively small. The resources of nature (non-renewables) categories such as non-renewable fossil, non-renewable nuclear and non-renewable metals impact categories present the largest demand with a value higher than 99%.

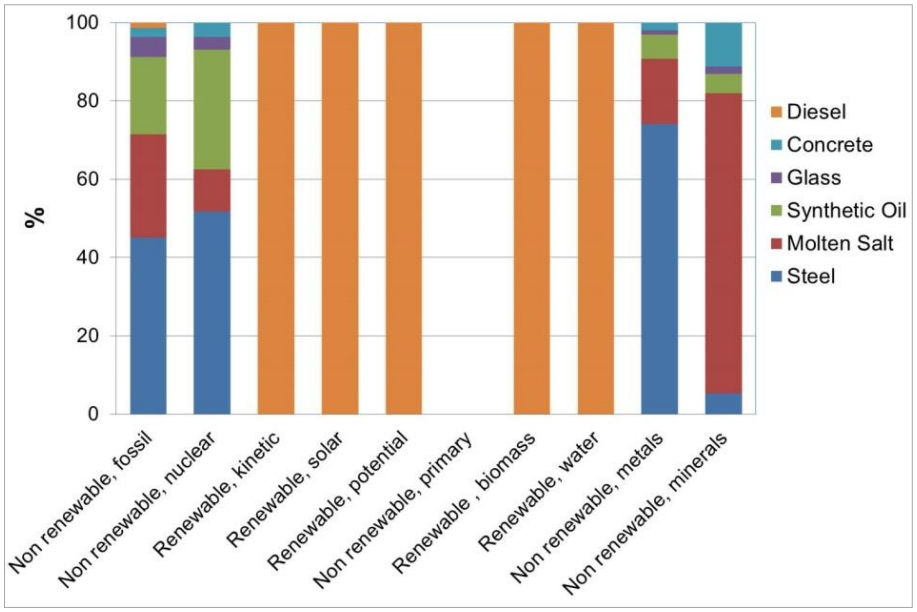

Figure 5.13: ELCA graphical representation of the characterization.

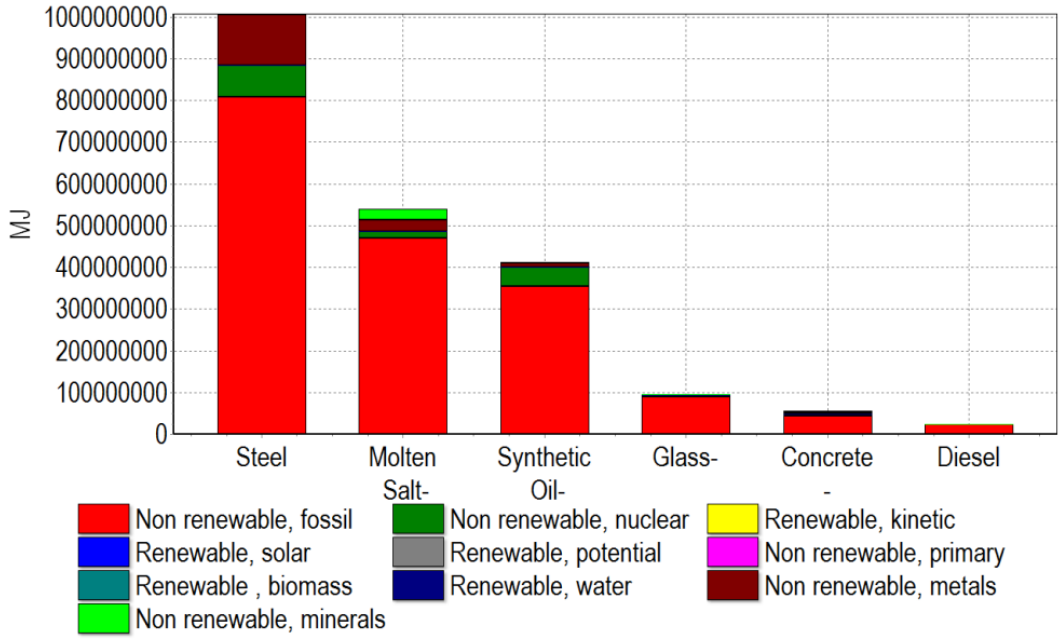

Figure 5.14: The attribution of the total CExD according to the single score indicator.

The material with highest exergy demand is steel (about 47% out of the total demand); the most important component of the exergy demand for steel is due to the non-renewable fossil fuel impact category, which has a contribution close to 82%. In addition, there is a considerable exergetic demand due to the molten salt and synthetic oil with percentages of 25% and 19%, respectively; the demand for other materials is relatively small. The resources of nature (non-renewables) categories such as non-renewable fossil, non-renewable nuclear and non-renewable metals impact categories present the largest demand with a value higher than 99%.

The study of Lechón et al. [23] reports the estimated cumulative fossil energy demand (CED) for the life cycle of the solar thermal power plants as summarized in Table 5.9. The study shows that the most of the fossil energy required is during the operation stage and it is mainly due to the natural gas and electricity consumption. The energy demanded for building and dismantling is found to be 0.16 MJ/kW h in the present study, where other studies report 0.19 MJ/kW h [23] of Spanish PTPP (the same plant considered in the present study) and 0.14 MJ/kW h for a SEGS plant

[120]. The present work has a few similarities with published work [26,120]; however, it is unique in what concerns the analysis and determination of the cumulative exergy demand (CExD).

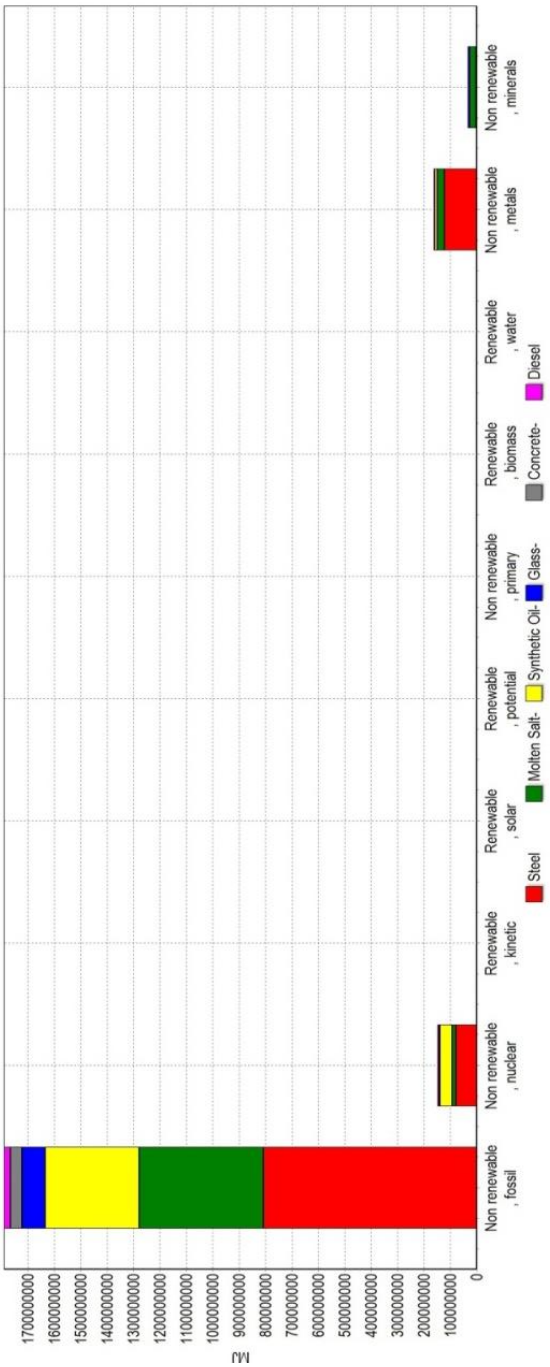

Figure 5.15: The weighting indicator of the total CExD referred to the individual impact categories.

Table 5-9: Cumulative energetic and exergetic demand of the parabolic trough-CSP plant.

	Lechón et al. [23]	The present study	
Component (MJ/kW h)	CED	CED	CExD
Solar field	0.09	0.13	0.15
Power block	0.004	0.003	0.006
Storage system	0.08	0.035	0.04

5.4.1.3 Comparison with Fossil Power Plants

To have a preliminary assessment of conventional power production practices as compared to a solar option, an environmental impact comparison of two fossil plants was conducted – one a natural gas combined cycle (NGCC) plant and the other an oil thermal power plant, with the CSP plant selected for the present study. These fossil plants are commonly used in Libya, since the country has large natural gas and oil resources; coal-fired plants or other plants using renewable technologies such as biomass are not considered in the present study because these plants do not exist in Libya. For the purpose of using the Eco-invent database, the fossil plants were selected based on the average of the European power plants. The results of this particular analysis indicate the CSP plant has the lowest environmental impact as compared to other plants with 20.8 Mpt, while the oil power plant presents the worst environmental performance with 430 Mpt, while the NGCC plant yields 150 Mpt. The CSP parabolic power plant has the advantage over the oil plant in all damage categories and over the NGCC power plant in the Resources and Human Health damage categories. However, the Ecosystem Quality damage category presents very small impact for the NGCC power plant (0.3 Mpt). The Resources damage category presents 77% for the NGCC plant and 53% for the oil plant. Oil and NGCC power plants demonstrate positive indicators in the land use category. The CSP technologies do not emit fossil carbon throughout the operational stage; therefore, the impact is primarily due to the construction (including materials) stage, which is higher due to the demand of materials per generated MWh.

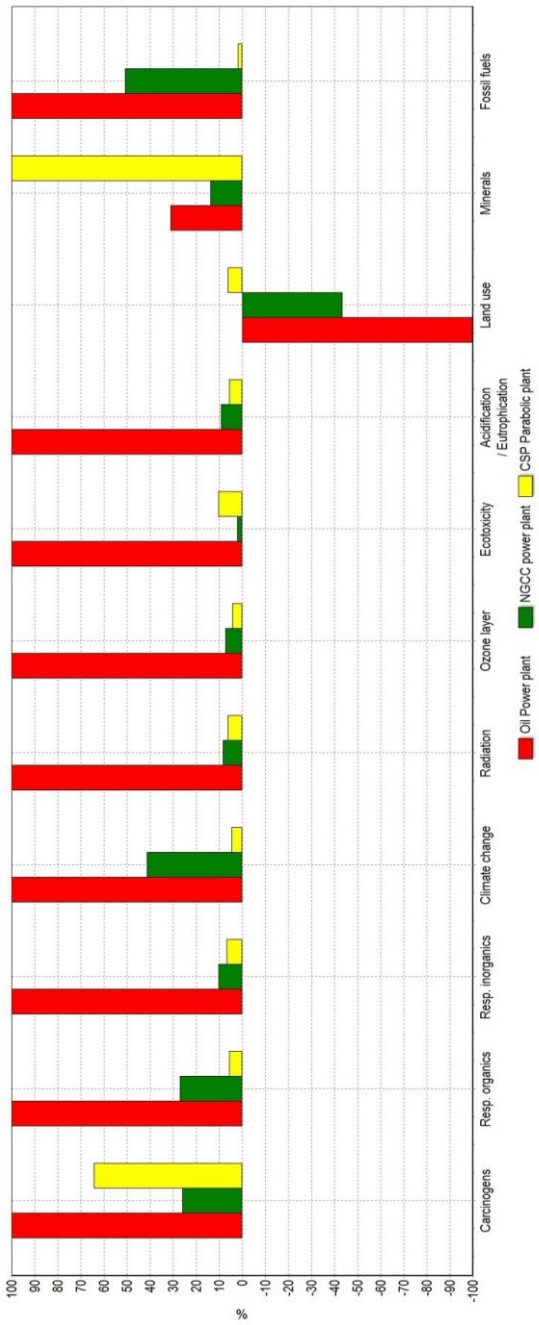

Figure 5.16: Comparison of the three power plants in attribution of a damage assessment indicator.

Table 5.10 summarizes the total damage impact of each category for each plant. This result was expected considering that fossil fuels are used in NGCC and oil plants; moreover, as known, the use of oil yields higher pollution than that for natural gas.

Table 5-10: Total damage associated with the three plants.

Damage category	Unit	NGCC power plant	Oil power plant	PTPP
Human Health	DALY	725	4E+03	325
Ecosystem Quality	PDF*m²*yr	4.2E+06	2E+08	2E+07
Resources	MJ surplus	4.4E+09	8.6E+09	1.9E+08

The study of Garcia et al. [121] reports the cumulative energetic demand of electric systems in Portugal. The oil power plant is the one with the highest value of CED (13.6 MJ/kW h), and the NGCC power plant presents 7.4 MJ/kW h. Lechón et al. [23] report a CED value of 2.5 MJ/kW h for the parabolic trough-CSP plant; it should be noted their study presents results close to those of the present study, as shown in Table 5.9. Therefore, from this comparison it is clear that the CSP plant is the one, among all the studied plants, with the lowest environmental impact and demand of energy.

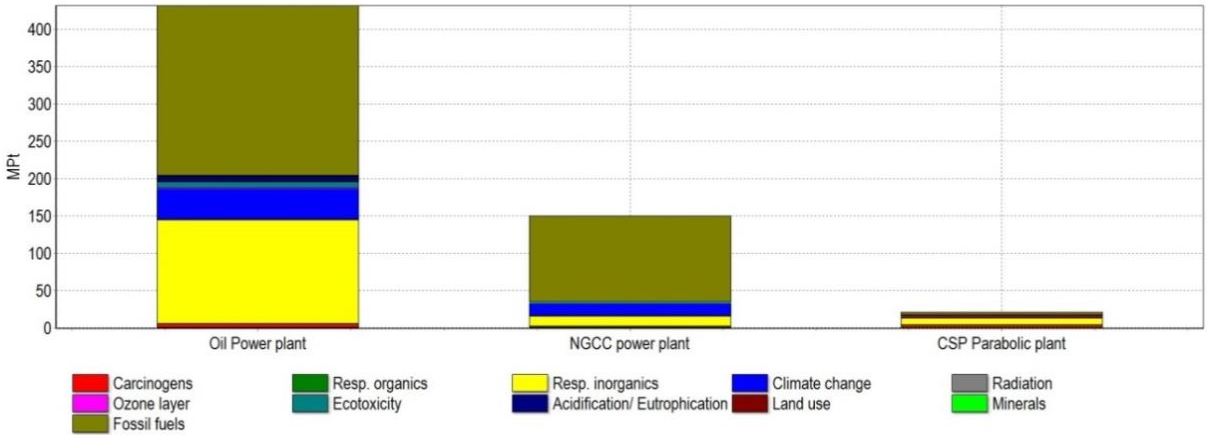

Figure 5.17: Comparison of the three power plants in terms of the single score indicator.

5.4.2 Results of the Thermoeconomic Analysis

The exergetic destruction of each product used is obtained from the results presented in chapter 3 with the exception of the values of exergy destruction for the solar field and condenser, which are taken from [18]. Table 5.11 summarizes the exergetic destruction and the cost rate per hour for the main components of the plant.

The values of cost rate per unit exergy of the components follows largely the work reported in [49]; however, for the boiler, it is calculated based on the data presented in [122]. In the absence of a SPECO analysis for this specific plant, the work of Elsafi [49] is used for comparison; the results are in close agreement; the highest cost rate takes place at the solar field, and the boiler is the component with the largest cost rate for the power cycle followed by the condenser, turbines and the pump. The reason for the high cost rate value related to the boiler is due to the extensive use of materials in the construction of numerous heat exchangers associated with the energy transfer between the solar field and the power cycle, and those required to accomplish the four stages for steam production - preheating, steam generation, superheating and reheating.

Table 5-11: Exergo-economic results.

Component	$\dot{E}_D$ (kW)	c ($/kW h)	$\dot{C}_D$ ($/h)	$\dot{C}_D$ ($/h) Elsafi study [49]
Solar field	89521	0.19	17636	12506
Boiler	10796	0.23	2526	X
HP Turbine	1252	0.24	303	302
LP Turbine	4063	0.24	983	998
Condenser	4440	0.25	1104	1040
Pump	124	0.3	38	43.5

5.5 Chapter Summary

The present research addresses the exergetic life cycle assessment of CSPs with the analysis focused on a 50 MWe parabolic trough-CSP plant. The Eco-indicator 99 (H) and Cumulative Exergy Demand methods were used to assess the midpoint and endpoint impacts from ‘the cradle to the grave’. The impact categories comprised global warming, acidification, eutrophication, ecotoxicity, carcinogens, respiratory organics, respiratory inorganic and climate change. The LCA reported that the Human Health damage category presents the most impact with 69% followed by Resource damage category with 24% and then Ecosystem Quality damage category

with 7%. The respiratory inorganics category presents the highest impact percentage (45.5%) followed by fossil fuels (20.4%) and carcinogens (14%), while other categories present low impacts. The materials with highest impact are: steel (47%), molten salt (25%) and synthetic oil (21%). The most important contribution impact lies with the solar field reporting a value of 79%. The impact of the storage system with a value of 20.6% was of the same order of magnitude of that of the solar field, while the power block and transportation impacts are relatively small. This apparent disparity is due to the large amounts of steel and synthetic oil being used in the solar field, and of molten salt in the storage system. The complete life cycle assessment analysis of the system included the waste disposal and reuse of the components after the useful life of the plant was conducted with the aim of learning about the environmental impact caused by the disposal and waste stages. Since there was no radioactive and fuel waste disposals, the impact of the disposal stage was low (8.7% out of the total impacts of all studied stages).

The ELCA analysis shows that the highest exergy demand was linked to the steel (approximately 47% out of the total demand), which is primarily due to the non-renewable fossil fuel impact category. In addition, there is a considerable exergetic demand related to the molten salt and synthetic oil with approximate values of 25% and 19%, respectively; while other demands are relatively small. The resources of the nature (non-renewables) categories such as non-renewable fossil, non-renewable nuclear and non-renewable metals impact categories presented the core of the demands with a value higher than 99%.

Comparing with two fossil technologies, the solar thermal power plant has the lowest environmental impact, while the oil power plant has the worst environmental performance. The solar thermal power plant has the advantage over the oil power plant for all damage categories, while the advantage over the NGCC power plant lies with the Resources and Human Health damage categories. It should be noted the NGCC power plant for the Ecosystem Quality damage category presents a very small

impact; however, in the Resources damage category, the highest impact is for the NGCC power with a value of 77%, while for the oil power plant for this indicator is 53%.

The thermo-economic analysis determines the average cost rates and the unit cost of components, specific cost per exergy unit of electricity. The solar field presents the maximum cost rate (17635 $/h ≈ 15532 €/h), and the boiler is the component with the highest cost rate (2526 $/h ≈ 2225 €/h) among power cycle components and the condenser (1104 $/h ≈ 972 €/h).

In concluding, the most important contribution impact is presented by the solar field and after by the storage system, however, CSPs present lower contribution impact than that of fossil systems. In addition, the highest cost rate is presented in the solar field that clearly due to the initial investments, which can be overcome by increasing the operation time due to the combined effect of cost savings related to the non-usage of fossil fuels in the power-generation process and the absence of a CO_2 tax.

Chapter 6

Numerical Analysis of Thermocline Thermal Energy Storage System for CSP Systems

6.1 Introduction

Energy storage is a crucial feature in the expansion of solar power systems for the sustained production of electricity. Thermal energy storage (TES) refers to the technology where heat can be stored in thermal reservoirs for later use. The application of TES technologies for such systems is necessary for the purpose of reducing the mismatch between energy supply and demand. The incorporation of TES into the operation of CSP plants offers the potential of delivering electricity without fossil-fuel backup even during peak demand, independent of weather conditions and daylight. The present chapter contributes to this specific area trough modeling and analysis of a thermocline energy storage system aiming better understanding of its dynamic temperature response. The reason is that the thermocline tank, as compared to other thermal storage systems such as the 2-tank technology, can decrease the construction costs due to the reduction of the materials usage and components; in this context, for large single-tank installations, the cost abatement can be as high as 33% [59].

Along this effort, the present study aims to develop a comprehensive analysis of the charging of a thermocline thermal energy storage tank for CSPs. There are several studies of thermocline thermal energy storage for CSPs, which, in general, examined the effect of varying different system parameters such as porosity, filler material characteristics, tank dimensions on overall performance of the thermal storage systems. In general, these studies perform the analysis of the thermocline storage tanks by considering packed-bed systems, and the numerical formulation is based on Schumann's one-dimensional model [123]. The model includes two heat transfer equations, when it is assumed the fluid and the packed-bed particles at different temperatures. For the particular case when the HTF is a liquid, a few studies point out that the difference between fluid and solid filler temperatures is small, because the heat transfer between them is very effective, as found by Bayon and Rojas [61]. Under these conditions, it can be assumed for that liquid and filler have the same temperature; hence, a single-phase model can be formulated, for which only one heat transfer equation is required.

A numerical model for the thermocline thermal storage system that can simulate its behavior and it has the potential of enabling enhancement of effectiveness, economics and operational characteristics of parabolic trough-CSP systems was developed. Comprehensive transient, charging stage was simulated and analyzed with particular emphasis on heat transfer and fluid dynamics within the thermocline thermal storage system. The thermocline thickness and effectiveness are examined as a function of the thermocline motion, effective thermal diffusivity and height of the tank. The main finding is that the predictions agree well with the experiments data that presented by the study of Zurigat et al. [72] for the time evolution of thermocline region, particularly for the regions away from the top-inlet. The deviations observed in the near-region of the inlet are most likely due to the high-level of turbulence in this region due to the localized level of mixing resulting; therefore, a simple analytical model to take into consideration this increased of turbulence level was developed and it led to some improvement in the predictions.

6.2 Thermal Storage Energy of CSP Systems

As already mentioned early in this chapter, the advantage of the incorporation of TES into the operation of CSP plants offers the potential of power generation without using fossil-fuel backup and meeting peak demand independent of weather conditions. The thermal storage is charged at the peak of solar energy availability for the duration of the day-time, and the stored heat will be released at night or during the time when there is not enough solar irradiation available [124]. In this way, CSPs become unique among renewable systems – they can provide utility-scale and dispatchable renewable energy when using TES systems. In addition, the long term use of TES can help to reduce the cost of the electricity production by allowing longer periods of operation time of the power cycle. The long-term strategy for CSP is to make them fully integrated into a power grid with adequate adaptation to auxiliary facilities, generator mix, including variable generation sources such as wind and solar photovoltaics. Solar thermal power plants with large storage capacity might be able to generate base-load solar electricity day and night, making it possible for low carbon to compete with fossil fuel power plants that emit high levels of pollutions. Therefore, CSP offers reliable and flexible electrical production capacity to utilities and grid operators, while also enabling effective management of a greater share of variable energy from other renewable sources.

There are three main technologies of TES that can be incorporated in the operation of CSP systems: sensible heat where a change of temperature occurs, latent heat where a change of phase occurs, and third technology is thermochemical energy where a reversible chemical reaction takes place; Figure 6.1 details these options. Among TES systems integrated with CSP power plants already in use, it should be mentioned that the Andasol power plant uses sensible heat storage in the liquid phase by using 2-tank molten salt system.

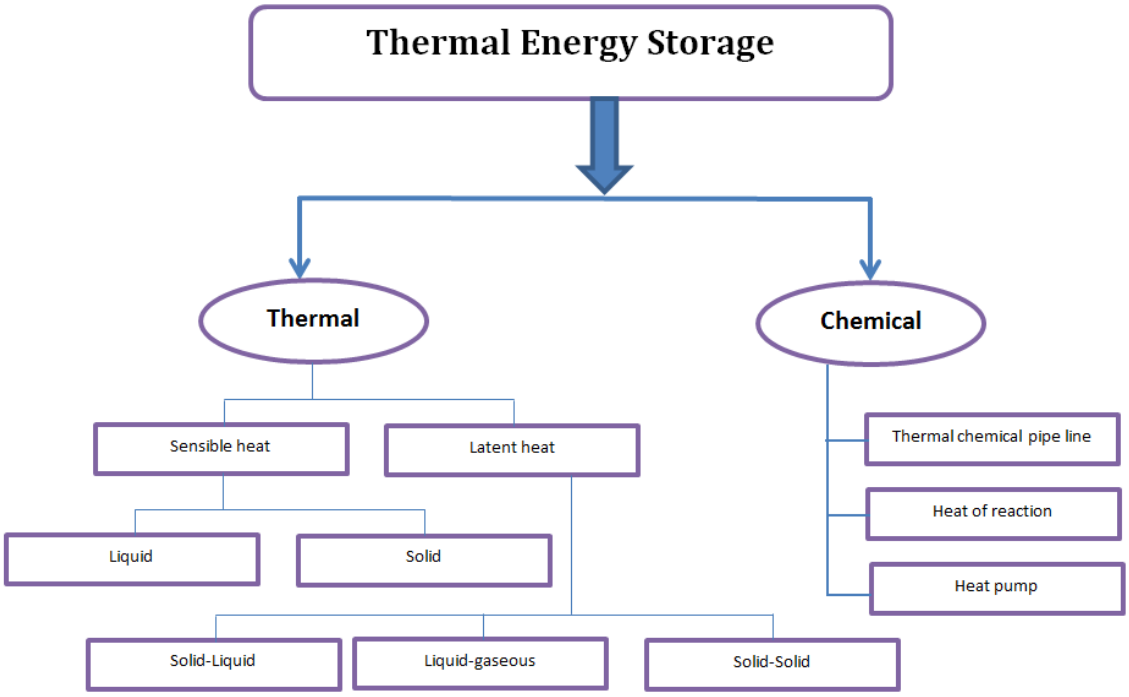

Figure 6.1: Different types of thermal storage of solar energy, Sharma et al. [125].

6.2.1 Sensible Heat Storage

Thermal energy sensible heat storage is the simplest form of storing thermal energy; in its simplest configuration, cold fluid contained in an insulated tank is heated up by the hot fluid coming from the solar field. Commonly in solar systems, the fluids in the solar field and in the storage system are the same; therefore, the heating is by direct contact, eliminating, in this way, the need for a heat exchanger. However, the problem with these systems is that the storage fluid reaches some average temperature between the starting storage temperature and the hot collector fluid temperature. If the quantity of thermal energy delivered by the collector field is insufficient to heat the entire storage to a temperature near that of the hot fluid, a significant loss in energy quality (availability) occurs in the storage system. Energy quality is usually an important factor in the design of high-temperature solar thermal energy systems. Otherwise, there would be no need to operate the solar collectors at high temperatures, which would decrease collector efficiency. Therefore, a 2-tank storage system can be used to avoid this particular problem.

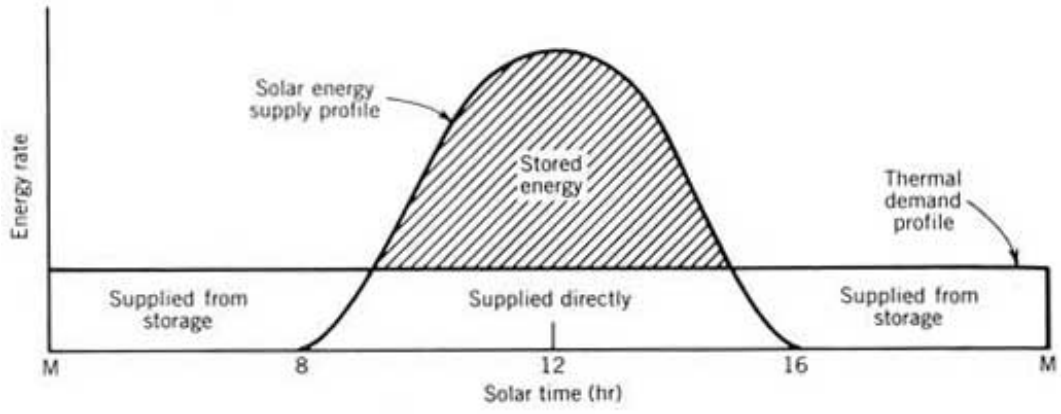

Figure 6.2: Overnight storage of thermal energy, [124].

A typical classification of sensible heat storage systems is:

- Multi-tank storage
- Thermocline energy storage (Single tank)
- Mixed-media thermocline storage
- High temperature sensible heat storage
- Pressurized Fluids.

The thermocline system is composed by a single tank including a packed bed used as the filling material; the hot and cold storage fluids occupy the same tank. Recently, these systems have received increased worldwide attention for their potential of providing extended storage capability with moderate capital costs due to the reduction of tank size as compared to the 2-tank systems; this is the reason why the present study is focused on the thermocline system. However, large-scale utilization of the packed-bed thermocline system is still hindered by several technical problems, among them the time-dependence of heat delivery and sizing requirements.

6.2.2 Latent Heat Storage

The most developed alternative to the sensible storage system is related to the use of phase change materials (PCM), which allows increasing stored energy density.

These materials store energy by undergoing a phase change either from solid to liquid, or liquid to vapor. To release the energy the reverse phase change will occur. Obviously, phase change materials have both latent and sensible enthalpies that contribute to the stored energy density; therefore, in this aspect, they have advantage over the purely sensible systems. However, one major issue with the PCM systems is the limitation to heat transfer during the charging and discharging of thermal energy. Typical values of PCM thermal conductivity range between 0.2 W/m-K and 0.7 W/m-K. This limitation results in low power density for PCM systems and will need to be overcome if PCM storage is to become a viable alternative. However, PCM storage is the most compatible storage system for the parabolic dish/Stirling concentrator because thermal energy delivery to the engine is isothermal.

6.2.3 Thermochemical Heat Storage

The last option, which is the thermochemical, offers perhaps the greatest advantage due to the large quantity of stored energy associated with the heat of reaction. Practical implementation of these systems is often limited by the loss of system performance when it goes through many charge/discharge cycles. System performance depends on maintaining consistent physical and chemical properties of the chemical components and of any solid-phase materials used in the system over many cycles. Over time, degradation of these material properties may result in reduction of both the system heat-transfer rate and storage capacity. In addition, some cycles require the handling of gas-phase reactants, which needs special construction materials. The advantage of very high energy densities and the possibility of storing reaction products at ambient temperature make thermochemical storage an interesting alternative for CSP technologies. The thermochemical energy storage system is one in which thermal power is used to break chemical bonds in a reversible manner. The breaking of chemical bond needs a large input of energy, allowing in this way effective thermal energy storage; the products of the thermochemical reaction are typically non-reactive at ambient temperature. At high

temperatures, the energy storing reaction is reversed, returning to the original chemical composition with the release of heat.

6.3 Life Cycle Assessment Comparative Analysis of Thermocline and 2-Tank Storage Systems

There are two prevailing design options for sensible liquid thermal energy storage: 2-tank and thermocline (single-tank) thermal energy storage systems. In 2-tank storage system, the hot and cold molten salt liquids are maintained in separate tanks. The system is charged or discharged by transferring excess heated fluid between the hot and cold tanks and delivering the stored heat to the power cycle. Up to date, the technology that was implemented in commercial CSPs is the 2-tank molten salt technology at Andasol plant, where the estimated cost is approximately 30 – 50 US$ (26 – 44 €) per thermal kWh [61]; it has been predicted that thermocline systems might have a significant cost reduction potential between 38% and 69% by 2020 [61,126]. In addition, as mentioned the cost of 2-tank storage technology can be reduced by combining the hot and cold tanks into single-tank (thermocline). Therefore, in addition to this advantage of reducing the cost, this analysis is aimed at finding whether reduction of environmental impacts can also be realized. Table 6.1 lists the materials used in both systems under study, which are designed to supply 6 hours of thermal storage for the 50 MW parabolic trough-CSP plant.

The result of the LCA analysis is summarized in Figures 6.3 and 6.4. As expected, the results show that the 2-tank system has the worst environmental performance due to the complexity of the design and because the materials and components used in 2-tank system are in much higher quantity than that required by the thermocline system. The result presents that the highest environmental impact is due to the molten salt since the amount of molten salt used in the 2-tank system is approximately three times that used by the thermocline system. The total single score impact of the 2-tank system is 5 MPt while 1.6 MPt for the thermocline system. The

main damage contribution is found in the Human Health category followed by the Resources and then the Ecosystem.

Table 6-1: The materials of 2-tank and thermocline systems of the plant under study [116].

Component	Eco-Invent V.3 equivalence	Quantity (kg)	
		Thermocline	2-tank
Refractory brick	Refractory, fireclay, packed {DE}| production | Alloc Def, U	157680	243455
Concrete	Concrete, normal {CH}| production | Alloc Def, U	3360000	5140000
Silica sand	Silica sand {DE}| production | Alloc Def, U	954070	x
Foam glass	Foam glass {GLO}| production | Alloc Def, U	16060	33105.5
Molten salt	Potassium nitrate {RER}| production | Alloc Def, U	7680000	25600000
Stainless steel	Reinforcing steel {RER}| production | Alloc Def, U	182080	417110
Carbon steel	Sheet rolling, steel {GLO}| market for | Alloc Def, U	801900	1357000
Mineral wool	Rock wool {CH}| production | Alloc Def, U	57670	103295
Nitrogen	Nitrogen, liquid {RER}| air separation, cryogenic | Alloc Def, U	28100	429000
Calcium silicate	Calcium silicate, blocks and elements, production mix, at plant, density 1400 to 2000 kg/m³ RER S	24476.9	49099

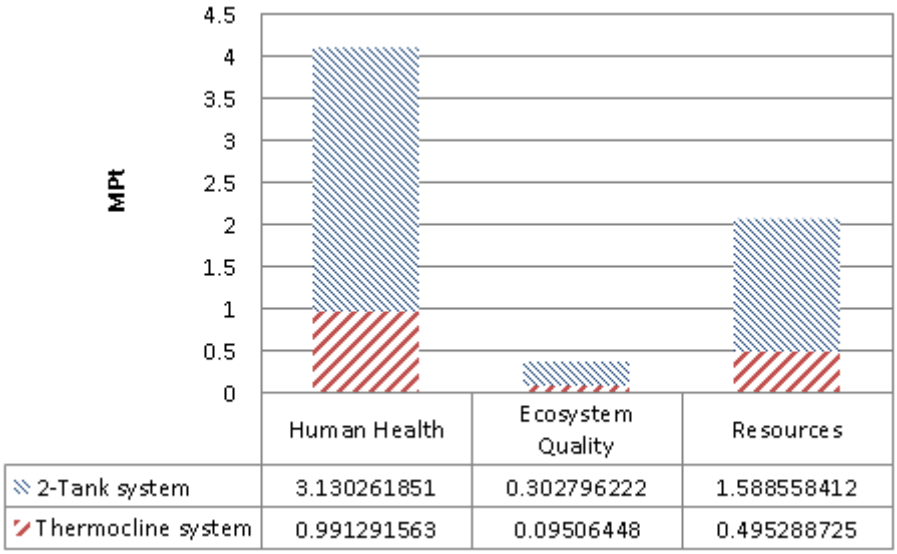

Figure 6.3: LCAs comparison of 2-tank and single storage systems.

As already mentioned, the single tank (thermocline) presents advantages in terms of cost and environmental impact; therefore, this system is to be further

analyzed in this study. The analysis intends to contribute to the better understanding of its operation in order to make it a viable alternative to the 2-tank technology.

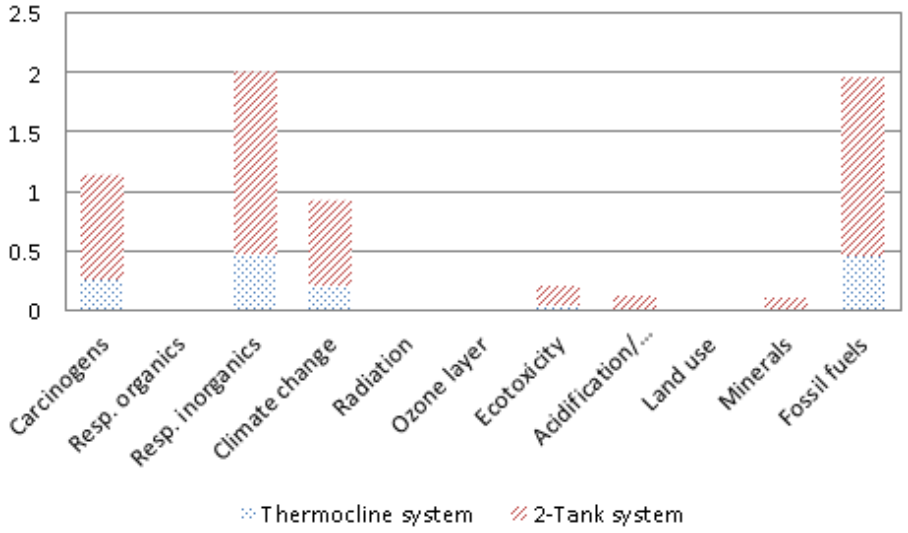

Figure 6.4: LCA comparison of 2-tank and single storage systems referred to individual impact categories.

6.4 Modeling of the Thermocline Thermal Storage System

The numerical investigation carried out follows largely [61] and the effectiveness is examined as a function of the thermocline motion, effective thermal diffusivity and height of the tank. The model is validated with the experimental data that presented by the study of Zurigat et al. [72]. The numerical model based on the resulting system of equations is solved by using time-implicit and space-backward finite differences within the Matlab environment. The aim of this component of the model is to describe the behavior of the selected storage tank by means of a result which accurately provides outlet temperature with time and can be implemented in any kind of code used for simulating the annual performance of a CSP power plant. The objective is to identify and solve a set of governing equations which economically and accurately characterize the dominant energy transfer mechanisms in a charging the storage

system. The packed bed filler and the heat transfer fluid (HTF) flowing through the free space, is characterized by a void fraction ε [127]:

$$\varepsilon = \frac{\forall_f}{\forall_f + \forall_s} \quad 6.1$$

Where $\forall_f$ and $\forall_s$ are the solid filler and fluid volumes, respectively. The energy balances are written in one dimension assuming that the significant temperature variations appear just in the axial (z) direction. The governing equations of the heat transfer fluid and packed bed are presented by Schumann [123] where they particles have different temperatures T_f and T_s, respectively:

$$\rho_f C_f \varepsilon \frac{\partial T_f}{\partial t} + \frac{\dot{m} C_f}{A} . \frac{\partial T_f}{\partial z} = h_v (T_s - T_f) \quad 6.2$$

$$\rho_s C_s (1 - \varepsilon) \frac{\partial T_s}{\partial t} = h_v (T_f - T_s) \quad 6.3$$

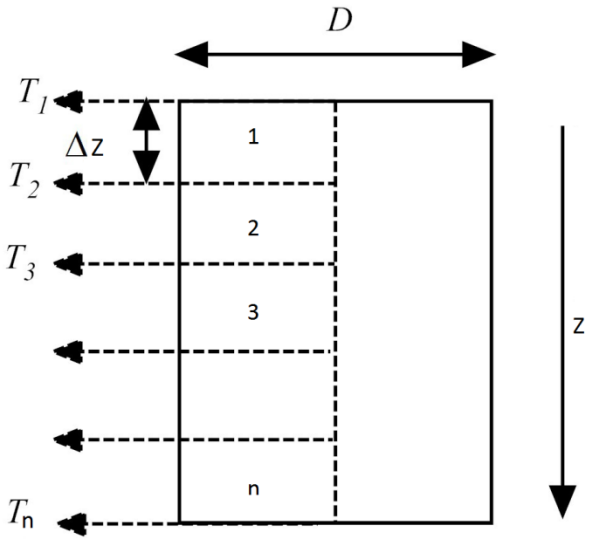

Figure 6.5: Differential control volume of the storage tank system.

The heat transfer between the fluid and the packed bed is accounted by a volumetric interstitial heat transfer coefficient h_v, which appears on the right-hand side of Equations 6.2 and 6.3; this interstitial heat transfer coefficient is related to

conventional convective heat transfer coefficient. However, in the present study, the thermal equilibrium between the HTF and the packed bed filler is assumed, i.e., their temperatures are at the same value. Therefore, equations (6.2) and (6.3) reduce to the equation 6.4, which describes the energy balance for the HTF within the storage system. The equation is solved iteratively for all control-volumes and time steps.

$$\left(\rho C_p\right)_{eff}\frac{\partial T}{\partial t}+\varepsilon\left(\rho C_p\right)_{liquid}\vartheta_{liquid}\frac{\partial T}{\partial z}=k_{eff}\frac{\partial^2 T}{\partial z^2}-U_w a_w(T-T_w) \quad 6.4$$

The thermal loss term $\mathrm{U_w a_w (T - T_w)}$ can be neglected because the tank is assumed to be reasonably well insulated and the main contribution to temperature variation with time and position is the movement of the thermocline zone; therefore Eq. (6.4) is simplified as follows:

$$\left(\rho C_p\right)_{eff}\frac{\partial T}{\partial t}+\varepsilon\left(\rho C_p\right)_{liquid}\vartheta_{liquid}\frac{\partial T}{\partial z}=k_{eff}\frac{\partial^2 T}{\partial z^2} \quad 6.5$$

The heat transfer equation is expressed in dimensionless coordinates aiming at the simplification of the solution procedure and to obtain general results in terms of performance parameters; consequently all variables are hence expressed in dimensionless form by means of the following normalization:

$$z^*=\frac{z}{L} \quad 6.6$$

$$t^*=\frac{t\alpha_{eff}}{L^2} \quad 6.7$$

$$\vartheta^*=\frac{\varepsilon\left(\rho C_p\right)_{liquid}L\vartheta_{liquid}}{k_{eff}} \quad 6.8$$

$$\Pi=\frac{T-T_{min}}{T_{max}-T_{min}} \quad 6.9$$

$$\alpha_{eff}=\frac{k_{eff}}{\left(\rho C_p\right)_{eff}} \quad 6.10$$

$$k_{eff}=\varepsilon k_{liquid}+(1-\varepsilon)k_{solid} \quad 6.11$$

$$\left(\rho C_p\right)_{eff}=\varepsilon\left(\rho C_p\right)_{liquid}+(1-\varepsilon)\left(\rho C_p\right)_{solid} \quad 6.12$$

The resulting dimensionless governing equation assuming the coefficients constant, is become:

$$\frac{\partial \Pi}{\partial t^*} + \vartheta^* \frac{\partial \Pi}{\partial z^*} = \frac{\partial^2 \Pi}{\partial z^{*2}} \quad 6.13$$

The energy stored as sensible heat by the tank filler and the energy either delivered in the discharging stage or accumulated in the charging stage are calculated using the following expressions:

$$Q_{Ideal} = AL\left(\rho C_p\right)_{eff}(T_{max} - T_m) \quad 6.14$$

$$\eta = \frac{Q_{delivered/stored}}{Q_{Ideal}} \quad 6.15$$

$$Q_{delivered/stored} = \left(C_p\right)_{liquid} \dot{m}_{liquid} t_{end}(T_{max} - T_m) \quad 6.16$$

The velocity of the fluid, ϑ_{liquid}, is directly related to $Q_{delivered/stored}$ as follows:

$$Q_{delivered/stored} = A\left(\rho C_p\right)_{liquid} \varepsilon \vartheta_{liquid} t_{end}(T_{max} - T_m) \quad 6.17$$

In the analysis of the process described by Eq. (6.13), the dimensionless volume tank is discretized in a certain number (n) of non-overlapping control volumes and each control volume at a temperature Π_i is represented by a spatial node Z^*_i. The finite control-volume method is used to discretize Eq. (6.13) combined with a backward implicit scheme; the resulting system of algebraic equations is solved using computer code within the Matlab environment. Formally, assuming the coefficients constant, the discretized equation is formulated as follows:

$$-\left(\frac{\Delta t^*}{\Delta z^{*2}} + \frac{\vartheta^* \Delta t^*}{\Delta z^*}\right)\Pi_{z-1}^{t+1} + \left(1 + \frac{2\Delta t^*}{\Delta z^{*2}} + \frac{\vartheta^* \Delta t^*}{\Delta z^*}\right)\Pi_z^{t+1} - \left(\frac{\Delta t^*}{\Delta z^{*2}}\right)\Pi_{z+1}^{t+1} = \Pi_z^t \quad 6.18$$

$$-A\Pi_{z-1}^{t+1} + B\Pi_z^{t+1} - C\Pi_{z+1}^{t+1} = \Pi_z^t \quad 6.19$$

Where $A = \left(\frac{\Delta t^*}{\Delta z^{*2}} + \frac{\vartheta^* \Delta t^*}{\Delta z^*}\right)$, $B = \left(1 + \frac{2\Delta t^*}{\Delta z^{*2}} + \frac{\vartheta^* \Delta t^*}{\Delta z^*}\right)$ and $C = \left(\frac{\Delta t^*}{\Delta z^{*2}}\right)$; which are organized in matrix form yields the following tri-diagonal matrix equation of the standard form ax=b:

$$\begin{bmatrix} B & -C & 0 & 0 & 0 & \cdots & \cdots & 0 \\ -A & B & -C & 0 & 0 & \cdots & \cdots & 0 \\ 0 & -A & B & -C & 0 & \cdots & \cdots & 0 \\ 0 & 0 & -A & B & -C & \cdots & \cdots & 0 \\ 0 & 0 & 0 & -A & B & \cdots & \cdots & 0 \\ 0 & 0 & 0 & 0 & -A & \cdots & \cdots & 0 \\ 0 & 0 & 0 & 0 & 0 & \cdots & \cdots & 0 \\ \vdots & \vdots & \vdots & \vdots & \vdots & \cdots & \cdots & \vdots \\ 0 & 0 & 0 & 0 & 0 & \cdots & -A & B \end{bmatrix} \begin{bmatrix} \Pi_1^{t+1} \\ \Pi_2^{t+1} \\ \Pi_3^{t+1} \\ \Pi_4^{t+1} \\ \Pi_5^{t+1} \\ \vdots \\ \vdots \\ \vdots \\ \Pi_{n-1}^{t+1} \end{bmatrix} = \begin{bmatrix} \Pi_1^{t+1} + A\Pi_0^{t+1} \\ \Pi_2^{t+1} \\ \Pi_3^{t+1} \\ \Pi_4^{t+1} \\ \Pi_5^{t+1} \\ \vdots \\ \vdots \\ \vdots \\ \Pi_1^{t+1} + C\,\Pi_{n-1}^{t+1} \end{bmatrix}$$

6.4.1 Simulation Results

The numerical code developed to systematically investigate the behavior of a thermocline energy storage system was validated in terms of solution accuracy and mesh convergence. Furthermore, the code was compared with a version using a time explicit scheme; although the predictions are similar, the proposed code shows a marked reduction (~20%) in terms of CPU time. In order to benchmark the numerical model, which is the core of the code, comparisons were conducted for particular types of thermocline tanks for which experimental results are available in the literature [72]. The test tank used in study of Zurigat et al. [72] is 0.4064 m in diameter, 1.4465 m in height and the impingement inlet is 0.018 m. The behavior of the tank with water only was investigated by taking into consideration the experimental data in [72]. The predictions with the proposed model are compared against the experimental data shown in Figure 6.6. The experimental results correspond to transient temperature profiles with minimum temperature (T_{min}), equal to 25.9˚C and the maximum temperature (T_{max}) is 50.8˚C. The main characteristics and design parameters of these tanks, and the physical properties corresponding to the storage media used in the simulations are reported in [72]. The numerical simulations allow the investigation of the thermal gradient, as well as temperatures, at all nodes of the HTF (water) as a function of time. Consequently, this information can be used for the analysis and

preliminary design of thermocline thermal storage systems. The results reported in this section are only concerned with the charging stage.

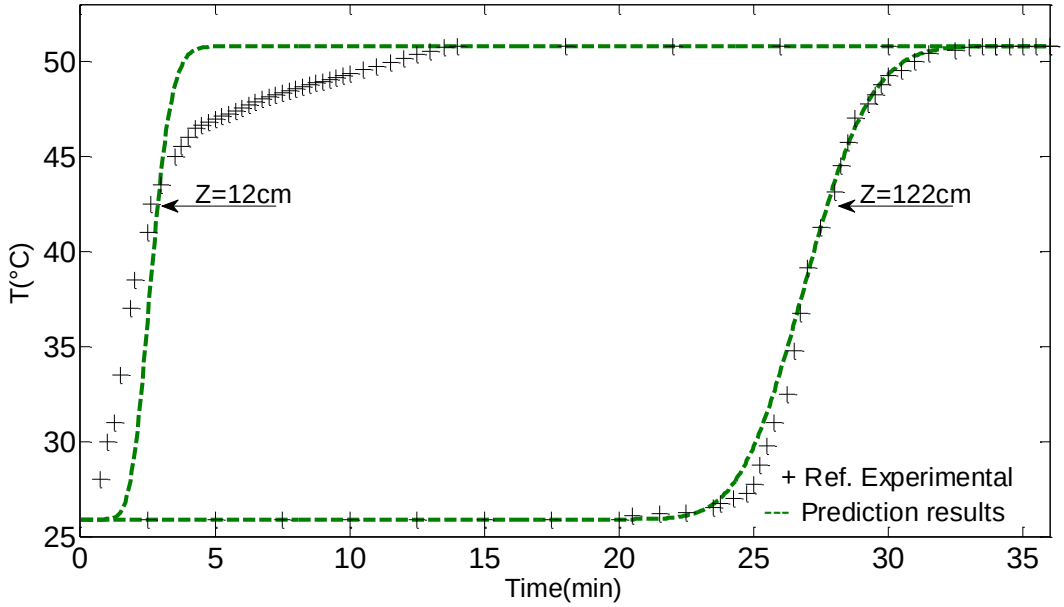

Figure 6.6: Transient temperature profiles at two different locations in the charging process comparison with the experimental data taken from Ref. [72].

The predictions show good agreement for the time evolution of the storage tank region of the experiments, particularly for regions away from the top-inlet region. Near the inlet region, the deviations observed, most likely, are due to the high level of mixing leading to high-level of turbulence - a situation that was anticipated for this particular model; therefore, the apparent mismatch between predictions and experimental results in this region should not be surprising. There are possible avenues for model enhancement by taking into account the presence of turbulence in the inlet region; however, the objective in this particular case is to improve the prediction capability of the model in what concerns the quantification of the turbulent mixing in the thermal storage tanks with minor increase in computational effort. Under these circumstances, one possible formulation relies on the mixing length relations for a round jet, in which the underlying assumption is that whenever a moving fluid enters a quiescent body of the same fluid, a velocity shear is created between the entering

and ambient fluids, causing turbulence and mixing. The turbulence characteristics greatly depend on the geometry of the flow domain; therefore, particular consideration should be given to this particular constraint. In addition, the mismatch between predicted and experimental temperature profiles observed in the vicinity of inlet region is due to local turbulence enhancement, different values for the effective thermal diffusivity are considered where the thermal conductivity and diffusivity are the most important thermophysical material parameters for describing the heat transport properties. Figures 6.7 and 6.8 report the impact of changing turbulent diffusivity at the inlet and outlet zones. The effective diffusivity is suggested to be 1, 10, 200 and 300 times, respectively, that of the momentum diffusivity for the location in the vicinity of the entering zone at z equal to 0.12 m; while, the effective diffusivity at z equal to 1.22 m is suggested to be 1, 2, 3 and 4 times, respectively, of momentum diffusivity. At the inlet zone, the value of the effective diffusivity that leads to the best agreement with the experimental results is 300 times that of momentum diffusivity, while in the region away from the inlet the effective diffusivity equals the momentum diffusivity, i.e., the turbulent diffusivity is practically negligible.

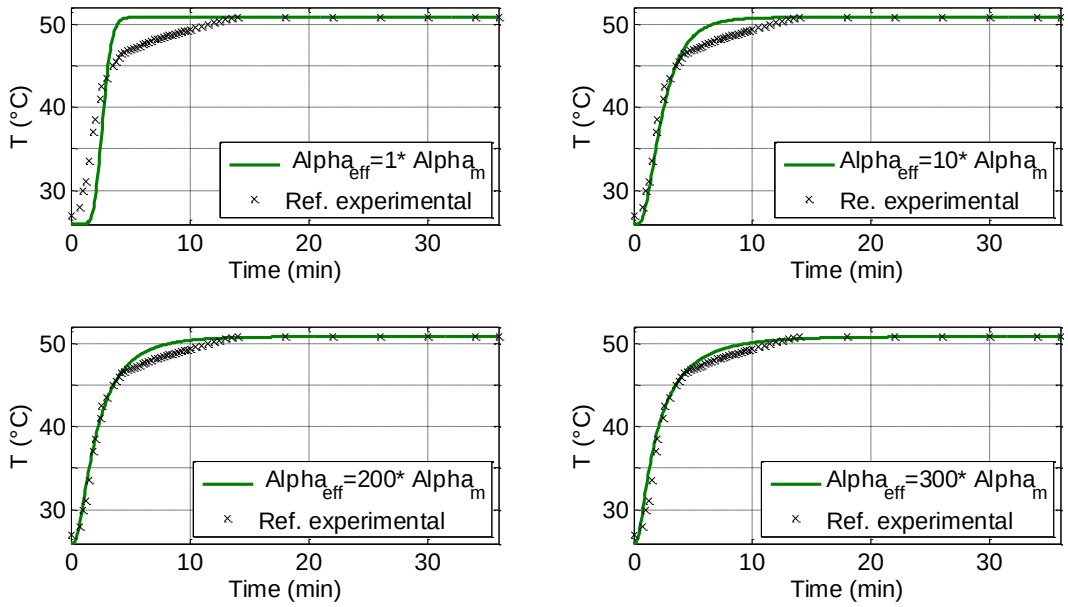

Figure 6.7: Predicted temporal temperature development for different values of the effective thermal diffusivity at the location z = 0.12 m compared with the reference experimental data.

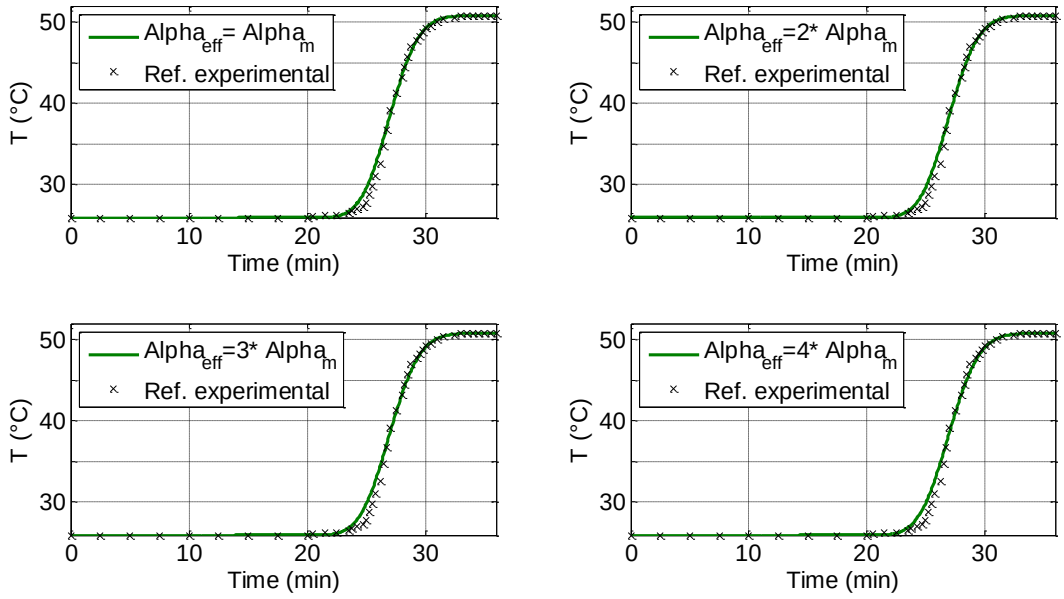

Figure 6.8: Predicted temporal temperature development for different values of the effective thermal diffusivity at the location z = 1.22 m compared with the reference experimental data.

These results give clear evidence that turbulence decay occurs along the downstream direction of the flow. Therefore, as mentioned before, one possible way of taking into consideration the effect of turbulence is using a scaled mixing length formulation for the round turbulent jet, which is based on the consideration the velocity structure. A suitable mixing length model may be capable of predicting the temperature time development along the downstream direction of the flow.

The effective diffusivity (α_{eff}) is equal to the summation of turbulent diffusivity and momentum diffusivity Eq. (6.20), where the turbulent diffusivity is equal to zero at the steady state zones for the undisturbed region, i.e., the effective diffusivity is constant and equal to the momentum diffusivity.

$$\alpha_{eff} = \alpha_M(1 + \alpha_T/\alpha_M) \qquad 6.20$$

Where α_M and α_T are the thermal diffusivity and the turbulent diffusivity, respectively. The turbulent diffusivity will be calculated based on the kinematic eddy viscosity (ν_T), by assuming the turbulent Prandtl number σ_T, has a constant value; therefore

$$\alpha_T = \nu_T/\sigma_T \qquad 6.21$$

The normalized governing equation 6.14 becomes:

$$\frac{\partial \Pi}{\partial t^*} + \vartheta^* \frac{\partial \Pi}{\partial z^*} = \frac{\partial}{\partial z^*}\left[\left(1 + \varepsilon \frac{k_{liquid}}{k_{eff}} \frac{\alpha_T}{\alpha_{liquid}}\right)\frac{\partial \Pi}{\partial z^*}\right] \qquad 6.22$$

Under these conditions the objective is to determine an appropriate relation for the eddy diffusivity. The procedure involves the following steps:

1. Calculate the inlet value of the eddy viscosity using the mixing length theory with the assumption the inflow behaves as a submerged round jet; and
2. Determine a damping function as a function of the distance away from the inlet.

Following the description of a turbulent round jet proposed by Cushman-Roisin [128], it can be simplified as depicted in Figure 6.9.

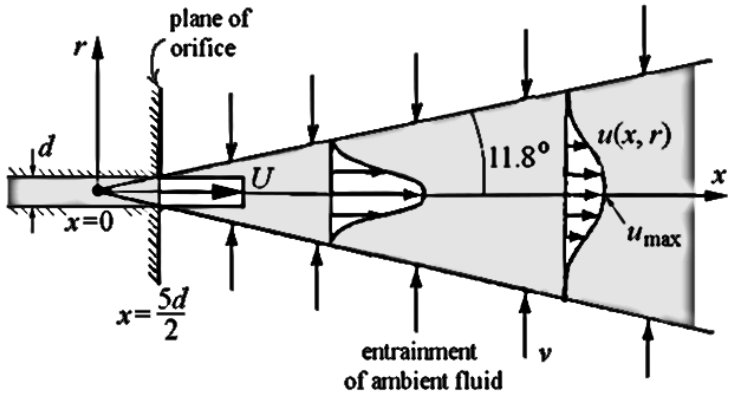

Figure 6.9: Simplified representation of a turbulent round jet penetrating a fluid at rest. The spreading is linear with the distance away from the inlet and the cross-jet velocity profiles, with the exception of that at the inlet are similar one to another [128]. The virtual source is at x=0

It should be noted that there is a universal angle of 11.8º yielding, since *tan(11.8◦) ≃ 1/5*, the relation between the jet radius (*r*) and the downstream distance (*x*) from the virtual source (Figure 6.9) is:

$$\delta(x) = \frac{1}{5}\, x \tag{6.23}$$

Where $\delta(x)$ is the distance from the centerline to the edge of the spreading. The initial jet radius is equal to half the exit diameter *d*; therefore, the distance *x* must be counted from a distance *5d/2* into the conduit, which is known as virtual source (Figure 6.9). The velocity profile across the jet presents a nearly Gaussian shape, which can be written as:

$$u(x,r) = u_{max}\, exp(-\frac{r^2}{2\sigma^2}) \tag{6.24}$$

Where *x* is the downstream distance along the jet (counted from the virtual source), *r* is the cross-jet radial distance from its centerline, $u_{max}(x)$ is the maximum speed at the centerline, and $\sigma(x)$ is the standard deviation related to the spread of the profile across the centerline. The value of σ is equal to *x/10* [128], and Eq. 6.24 can be rewritten as:

$$u(x,r) = u_{max}\, exp(-\frac{50r^2}{x^2}) \tag{6.25}$$

In [128] the relations for maximum velocity (u_{max}) and the average velocity ($\overline{u}$), respectively, are as follows:

$$u_{max} = \frac{5d}{x} U \tag{6.26}$$

and

$$\overline{u} = \frac{5d}{2x} U \tag{6.27}$$

Where U and *d* are respectively the average exit velocity and the orifice diameter. Therefore, the velocity along the centerline of the jet decreases inversely with distance from the virtual source (i.e. the ratio U/u_{max} increases linearly with distance as shown in Figure 6.10). Taking the mixing length hypothesis leads to the formulation of the kinematic eddy viscosity [129]:

$$\nu_T = l_{mix}^2 \left|\frac{\partial u}{\partial r}\right| \quad 6.28$$

Where l_{mix} is the mixing length; and introducing $\frac{\partial u}{\partial r}$, which is derived from Eq. 6.25, into Eq. 6.28, it results:

$$\nu_T = l_{mix}^2 u_{max} \frac{100r}{x^2} exp(-\frac{50r^2}{x^2}) \quad 6.29$$

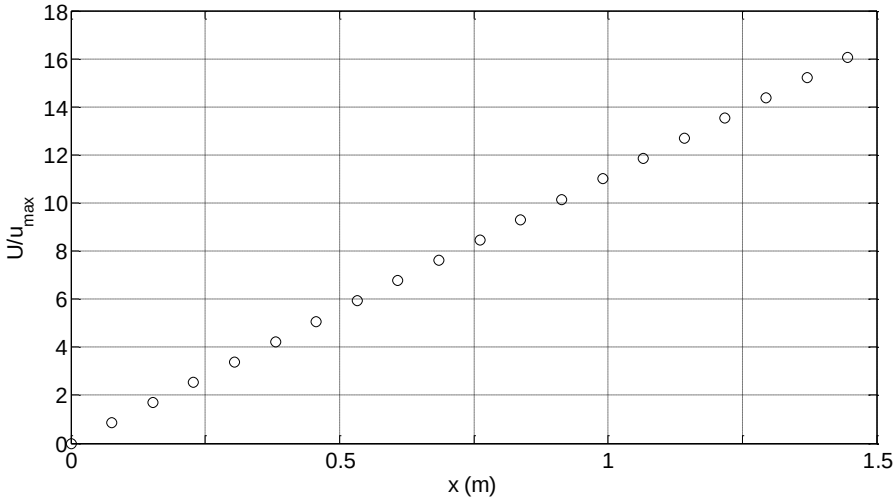

Figure 6.10: The ratio (U/u_{max}) increase linearly with the distance away from the tank inlet.

Considering the aim is to develop a one-dimensional model, in Eq. 6.29 the radial position r will be taken at $\delta(x)$ leading to:

$$\nu_T = l_{mix}^2 u_{max} \frac{100\delta(x)}{x^2} exp(-\frac{50\delta(x)^2}{x^2}) \quad 6.30$$

Taking the relation given in [129] between l_{mix} and $\delta(x)$

$$l_{mix} = \xi\delta(x) \quad 6.31$$

into Eq. 6.31, it results

$$\nu_T = (\xi\delta)^2 u_{max} \frac{100\delta}{x^2} exp(-\frac{50\delta^2}{x^2}) \quad 6.32$$

Where ξ is a constant equal to 0.08 [129]. By introducing the relations for $\delta(x)$ and u_{max} into Eq. 6.32, it yields

$$\nu_T = (\xi \frac{1}{5} x)^2 \frac{5d}{x} U \frac{100(\frac{1}{5}x)}{x^2} exp(-\frac{50(\frac{1}{5}x)^2}{x^2}) \quad 6.33$$

or

$$\nu_T = 0.04dU \quad 6.34$$

Therefore with a value of σ_T equal to 0.9, the thermal diffusivity is

$$\alpha_T = 0.05dU \quad 6.35$$

This relation for α_T is a constant value along the axis of the jet; and several time-dependent simulations indicate that is suitable for the inlet mixing region; however, it predicts poorly outside this region. Under these circumstances, it is proposed to introduce an exponential decay of α_T as a function of *x*. Similarly to the Van Driest damping function [130], although this physical situation is different, the model takes the following form:

$$\alpha_T = 0.05dUexp(-ax) \quad 6.36$$

Where a is a fitting constant designed to have the value of α_T reduced to 10% of its original value at the end of the zone of flow establishment (ZFE). According to [131] the length of the zone of flow establishment, x_{ZFE}, is

$$x_{ZFE} = K_1 d \quad 6.37$$

where K_1 is a constant and equal to 5.1 [131]. If *z* is the distance away from the inlet, then

$$z_{ZFE} = K_1 d - \frac{5d}{2} \quad 6.38$$

The resulting equation using the distance away from the inlet and based on Eq. 6.36 is

$$\alpha_T = 0.05dUexp(-50z) \quad 6.39$$

Figure 6.11 shows the profiles of the effective thermal diffusivity variation with the height of the tank (z). It can be seen that the effect of thermal diffusivity reflects reasonably well to the presence of turbulence caused by the mixing originating from the tank inflow. As the thermal diffusivity is depending on the velocity, they steady declines with the height of the tank.

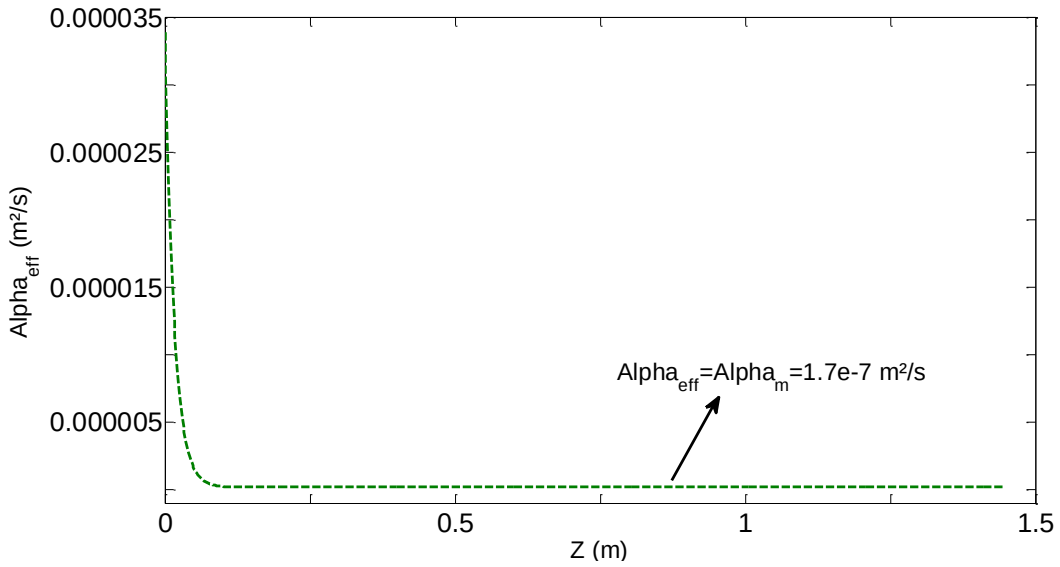

Figure 6.11: Actual effective diffusivity variation with the height of the tank.

Figure 6.12 presents the temperature profiles predicted by mixing length model comparison with experimental data taken from [72] and the first result (Figure 6.6), it can be observed that the result fits well the experimental data bringing a marked improvement to the prediction at the inlet region.

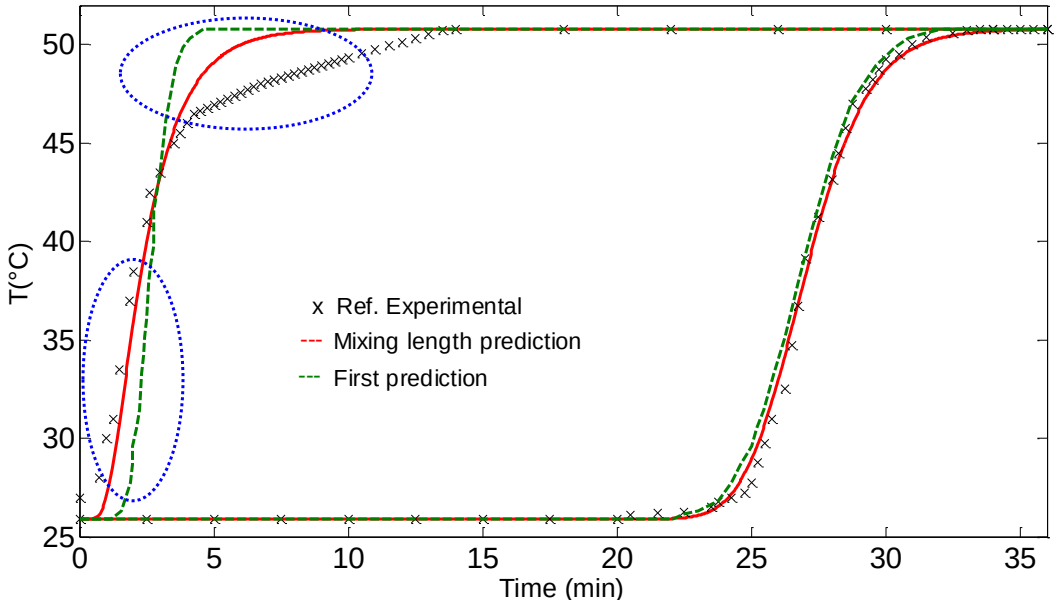

Figure 6.12: Transient temperature profiles obtained by mixing length model comparison with the experimental data taken from Ref. [72] and the results presented in Fig.6.6.

6.5 Chapter Summary

The environmental assessment analysis shows that the thermocline system has markedly less environmental impact than the 2-tank system. This fact and the lower cost of the thermocline system supported the selection of this system for the present study. A numerical model based on the resulting system of equations is solved by using time-implicit and space-backward finite differences within the Matlab environment. The model developed allows the comprehensive analysis of the transient charging/discharging phase. The mathematical formulation of the model is based on the one-dimensional Schumann equations, which allows the specification of the inlet temperature and velocity, physical properties, and initial conditions. The analyses of the selected storage system during the charging phase led to the following findings: the predictions agree well with the experiments in what concerns the time evolution of the tank region, particularly for the regions away from the immediate vicinity of the top-inlet. The deviations observed in the near-region of the inlet are most likely due to the high-level of turbulence in this region and are due to

the resulting localized level of mixing; a simple analytical model to take into consideration this increased turbulence level was developed and it leads to improved predictions. This approach requires practically no additional computational effort and it relates, through the mixing length, the effective thermal diffusivity to the velocity profile of the fluid at each particular height of the system. For the implementation of the model to a packed bed thermocline system is envisaged the influence of the void fraction will be critical in the definition of the flow characteristics. The model will only affect the effective diffusivity referring to the liquid component.

Conclusion

Summary

The PhD project addresses the potential of concentrating solar power (CSP) plants as a viable alternative clean energy producing system in Libya. Exergetic, energetic, economic performance and environmental impact analyses were carried out for a particular type of CSP plant - a 50 MWe parabolic trough-CSP plant. The novelty of the study, in addition to the configuration that was considered, lies in the use of a state-of-the-art exergetic analysis combined with Life Cycle Assessment (LCA). The Libyan territory is taken into consideration as the specific location of the CSP plant based on its high solar irradiation, consumer proximity and density, and condenser cooling water availability. In this region, a large-scale Mediterranean climate prevails with high average annual levels of irradiation, which make the establishment of commercial CSPs highly favorable in terms of rentability return.

Altogether the study indicates that the selected parabolic trough-CSP plant has the edge over alternative competing technologies for locations where DNI is high and where land usage is not an issue such as the shoreline of Libya, in this way, after the restoration of stability in the region, it will be viable to implement several European initiatives that aim to import electricity generated by CSPs. In addition, further financial and energy costs reduction incentives can be achieved by having the participation of local manufacturing.

Concluding Remarks

- Modeling and simulation analysis of a 50 MWe parabolic trough-CSP plant was carried out in Chapter Three. The analysis was divided into two components: solar field and power generation cycle. A computer model was developed for the analysis of the selected plant based on algebraic equations describing the power cycle and the solar field. The model allowing the definition of the properties at each state point of the cycle and then, sequentially, determined energy, efficiency and irreversibility for each component. The solar field model was based on the simplified methodology proposed by Forristall [69], the heat transfer model of the heat collection is one dimensional and steady-state and based on a thermal resistance analysis. The maximum and minimum annual solar days of the Tripoli region was tested within the model.

  The main findings reported that the energetic thermal efficiency of the power cycle is 36% and the gross power output is 48 MW. In addition, the exergetic losses reach a maximum at the boiler (10796 kW), and the daily averaged amount of energy needed to be delivered to the train heat exchanger is 3289 MWh. The collected heat at the collector is 1267 W/m and the collector efficiency 70% in the middle of July; while they are 4833 W/m and 50%, respectively, in the middle of December. In concluding, the developed model has the potential of becoming a useful tool for the preliminary design of CSPs and, in particular, for the configuration of the solar field using existing commercial plants. Moreover, it has the ability of analyzing the energetic, economic and environmental feasibility of using CSPs in different regions of the world, which was illustrated for the Tripoli region (Libya) in this study.

- The overall energy scenario for the CSP in terms of behavior and performance of its components was completed through an hourly analysis on an annual

basis in Chapter Four. This analysis allows the comparison of different systems and, eventually of a particular selection, and it includes both the economic and performance elements, which was simulated within the “greenius” environment. The analysis also examined the impact of project financing and incentives on the cost of energy. The analysis uses the levelized cost of electricity (LCE) as the primary metric of the financial performance.

The findings make a sound case, based on the current cost of energy, for the potential of reducing the cost of energy from parabolic trough solar power plant technology. An interesting, and to a great extent surprising, finding of the present study is higher values for performance and potentially lower LCE for Tripoli (Libya) as compared to Andalucía (Spain). Libya, in technological terms, has the potential of becoming attractive for establishing CSPs in its territory and, in this way, to facilitate the realization of several European initiatives that aim to import electricity generated by renewable sources from North African and Middle East countries. Moreover, the model has the ability of analyzing the energetic, economic and environmental feasibility of using CSPs in different regions of the world, which was illustrated by analyzing four different sites in Libya.

In addition, a comparative analysis was conducted for three different sites in Libya in addition to the Tripoli region - the cities of Al Ugaylah, Dirj and Al Jawf, which are located in the middle of coastline (North), the Southwest and the Southeast, respectively. Al Jawf presents the highest efficiencies 48.6% in the solar field and 15% in the plant, while Dirj presents the highest annual net output of gross electricity of 244 MWhe. In addition, both locations have the advantage of their closeness to the Sahara, where vast free land is available. However, Al Ugaylah has the advantage of being close to the sea with total availability of water for condenser cooling. The other two locations would require additional infrastructures for condenser cooling such as cooling

towers, where the use of freshwater is desirable, and water ponds. These facilities will require considerable capital and maintenance costs.

- Chapter Five addresses the exergetic life cycle assessment of CSP plants; the analysis focused on 50 MWe parabolic trough-CSP plant. The Eco-indicator 99 (H) and Cumulative Exergy Demand methods were used to assess the midpoint and endpoint impacts from 'the cradle to the grave'. The impact categories comprised global warming, acidification, eutrophication, ecotoxicity, carcinogens, respiratory organics, respiratory inorganic and climate change. The LCA reported that the Human Health damage category presents the largest impact with 69% followed by the Resource damage category with 24% and then the Ecosystem Quality damage category with 7%. The respiratory inorganics category presents the highest impact percentage (45.5%) followed by fossil fuels (20.4%) and carcinogens (14%), while other categories present low impacts. The materials with highest impact are: steel (47%), molten salt (25%) and synthetic oil (21%). The most important contribution impact lies with the solar field reporting a value of 79%. The impact of the storage system with a value of 20.6% was of the same order of magnitude of that of the solar field, while the power block and transportation impacts are relatively small. This apparent disparity is due to the large amounts of steel and synthetic oil being used in the solar field, and of molten salt in the storage system. The complete life cycle assessment analysis of the system included the waste disposal and reuse of the components after the useful life of the plant, and it was conducted with the aim of learning about the environmental impact caused by the disposal and waste stages. Since there was no radioactive and fuel waste disposals, the impact of the disposal stage was low (8.7% out of the total impacts of all studied stages).

The ELCA analysis demonstrated that the highest exergy demand was linked to the steel (47%); which is primarily due to the non-renewable fossil fuel impact category. In addition, there is a considerable exergetic demand related to the molten salt and synthetic oil with approximate values of 25% and 19%, respectively; while other demands are relatively small. The resources of the nature (non-renewables) categories such as non-renewable fossil, non-renewable nuclear and non-renewable metals impact categories presented the core of the demands with a value higher than 99%.

Comparing with the two fossil technologies considered in this study, the solar thermal power plant has the lowest environmental impact, while the oil power plant has the worst environmental performance. The solar thermal power plant has the advantage over the oil power plant for all damage categories, while the advantage over the NGCC power plant lies with the Resources and Human Health damage categories. It should be noted the NGCC power plant for the Ecosystem Quality damage category presents a very small impact; however, in the Resources damage category, the highest impact is for the NGCC power plant with a value of 77%, while for the oil power plant for this indicator is 53%.

Although, the most important contribution impact is presented by the solar field and then by the storage system, due to the large amount of steel and synthetic oil used in the solar field and molten salt used in the storage system. However, CSPs present lower contribution impact than that of fossil systems. Furthermore, the highest cost rate is presented in the solar field, due to the initial capital investment, which can be overcome by increasing the operation time due to the combined effect of cost savings related to the non-usage of fossil fuels in the power-generation process and the absence of a CO2 tax.

The thermo-economic analysis determines the average cost rates and the unit cost of components, specific cost per exergy unit of electricity. The solar field presents the maximum cost rate, and the boiler is the component with the highest cost rate among power cycle components.

- Chapter Six, through modeling and analysis, contributes to an improved understanding of the dynamic temperature response of a thermocline energy storage system. The model, although simplified, is comprehensive and accurate in predicting the charging phase of a thermocline thermal energy storage tank for CSP plants. This numerical model can simulate the thermocline storage systems, which have a key role in the enhancement of effectiveness, economics and operational characteristics of solar parabolic trough electric systems. The thermocline thickness and effectiveness are examined as a function of the thermocline motion, effective thermal diffusivity and height of the tank; and the model was validated with the experimental data. The analysis of the results obtained for the charging phase of the thermal storage system leads to the following findings: the predictions agree well with the experiments for the time evolution of thermocline region, particularly for the regions far-away from the top-inlet. The deviations observed in the near-region of the inlet are most likely due to the high-level of turbulence in this region due to the localized level of mixing; a simple analytical model to take into consideration this increased turbulence level was developed and it leads to some improvement in the predictions.

Potential Future Work

All North African countries have an outstanding potential for solar energy applications, while most of them are afflicted by extreme water scarcity. Libya, in particular, it depends almost exclusively on ground water and desalination of seawater. Until recently, it was being considered to use extra fossil fuel for seawater desalination to cover the dramatic increase in demand of potable water. In these circumstances, the use of CSPs to power seawater desalination either by electricity or in integrated generation with process steam to solve the water scarcity problem is a rather obvious approach.

The viability of an integrated plant under different scenarios including those of electricity generation for external-to-the-plant consumption will be an interesting and appropriate extension of the present work. The main purpose of this possible study will be to develop a methodology to assess the best configuration for an integrated solar power and desalination plant. The assessment should be conducted not only in terms of overall efficiency, but also in terms of environmental impact using the LCA method. The solar plant itself will use CSP technologies; however, as a function of the scenario to be analyzed, the most appropriate solution for the energy receiver-storage system, most likely, will not be universal. In what concerns the desalination process itself, as indicated by a preliminary study [132], there are a considerable number of options, namely: low temperature multi-effect distillation, thermal vapor compression multi-effect distillation coupled with solar power, and reverse osmosis using power supplied by the solar power plant.

References

[1] Dadax. Worldometers. http://www.worldometers.info/world-population/ (accessed April 4, 2016).

[2] EIA. International Energy Outlook 2013. 2013. doi:EIA-0484(2013).

[3] U.S. Department of Commerce, National Oceanic & Atmospheric Administration NOAA. Earth System Research Laboratory Global Monitoring Division 2014. http://www.esrl.noaa.gov/gmd/ccgg/trends/.

[4] The State of Food Insecurity in the World. Food and agriculture organization of the united nations, ISBN 978-92-5-107316-2; 2012.

[5] Becker M, Meinecke W, Geyer M, Trieb F, Blanco M, Romero M, et al. Solar Thermal Power Plants, report prepared for the EUREC-Agency, 2000.

[6] Cheng Z-D, He Y-L, Du B-C, Wang K, Liang Q. Geometric optimization on optical performance of parabolic trough solar collector systems using particle swarm optimization algorithm. Applied Energy 2015;148:282–93.

[7] Rodriguez-Sanchez D, Rosengarten G. Improving the concentration ratio of parabolic troughs using a second-stage flat mirror. Applied Energy 2015;159:620–32.

[8] Aichmayer L, Spelling J, Laumert B. Thermoeconomic Analysis of a Solar Dish Micro Gas-turbine Combined-cycle Power Plant. Energy Procedia 2015;69:1089–99.

[9] Gil A, Medrano M, Martorell I, Lázaro A, Dolado P, Zalba B, et al. State of the art on high temperature thermal energy storage for power generation. Part 1—Concepts, materials and modellization. Renewable and Sustainable Energy Reviews 2010;14:31–55.

[10] Blake D, Moens L, Hale M. New heat transfer and storage fluids for parabolic trough solar thermal electric plants. Proceedings of the 11th SolarPACES

International Symposium On concentrating Solar Power and Chemical Energy Technologies, Zurich, Switzerland: 2002.

[11] Desideri U, Zepparelli F, Morettini V, Garroni E. Comparative analysis of concentrating solar power and photovoltaic technologies: Technical and environmental evaluations. Applied Energy 2013;102:765–84.

[12] DESERTEC Foundation. http://www.desertec.org/.

[13] Poullikkas A, Hadjipaschalis I, Kourtis G. Techno-economic analysis of CSP plants for isolated Mediterranean power systems. 7th Mediterranean Conference and Exhibition on Power Generation, Transmission, Distribution and Energy Conversion (MedPower 2010), IET; 2010.

[14] He Y-L, Mei D-H, Tao W-Q, Yang W-W, Liu H-L. Simulation of the parabolic trough solar energy generation system with organic Rankine cycle. Applied Energy 2012;97:630–41.

[15] Derbal H, Bouaichaoui S, El-Gharbi N, Belhamel M, Benzaoui A. Modeling and numerical simulation of an integrated solar combined cycle system in Algeria. Procedia Engineering 2012;33:199–208.

[16] Montes M, Abánades A, Martínez-Val J, Valdés M. Solar multiple optimization for a solar-only thermal power plant, using oil as heat transfer fluid in the parabolic trough collectors. Solar Energy 2009;83:2165–76.

[17] Lippke F. Simulation of the Part Load Behavior of a 30MWe SEGS Plant. Albuque; Prepared for Sandia National Laboratories, SAND95-1293; 1995.

[18] Reddy V, Kaushik S, Tyagi S. Exergetic analysis and performance evaluation of parabolic trough concentrating solar thermal power plant (PTCSTPP). Energy 2012;39:258–73.

[19] Poullikkas A. Economic analysis of power generation from parabolic trough solar thermal plants for the Mediterranean region - A case study for the island of Cyprus. Renewable and Sustainable Energy Reviews 2009;13:2474–84.

[20] Sui X, Zhang Y, Shao S, Zhang S. Exergetic life cycle assessment of cement production process with waste heat power generation. Energy Conversion and Management 2014;88:684–92.

[21] Cornelissen R, Hirs G. The value of the exergetic life cycle assessment besides the LCA. Energy Conversion and Management 2002;43:1417–24.

[22] Bösch M, Hellweg S, Huijbregts M, Frischknecht R. Applying Cumulative Exergy Demand (CExD) Indicators to the ecoinvent Database. Int J LCA, 2007;12:181–90.

[23] Lechón Y, Rúa C, Sáez R. Life Cycle Environmental Impacts of Electricity Production by Solar thermal Power Plants in Spain. ASME - Journal of Solar Energy Engineering 2008;130:021012/1–7.

[24] Piemonte V, Falco M De, Tarquini P, Giaconia A. Life Cycle Assessment of a high temperature molten salt concentrated solar power plant. Solar Energy 2011;85:1101–8.

[25] Weinrebe G, Böhnke M, Trieb F. Life Cycle Assessment of an 80MW SEGS plant and a 30MW PHOEBUS power tower. International solar energy conference “Solar Engineering” Albuquerque, 1998.

[26] Oró E, Gil A, de Gracia A, Boer D, Cabeza L. Comparative life cycle assessment of thermal energy storage systems for solar power plants. Renewable Energy 2012;44:166–73.

[27] Aurelie K, Germain A, Leda G, Francois M. Life cycle assessment and envirnomic optimization of concentrating solar thermal power plants. 26th International Conference on Efficiency, Cost, Optimization, Simulation and Environmental Impact of Energy Systems , Guilin, China, 2013; EPFL–CONF–186393.

[28] Klein S, Rubin E. Life cycle assessment of greenhouse gas emissions, water and land use for concentrated solar power plants with different energy backup

systems. Energy Policy 2013;63:935–50.

[29] Asdrubali F, Baldinelli G, D'Alessandro F, Scrucca F. Life cycle assessment of electricity production from renewable energies: Review and results harmonization. Renewable and Sustainable Energy Reviews 2015;42:1113–22.

[30] Hepbasli A. A key review on exergetic analysis and assessment of renewable energy resources for a sustainable future. Renewable and Sustainable Energy Reviews 2008;12:593–661.

[31] Ozgener L, Hepbasli A, Dincer I. Thermo-Mechanical Exergy Analysis of Balcova Geothermal District Heating System in Izmir, Turkey. Journal of Energy Resources Technology 2004;126:293–301.

[32] Hepbasli A, Utlu Z. Evaluating the energy utilization efficiency of Turkey's renewable energy sources during 2001. Renewable and Sustainable Energy Reviews 2004;8:237–55.

[33] Hepbasli A. A review on energetic, exergetic and exergoeconomic aspects of geothermal district heating systems (GDHSs). Energy Conversion and Management 2010;51:2041–61.

[34] Ozgener O, Hepbasli A. A review on the energy and exergy analysis of solar assisted heat pump systems. Renewable and Sustainable Energy Reviews 2007;11:482–96.

[35] Hepbasli A, Alsuhaibani Z. Exergetic and exergoeconomic aspects of wind energy systems in achieving sustainable development. Renewable and Sustainable Energy Reviews 2011;15:2810–25.

[36] Ozgener L, Hepbasli A, Dincer I. Energy and exergy analysis of the Gonen geothermal district heating system, Turkey. Geothermics 2005;34:632–45.

[37] Ozgener O, Hepbasli A. Exergoeconomic analysis of a solar assisted ground-source heat pump greenhouse heating system. Applied Thermal Engineering 2005;25:1459–71.

[38] Oztop HF, Bayrak F, Hepbasli A. Energetic and exergetic aspects of solar air heating (solar collector) systems. Renewable and Sustainable Energy Reviews 2013;21:59–83.

[39] Sciubba E. Beyond thermoeconomics? The concept of Extended Exergy Accounting and its application to the analysis and design of thermal systems. Exergy, An International Journal 2001;1:68–84.

[40] Sciubba E. Extended exergy accounting: towards an exergetic theory of value. ECOS '99, Tokyo, Japan: 1999; 85–94.

[41] Sciubba E. Exergy as a direct measure of environmental impact. ASME, Advanced Energy Systems Division, Nashville, USA, 1999; 39: 573–81.

[42] Sciubba E. A nested black-box exergetic method for the analysis of complex systems. Adv. In Energy Studies, Venere, Italy: 1998; 471–82.

[43] Sciubba E, Bastianoni S, Tiezzi E. Exergy and extended exergy accounting of very large complex systems with an application to the province of Siena, Italy. Journal of Environmental Management 2008;86:372–82.

[44] Singh N, Kaushik SC, Misra RD. Exergetic analysis of a solar thermal power system. Renewable Energy 2000;19:135–43.

[45] Khaljani M, Khoshbakhti Saray R, Bahlouli K. Comprehensive analysis of energy, exergy and exergo-economic of cogeneration of heat and power in a combined gas turbine and organic Rankine cycle. Energy Conversion and Management 2015;97:154–65.

[46] Fellah G, Mgherbi F, Aboghres S. Exergoeconomic analysis for unit Gt14 of South Tripoli gas. Jordan Journal of Mechanical and Industrial Engineering 2010;4:507–16.

[47] Lazzaretto A, Tsatsaronis G. On the calculation of efficiencies and costs in thermal systems. In: Aceves SM, Garimella S, Peterson R, editors. Proceedings of the ASME advanced energy systems division, New York, 1999;39:421–30.

[48] Tsatsaronis G, Lin L, Pisa J. Exergy costing in exergoeconomics. Journal of Energy Resources Technology 1993;115:9–16.

[49] Elsafi A. Exergy and exergoeconomic analysis of sustainable direct steam generation solar power plants. Energy Conversion and Management 2015;103:338–47.

[50] Cavalcanti EJC, Motta HP. Exergoeconomic analysis of a solar-powered/fuel assisted Rankine cycle for power generation. Energy 2015;88:555–62.

[51] Colpan CO, Yeşin T. Energetic, exergetic and thermoeconomic analysis of Bilkent combined cycle cogeneration plant. International Journal of Energy Research 2006;30:875–94.

[52] Ozbilen A, Dincer I, Rosen MA. Exergetic life cycle assessment of a hydrogen production process. International Journal of Hydrogen Energy 2012;37:5665–75.

[53] Granovskii M, Dincer I, Rosen M a. Exergetic life cycle assessment of hydrogen production from renewables. Journal of Power Sources 2007;167:461–71.

[54] Koroneos C, Tsarouhis M. Exergy analysis and life cycle assessment of solar heating and cooling systems in the building environment. Journal of Cleaner Production 2012;32:52–60.

[55] De Meester B, Dewulf J, Verbeke S, Janssens A, Van Langenhove H. Exergetic life-cycle assessment (ELCA) for resource consumption evaluation in the built environment. Building and Environment 2009;44:11–7.

[56] Talens Peiró L, Lombardi L, Villalba Méndez G, Gabarrell i Durany X. Life cycle assessment (LCA) and exergetic life cycle assessment (ELCA) of the production of biodiesel from used cooking oil (UCO). Energy 2010;35:889–93.

[57] Lombardi L. Life cycle assessment (LCA) and exergetic life cycle assessment (ELCA) of a semi-closed gas turbine cycle with CO2 chemical absorption. Energy Conversion and Management 2001;42:101–14.

[58] Koroneos C, Dimou D, Andrinopoulos N, Moussiopoulos N. Application of life cycle assessment and exergy analysis in a combined cycle power plant using natural gas at Lavrion, Greece. International Journal of Power and Energy Conversion 2011;2:365–86.

[59] Libby C. Solar thermocline storage systems: preliminary design study. 2010. Report no. 1019581, EPRI, California.

[60] Tesfay M, Venkatesan M. Simulation of Thermocline Thermal Energy Storage System Using C. International Journal of Innovation and Applied Studies 2013;3:354–64.

[61] Bayón R, Rojas E. Simulation of thermocline storage for solar thermal power plants: From dimensionless results to prototypes and real-size tanks. International Journal of Heat and Mass Transfer 2013;60:713–21.

[62] Yang Z, Garimella S. Thermal analysis of solar thermal energy storage in a molten-salt thermocline. Solar Energy 2010;84:974–85.

[63] Yang Z, Garimella S. Molten-salt thermal energy storage in thermoclines under different environmental boundary conditions. Applied Energy 2010;87:3322–9.

[64] Flueckiger S, Yang Z, Garimella S. An integrated thermal and mechanical investigation of molten-salt thermocline energy storage. Applied Energy 2011;88:2098–105.

[65] Xu C, Wang Z, He Y, Li X, Bai F. Sensitivity analysis of the numerical study on the thermal performance of a packed-bed molten salt thermocline thermal storage system. Applied Energy 2012;92:65–75.

[66] Xu C, Wang Z, He Y, Li X, Bai F. Parametric study and standby behavior of a packed-bed molten salt thermocline thermal storage system. Renewable Energy 2012;48:1–9.

[67] Xu C, Li X, Wang Z, He Y, Bai F. Effects of solid particle properties on the thermal performance of a packed-bed molten-salt thermocline thermal storage

system. Applied Thermal Engineering 2013;57:69–80.

[68] EES: Engineering Equation Solver Software. F-Chart Software. http://www.fchart.com/ees/index.php.

[69] Forristall R. Heat Transfer Analysis and Modeling of a Parabolic Trough Solar Receiver Implemented in Engineering Equation Solver. National Renewable Energy Laboratory. Technical report NREL/TP-550-34169, 2003.

[70] greenius software. German Aerospace Centre (DLR). http://freegreenius.dlr.de/.

[71] Meteonorm7 Software. METEOTEST Genossenschaft. http://meteonorm.com/en/downloads.

[72] Zurigat Y, Liche P, Ghajar A. Influence of inlet geometry on mixing in thermocline thermal energy storage. Int J Heat Mass Transfer 1991;34:115–25.

[73] Goswami D, Kreith F, Kreider J. Principles of solar engineering. Second Edi. Taylor & Francis, 2000; ISBN: 1-56032-714-6.

[74] Li H, Lian Y, Wang X, Ma W, Zhao L. Solar constant values for estimating solar radiation. Energy 2011;36:1785–9.

[75] Padilla R. Simplified Methodology for Designing Parabolic Trough Solar Power Plants. PhD Thesis, University of South Florida, 2011.

[76] World map of global horizontal irradiation. SolarGIS 2013. http://solargis.info/ (accessed February 3, 2015).

[77] Reddy V, Kaushik S, Ranjan K, Tyagi S. State-of-the-art of solar thermal power plants—A review. Renewable and Sustainable Energy Reviews 2013;27:258–73.

[78] 7Practical applications of CSP and heat - solar Novus today. http://www.solarnovus.com/7-practical-applications-of-csp-and-heat_N9089.html (accessed August 14, 2015).

[79] International Renewable Energy Agency (IRENA). Renewable energy

technologies: cost analysis series - Concentrating Solar Power, 2012;1:(2-5).

[80] Weinstein L, Loomis J, Bhatia B, Bierman D, Wang E, Chen G. Concentrating Solar Power. American Chemical Society, CHEMICAL REVIEWS - Special Issue: Solar Energy Conversion 2015.

[81] REN21. Global status report. 2015. doi:SAIREC, South Africa International Renewable Energy Conference.

[82] Concentrating Solar Power Projects Home Page. National Renewable Energy Laboratory. http://www.nrel.gov/csp/solarpaces/ (accessed November 12, 2015).

[83] Salazar C. An overview of CSP in Europe, North Africa and the Middle East. CSP Today, London 2008:1–64.

[84] IEA. Technology Roadmap: Concentrating Solar Power. International Energy Agency; 2010.

[85] Khaled A. Technical and Economic Performance of Parabolic Trough in Jordan. Thesis, University of Kassel, 2012.

[86] Aldali Y. Solar thermal and photovoltaic electrical generation in Libya. PhD Thesis, Edinburgh Napier University, 2012.

[87] Ehtiwesh I, Coelho M, Sousa A. Exergetic and environmental life cycle assessment analysis of concentrated solar power plants. Renewable and Sustainable Energy Reviews 2016;56:145–55. doi:10.1016/j.rser.2015.11.066.

[88] Ehtiwesh I, Neto da Silva F, Sousa A. Performance and economic analysis of concentrated solar power plants in Libya. 2nd International Conference on Energy and Environment: bringing together Engineering and Economics Guimarães, Portugal, 2015.

[89] Duffie J, Beckman W. Solar Engineering of Thermal Processes. Third Ed. Wiely, John; 2006.

[90] Moran M, Shapiro H, Boettener D, Bailey M. Fundamentals o f engineering thermodynamics. Seven Ed. John Wiley & Sons, Inc.; 2011.

[91] Pantnode A. Simulation and Performance Evaluation of Parabolic Trough Solar Power Plants. Thesis, University of Wisconsin-Madison, 2006.

[92] Cengel Y. Heat Transfer: A Practical Approach. Second Ed. McGraw-Hill Companies; 2002.

[93] Habib M, Said S, Al-Zaharna I. Thermodynamic optimization of reheat regenerative thermal-power plants. Applied Energy 1999;63:17–34.

[94] Cengel YA, Boles M, Boles MA. Thermodynamics: an engineering approach. second Ed. McGraw-Hill Education; 1989.

[95] El-Wakil M. Power plant Technology. McGraw-Hill; 1988.

[96] Dudley E, Kolb J, Mahone R. Test Results: SEGS LS-2 Solar Collector, report: SAND94-1884 1994.

[97] Burkholder F, Kutscher C. Heat Loss Testing of Schott's 2008 PTR70 Parabolic Trough Receiver, Technical report: NREL/TP-550-45633. 2009.

[98] Incropera F, Bergman T, Lavine A, Dewitt D. Fundamentals of Heat and Mass Transfer. Seventh Ed. John Wiley & Sons, Inc; 2011.

[99] Price H, Lüpfert E, Kearney D, Zarza E, Cohen G, Gee R, et al. Advances in Parabolic Trough Solar Power Technology. Journal of Solar Energy Engineering, ASME 2002;124:109–25.

[100] Bartlett R. Steam turbine performance and economics. New York : McGraw-Hill; 1958.

[101] greenius User manual - version 4.1. DLR; 2014.

[102] Solar Millennium AG. The Parabolic Trough Power Plants Andasol 1 to 3. Germany: 2008.

[103] Schulte-Fischedick J, Tamme R, Herrmann U. CFD analysis of the cool down behaviour of molten salt thermal. Proceedings of the ES2008, Energy Sustainability, Jacksonville, Florida: 2008.

[104] SimaPro 8 - World's Leading LCA Software Package, PRé Consultants. PRé Consultants.

[105] ISO 14044 (2006): Environmental management - Life cycle assessment - Requirements and guidelines. International Organisation for Standardisation (ISO), Geneve.

[106] Arachchilage K. Life Cycle Analysis of Alfalfa stem-based bioethanol production system. University of Saskatchewan, 2011.

[107] Jensen A, Hoffman L, Moller B, Schmidt A, Christiansen K, Elkington J, et al. Life Cycle Assessment – A guide to approaches, experiences and information sources. Environmental Science and Pollution Research, European Environment Agency 1997.

[108] Erixon M. Practical strategies for acquiring life cycle inventory data in the electronics industry. Center for Environmental Assessment of Product and Material Systems, CPM Report 1999:3.

[109] ISO 14040 (2006): Environmental management - Life cycle assessment - Principles and framework. ISO, Geneve.

[110] PRé. The Eco-indicator 99–a damage oriented method for life cycle impact assessment, Methodology report. Pré Consultants B.V., Amersfoort, The Netherlands: 2001.

[111] Ortiz O, Castells F, Sonnemann G. Sustainability in the construction industry: A review of recent developments based on LCA. Construction and Building Materials 2009;23:28–39.

[112] Blengini G. Life cycle of buildings, demolition and recycling potential: A case study in Turin, Italy. Building and Environment 2009;44:319–30.

[113] Bravo Y, Carvalho M, Serra LM, Monné C, Alonso S, Moreno F, et al. Environmental evaluation of dish-Stirling technology for power generation. Solar Energy 2012;86:2811–25.

[114] Szargut J, Morris D, Steward F. Exergy Analysis of Thermal, Chemical, and Metallurgical Processes. New York: Hemisphere Publishing Corporation; 1997.

[115] Viebahn P, Kronshage S, Trieb F, Lechon Y. Final report on technical data, costs, and life cycle inventories of solar thermal power plants 2008:NEEDS, Project no: 502687.

[116] Nandi BR, Bandyopadhyay S, Banerjee R. Analysis of high temperature thermal energy storage for solar power plant. IEEE - ICSET, Nepal 2012:438–44.

[117] Pihl E, Kushnir D, Sandén B, Johnsson F. Material constraints for concentrating solar thermal power. Energy 2012;44:944–54.

[118] Tsatsaronis G, Moran MJ. Exergy-aided cost minimization. Energy Conversion and Management 1997;38:1535–42.

[119] Abusoglu A, Kanoglu M. Exergetic and thermoeconomic analyses of diesel engine powered cogeneration: Part 1 - Formulations. Applied Thermal Engineering 2009;29:234–41.

[120] Pehnt M. Dynamic life cycle assessment (LCA) of renewable energy technologies. Renewable Energy 2006;31:55–71.

[121] Garcia R, Marques P, Freire F. Life-cycle assessment of electricity in Portugal. Applied Energy 2014;134:563–72.

[122] Shokati N, Ranjbar F, Yari M. A comparative analysis of rankine and absorption power cycles from exergoeconomic viewpoint. Energy Conversion and Management 2014;88:657–68.

[123] Schumann T. Heat transfer: A liquid flowing through a porous prism. Journal of

the Franklin Institute 1929;208:405–16.

[124] Stine W, Geyer M. Power From The Sun 2001. http://www.powerfromthesun.net/book.html (accessed November 18, 2014).

[125] Sharma A, Tyagi VV, Chen CR, Buddhi D. Review on thermal energy storage with phase change materials and applications. Renewable and Sustainable Energy Reviews 2009;13:318–45.

[126] Flueckiger S, Yang Z, Garimella S. Review of Molten-Salt Thermocline Tank Modeling for Solar Thermal Energy Storage. Heat Transfer Engineering 2013;34:787–800.

[127] Mcmahan A. Design & optimization of organic Rankine cycle solar-thermal power plants. Thesis, University of Wisconsin-Madison, 2006.

[128] Cushman-roisin B. Environmental fluid mechanics. New York: John Wiley & Sons, Inc.; 2014.

[129] Wilcox D. Turbulence Modeling for CFD. Third Ed. La Cañada, California: DCW Industries, Inc.; 2006.

[130] Driest Van. On Turbulent Flow Near a Wall. Journal of the Aeronautical Sciences 1956;23:1007–11.

[131] Or CM, Lam KM, Liu P. Potential core lengths of round jets in stagnant and moving environments. Journal of Hydro-Environment Research 2011;5:81–91.

[132] Trieb F. Concentrating Solar Power for Seawater Desalination. German Aerospace Center, Institute of Technical Thermodynamics, DLR Final Report 2008.